FPL

L-2015-196
10 CFR 52.3

July 15, 2015

U.S. Nuclear Regulatory Commission
Attn: Document Control Desk
Washington, D.C. 20555-0001

Re: Florida Power & Light Company
Proposed Turkey Point Units 6 and 7
Docket Nos. 52-040 and 52-041
Response to NRC Request for Additional Information Letter No. 081 (eRAI 7804)
SRP Section 02.05.01 – Basic Geologic and Seismic Information

References:

1. NRC Letter to FPL dated February 18, 2015, Request for Additional Information Letter No. 081 Related to SRP Section 02.05.01 – Basic Geologic and Seismic Information for the Turkey Point Nuclear Plant Units 6 and 7 Combined License Application
2. FPL Letter L-2015-069 to NRC dated March 20, 2015, Schedule for Response to NRC Request for Additional Information Letter No. 081 (eRAI 7804) SRP Section 02.05.01 – Basic Geologic and Seismic Information
3. FPL Letter L-2015-123 to NRC dated April 10, 2015, Updated Schedule for FSAR Chapter 2 RAI Responses and FSAR Chapter 19

Florida Power & Light Company (FPL) provides, as an attachment to this letter, its response to the Nuclear Regulatory Commission's (NRC) request for additional information (RAI) 02.05.01-34 provided in Reference 1. In References 2 and 3 FPL provided schedule information for the response to this RAI. The attachment identifies changes that will be made in a future revision of the Turkey Point Units 6 and 7 Combined License Application (if applicable).

If you have any questions, or need additional information, please contact me at 561-691-7490.

I declare under penalty of perjury that the foregoing is true and correct.

Executed on July 15, 2015.

Sincerely,

William Maher
Senior Licensing Director – New Nuclear Projects

WDM/RFB

Florida Power & Light Company
700 Universe Boulevard, Juno Beach, FL 33408

D097
NRO

Attachment: FPL Response to NRC RAI No. 02.05.01-34 (eRAI 7804)

cc:
PTN 6 & 7 Project Manager, AP1000 Projects Branch 1, USNRC DNRL/NRO
Regional Administrator, Region II, USNRC
Senior Resident Inspector, USNRC, Turkey Point Plant 3 & 4

**NRC RAI Letter No. PTN-RAI-LTR-081**

**SRP Section: 02.05.01 - Basic Geologic and Seismic Information**

Questions from Geosciences and Geotechnical Engineering Branch 2 (RGS2)

**NRC RAI Number: 02.05.01-34 (eRAI 7804)**

Newly published data (D. Kula, August, 2014*) (high resolution seismic reflection, multibeam bathymetry and sub-bottom parasound profiles) reveal Quaternary-aged tectonic structures in the Santaren Channel and the Straits of Florida within 80 miles of TPNPP. Seafloor displacements are observed in all data types.

a) In support of 10 CFR 100.23 please provide a discussion of these tectonic features and integrate into the regional tectonic setting for TPNPP COLA.

b) Several investigations, published by authors such as Eberli, Massafero, Bergman and Kula, make a strong case for extending the Cuba Fold and Thrust belt beneath Cay Sal Bank and as far as the northwestern end of the Santaren Channel. Even though there is no seismicity in the area beneath Cay Sal Bank and the Santaren Channel, distinct seafloor scarps argue for very recent and significant displacement. Provide an analysis of how this northward extension of the Cuban Fold and Thrust belt terrane with associated Quaternary fault displacement and seafloor scarps on at least 2 faults impacts the site seismic hazard assessment and seismotectonic boundaries.

c) Provide appropriate illustrations and maps to support your analyses and discussions. Update any RAI responses and associated COLA revisions that pertain to the Santaren Anticline; the Cuban Fold and thrust belt; boundaries of the Cuba Areal source term, and sensitivity analysis for the Cuban source term. Include interpretation of Santaren Anticline based on Bergman, 2005**.

References:

* Kula, Deniz, "Neotectonics on the Edge of the Cuban Fold and Thrust Belt" (2014). Open Access Theses. Paper 498.

** Bergman, K.L., 2005, Seismic Analysis of Paleocurrent Features in the Florida Straits: Insights into the Paleo-Florida Current, Upstream Tectonics, and the Atlantic-Caribbean Connection, University of Miami, Coral Gables, Florida, p. 238. (FSAR reference 906)

**FPL RESPONSE:**

This response provides additional information pertaining to a recent MS thesis (Kula, 2014) (Reference 1) from the University of Miami that includes interpretations of Quaternary-aged tectonic structures along the northern and eastern margins of the Cay Sal Bank. Kula (Reference 1) documents processing and interpretation of newly obtained, high-resolution seismic data from the area north and east of Cay Sal Bank. Kula used the new 2D seismic profiles to map seismic facies, map and correlate seismic horizons to existing regional well control, and identify geologic structures in these profiles. Kula interprets two distinct types of fault systems: (1) strata-bound faults; and

(2) deep-rooted faults. The strata-bound faults in seismic profiles are noted to be associated with non-tectonic polygonal fault patterns in plan view, and interpreted as related to intra-formational compaction and fluid escape processes. The deep-rooted faults are described as reminiscent of wrench faults and thrust faults. Kula interprets the reactivation of these deep-rooted faults on the eastern side of the Cay Sal Bank as reason to extend the Cuba fold and thrust belt east and northeast to include Cay Sal Bank and into the Santaren Channel. A seafloor break, described as 40 km long, and 50 m in height, is interpreted as evidence of neotectonic activity along the outer fringe of the fold belt along the northeast margin of Cay Sal Bank. Five earthquakes in 2014 along the northern coast of Cuba, about 100 km (about 60 miles) to the west, are cited as evidence for ongoing tectonism within the Cuba fold and thrust belt in the region. Based on the data near Cay Sal Bank, a new structural model that extends the Cuba fold and thrust belt northeast of Cay Sal Bank and includes much of the Santaren Channel is proposed.

Most of the data presented by Kula (Reference 1) was acquired during the University of Hamburg M95 research cruise of the R/V *Meteor* in 2013 and are not publicly available. However, these data and other recently acquired high-resolution data in the same region form the basis of a larger body of research through the University of Miami Comparative Sedimentology Laboratory - Center for Carbonate Research and several cooperating European institutions. Through contacts with researchers and advisors to Kula's thesis research, additional data (published and unpublished) that pertain to the interpretations of Kula (Reference 1) have been obtained. These data, contacts, and the responses from researchers are documented and evaluated in a new SSHAC Level 2 (FSAR Reference 2.5.2-318) study of the potential Quaternary faults proposed by Kula (Reference 1) as part of this response.

To analyze how the potential Quaternary tectonic features interpreted by Kula (Reference 1) may impact site seismic hazard assessments and seismotectonic boundaries, additional publicly available marine seismic data were reviewed and are provided in this response. These data were obtained during commercial survey cruises in 1981 and 1982, and subsequently released to the public domain. These older data have somewhat lower resolution of small features, in comparison to the new 2013 data, but provide a much deeper view (up to 10 km) of potential fault structure. Images of some of these data appear and are interpreted in prior publications in the region (e.g., Ball et al., 1985; Masaferro, 1997; Masaferro et al., 1999, 2002; Bergman, 2005) (FSAR References 2.5.1-501, 2.5.1-477, 2.5.1-426, 2.5.1-479, and 2.5.1-906). For this response, digitally processed images of these data were obtained from the U.S. Geological Survey in order to evaluate the relationships of the shallow features interpreted by Kula (Reference 1) to deeper tectonic structure and to evaluate the potential continuity of these features along Kula's proposed northern extension of the Cuba fold and thrust belt.

Part (a) of this response provides a detailed discussion of the potential tectonic features interpreted by Kula (Reference 1) along with new and additional high-resolution images and revised interpretations of these features provided by the principal advisor of the Kula MS thesis, Prof. Gregor Eberli. Also included in the response to Part (a) are the

Technical Integrator (TI) Team's interpretations of six high-energy, deep-penetration 2D industry seismic lines acquired from the U.S. Geological Survey. Finally, an assessment as to whether Kula's interpretations are technically defensible is provided.

Part (b) of this response provides an assessment of the potential impacts on the site seismic hazard from the features identified by Kula (Reference 1) and Kula's proposed alternative configurations of the Cuba fold and thrust belt. First, a summary is presented of why some authors have proposed the northward extension of the Cuba fold and thrust belt to include the Cay Sal Bank and how this interpretation is more strongly supported in the southern Santaren Channel in the vicinity of the Santaren anticline as opposed to the northern Santaren Channel. Second, Part (b) of this response discusses possible implications of an expanded Cuba fold and thrust belt on how the Cuba areal source zone is represented in the seismic source model. Third, Part (b) of this response addresses whether any of the structures identified by Kula (Reference 1), Bergman (2005) (FSAR Reference 2.5.1-906), and Masaferro et al. (1999; 2002) (FSAR References 2.5.1-426 and 2.5.1-479) could represent viable seismic sources. Finally, Part (b) presents a sensitivity analysis that demonstrates minimal impact on site seismic hazard for an assumed reverse fault coring the Santaren anticline.

Part (c) provides a summary of the updates to previous RAI responses and COLA revisions to text and figures developed as part of this current response.

**Response to Part (a):** ***In support of 10 CFR 100.23 please provide a discussion of these tectonic features and integrate into the regional tectonic setting for TPNPP COLA.***

Kula (Reference 1) processed and interpreted structure and stratigraphy in the vicinity of Cay Sal Bank and Santaren Channel primarily using limited-penetration, high-resolution multichannel data, subbottom profiles, and seafloor bathymetry data. Kula mapped two distinct types of fault systems, including: (1) strata-bound faults; and (2) deep-rooted faults (Figure 1). The strata-bound faults are noted to be associated with non-tectonic polygonal fault patterns, and are related to intra-formational compaction, acoustic pipes, and fluid escape processes (Figure 2).

The deep-rooted faults include both strike-slip ("wrench") faults and thrust faults. Only the deep-rooted faults are considered to be of tectonic origin, although Kula (2014, p. 88) (Reference 1) acknowledges that "their point of origin is not always visible on the seismic sections due to insufficient resolution or depth range of the data." Kula maps four north-northwest-striking faults (named Faults A through D) of variable length on the eastern side of Cay Sal Bank (Figure 1). Two of Kula's mapped faults (Faults C and D) extend from the southern Santaren Channel northward to the Straits of Florida.

Kula (Reference 1) divides the deep-rooted tectonic faults into two subgroups, including: (1) steeply dipping wrench faults, which include Faults A and B; and (2) thrust fault systems, which include Faults C and D (Figures 1 and 3). Kula suggests these faults range in length from 41 km (Fault A) to 180 km (Fault C), as illustrated on Figure 1. The interpreted fault lengths, vertical offsets, and activity of these faults are presented in Table 1. Only Faults A and B, the shorter faults directly east and north of Cay Sal Bank,

were suggested by Kula as younger features. Whereas Faults C and D are interpreted as being much longer (180 and 160 km, respectively), they are interpreted by Kula to be older, inactive structures.

Kula (Reference 1) suggests all four tectonic faults splay off an approximately 8-km-deep detachment horizon (decollement) (Figure 4), and may be related to detachment folding interpreted by Masaferro et al. (1999) (FSAR Reference 2.5.1-426) in the southern Santaren Channel. Kula presents a cross section X-X' illustrating >1 km of vertical separation of the top of an early Miocene horizon, as well as older units, across several faults (Figure 4). However, the amount of this vertical separation is not consistent with separation amounts described in the text of Kula's thesis (Table 1). Kula also suggests that tectonic shortening above the detachment is responsible for local folding on the Cay Sal anticline to the northeast.

Almost all of the profiles presented by Kula (Reference 1) are limited-penetration data, but Kula presents only one deep-penetration industry seismic profile (GSI Line BH81-34 shown on Figure 5) from northern Cay Sal Bank. On this profile, Kula maps pre-early Miocene faults near the margin of a buried carbonate platform margin. Kula suggests that drowning of the platform occurred in the early Miocene, and that low amplitude reflections observed in the buried platform facies likely result from differences in acoustic impedance resulting from alternating limestones and dolomites in the Lower Cretaceous, and evaporates in the Upper Cretaceous (Eberli et al., 2004) (Reference 2). Kula interprets high-amplitude, parallel, semi-continuous seismic reflections within the carbonate bank deposits to represent carbonate-anhydrite alterations. The faults mapped by Kula on GSI Line BH81-34 exhibit very little (less than 15 m) vertical separation of seismic reflections, and are shown to terminate well below a horizon mapped as 19.4 million years old (early Miocene). These faults may correspond with Kula's Faults C and D (Figure 1 and Table 1), but are not labeled as such on Figure 4-6 in Kula (Reference 1) (Figure 5).

Kula (Reference 1) cites seafloor breaks as evidence for neotectonic activity, and notes such breaks on seismic profiles (Figures 3 and 6) as well as multibeam bathymetry (MBES) data (Figures 7a and 7b). On Profile 20 (Figure 3), Kula suggests the break zone is about 1 km wide and 15 m deep. Profile 24A (Figure 6) is located along the northeast margin of Cay Sal Bank. On this line. Kula suggests that Fault A offsets the seafloor by about 50 m. Overall, the seafloor break is meandering and circuitous in map view, extending for about 40 km (Figures 7a and 7b), and is up to 1 km wide (Kula, 2014) (Reference 1).

Kula (Reference 1) interprets a north-northeast-trending anticline termed the Cay Sal anticline that is approximately coincident with the seafloor breaks and Fault A (westernmost fault) on Figure 8. As presented by Kula (Reference 1) in seismic sections, this feature is primarily expressed in post-Middle Cretaceous strata, with a short-wavelength and high-amplitude. The Cay Sal anticline interpreted by Kula (Reference 1) is distinctly different from an anticline mapped by Bergman (2005) (FSAR Reference 2.5.1-906). Bergman's mapped anticline is a broad wavelength feature that trends northeast with a very shallow dip on the western fold limb, and basin-bounding normal faults on the eastern limb (see Figures 6.6 and 6.8 in Bergman, 2005 [FSAR

Reference 2.5.1-906]) near the northen Cay Sal Bank. Kula's (Reference 1) interpretations of structural elements (faults and folds), seafloor breaks, and seismicity in northern Cuba are suggested to be evidence for neotectonic activity around the northeastern side of Cay Sal Bank. In turn, Kula uses these interpretations as support for the northward extension of the Cuba fold and thrust belt (Figure 8). Seismicity in northern Cuba and figures from Bergman (2005) (FSAR Reference 2.5.1-906) are presented in Part (b) of this response.

In summary, Kula (Reference 1) presents an interpretation suggesting the presence of four long faults along the eastern margin of Cay Sal Bank, and that these faults represent an extension of the Cuba fold and thrust belt a few hundred kilometers farther north and east than previously mapped by others. Kula suggests neotectonic activity on two of these faults along the eastern margin of Cay Sal Bank and north to the Straits of Florida splaying off a deep detachment beneath Cay Sal Bank (Figures 4 and 8; Table 1).

As part of the data gathering and evaluation process to develop this response, the TI Team reached out to more than 20 researchers with potential knowledge of the new offshore data in the region. Most of those contacted either did not respond, or indicated that they did not consider that they had current information to offer that would be of use to the TI Team. Prof. Eberli provided detailed responses and dialogue with the TI Team. Limited responses were received from Flavio Anselmetti, Kelly Bergman, Christian Betzler, Kevin Cunningham, Paul Mann, Sam Purkis, and Eduard Saura. These responses provided copies or links to published literature, and recommendations for the TI Team to reach out to other experts, with several suggestions to contact the research group at University of Miami headed by Prof. Eberli. A color copy of the Bergman (2005) (FSAR Reference 2.5.1-906) dissertation was provided by its author and includes much higher-resolution versions of figures relative to those previously available in the online version. Comments from Paul Mann recommended further discussions with Prof. Eberli and expressed the opinion that any faults along the margin of Cay Sal Bank likely are gravitational in nature and an unlikely source of large, crustal earthquakes.

The TI Team was unsuccessful in contacting Deniz Kula despite several attempts, but the TI Team was able to develop a long dialogue and series of information exchanges with Prof. Eberli, Kula's principal thesis advisor. In particular, Prof. Eberli provided detailed clarification of interpretations presented in Kula (Reference 1), both in phone calls and in writing to the TI Team. Prof. Eberli provided review comments on the preliminary TI Team evaluations, answers to TI Team questions, and high-resolution images of several marine seismic profiles presented in Kula's thesis.

Prof. Eberli provided two important points of background information to the TI Team:

- Kula is a geophysicist (not a structural geologist), and the first focus of the thesis was data processing. A secondary focus was data interpretation.
- Kula's forte is treatment of seismic data and not their interpretation.

Key points of clarification provided to the TI Team by Prof. Eberli are summarized in the bullets below and discussed in more detail in the text that follows.

- Kula's structural and neotectonic interpretations allow some reinterpretations.
- Interpretation of M95 seismic profiles acquired in 2013 is an ongoing project and Kula's interpretations are not the final product.
- Prof. Eberli disagrees with several of Kula's structural interpretations, which have not been peer reviewed.
- Prof. Eberli does not believe long through-going faults exist as mapped by Kula.
- Faults C and D mapped by Kula are ancient (pre-Miocene) faults that are no longer active. Kula believes that most of the faults are deeply buried and inactive.
- Kula interpreted two faults with local seafloor offset. The larger of the two seafloor breaks (the one with a 50-m-high scarp) that Kula mapped as fault scarps was misinterpreted. Only one fault (Fault A on Line 20) cuts to the seafloor and is considered active by Prof. Eberli.
- The 50-m-high, 30-km-long seafloor break on Line 24 has been reinterpreted by Prof. Eberli as being the result of a Mass Transport Complex (MTC) headscarp, and not the result of Quaternary faulting as suggested by Kula. The MTC is approximately 1.8 Myrs in age. Seismic reflections of Plio-Pleistocene strata beneath the MTC headscarp are unfaulted and provide evidence for no Quaternary fault activity in this area.
- Prof. Eberli does not believe that any faults mapped by Kula are seismogenic because they are very short and discontinuous and have extremely low slip rates.
- The Santaren anticline and Kula's (Reference 1) Cay Sal anticline are separate tectonic features, and are not connected.
- Neotectonic movement on the northern fringes of the Cuba fold and thrust belt are local and have very low slip rates.
- Prof. Eberli clarified how interpretations have changed through time, as reflected in his oral presentation at the 2015 American Association of Petroleum Geologists (AAPG) Convention in Denver. Prof. Eberli's AAPG abstract (Eberli et al., 2015) was largely written based on the findings of Kula over six months before the AAPG convention. Subsequent research has resulted in significant reinterpretations and corrections, as highlighted above.

Prof. Eberli summarized his opinions and interpretations for the TI Team as related to Kula (Reference 1) and related tectonic questions. In these discussions, Prof. Eberli provided improved images and illustrations of key figures from Kula (Reference 1), and updated interpretations of several features noted by Kula. Figure 9 shows the locations of publicly available seismic lines, as well as the Cruise M95 seismic profile locations that Kula interpreted. Figure 10 shows an updated interpretation of a portion of Cruise

M95 Profile 20 provided by Prof. Eberli. This is a higher resolution image of the same line presented by Kula (Figure 3), and intersects GSI Line BH81-34 also interpreted by Kula (Figure 5). One of the mapped faults (Fault A) in this image extends to the seafloor. Prof. Eberli interprets this as a minor wrench fault exhibiting both compressional and strike-slip motion, with no observed vertical offset of the Plio-Pleistocene boundary. Minor down-to-the-east normal faulting is apparent on middle Miocene and older strata on this profile.

Prof. Eberli stated in his discussions with the TI Team that within the entire M95 dataset, this feature (faulted Cay Sal anticline, Figures 3, 8, and 10) represents the only active tectonic structure. A re-interpretation of M95 Line 24 by Prof. Eberli is shown on Figure 11. The seafloor break on this line is interpreted by Prof. Eberli as the headscarp on a MTC that formed approximately 1.8 Myrs ago. The subsurface seismic data (Figure 11) and geomorphic expression (Figures 7a and 7b) of this MTC are similar to features described by Mulder et al. (2012) (FSAR Reference 2.5.1-984) and Tournador et al. (2015) (Reference 3) for other MTC complexes in the region. Prof. Eberli does not map a fault beneath the feature, as suggested by Kula (Figure 6). Unfaulted seismic reflections of Pliocene age underlie the MTC headscarp, providing evidence of no deeper faulting at this location.

This new interpretation of M95 Line 24 was presented and discussed by Prof. Eberli in the oral presentation at the 2015 AAPG Convention in Denver (Eberli et al., 2015) (Reference 4) as an example of an old MTC feature along the Cay Sal Bank, although it was not highlighted in the published abstract. A TI Team member attended, took notes on Eberli's AAPG presentation, and personally met with Prof. Eberli. The published abstract was written and submitted well in advance of the presentation and the oral presentation reflects Eberli's current thinking. Subsequent research prompted two main corrections to statements made in the abstract. The first is the interpretation of a 50-m-high and 30-km-long seafloor scarp as a slump scar rather than a fault displacing the seafloor on Profile 24, as discussed above. A small displacement of the seafloor on Profile 20 is still interpreted by Prof. Eberli as a fault, but even here there is some ambiguity. The second correction is in regards to the lateral offset of slope channels that were taken as an indication of strike slip movements along the eastern side of Cay Sal Bank. Prof. Eberli no longer believes this is a valid interpretation.

As previously stated, Prof. Eberli considers only one feature to be active. This is the fault-cored fold of the Cay Sal anticline apparent on Profile 20 (Figure 3). Prof. Eberli interprets this structure as a wrench fault system with components of both local compression and strike slip motion, and suggests it may be the far field expression of a lateral stress component along the American-Caribbean plate boundary. Prof. Eberli notes that the offset of seismic reflections along the fault is very small, indicating that no major vertical movement is associated with this structure. Prof. Eberli stated that the only other defensible technical explanation for the observed folding and faulting on Line 20 may be the compaction and subsidence difference along the buried platform margin along which fluid escape occurs, and suggests that this is not a likely seismic source.

Prof. Eberli concludes that while there is evidence for small neotectonic activity north of Cay Sal Bank, the offsets on faults and the amount of growth strata apparent on seismic

lines across the Cay Sal anticline are small and only local, indicating that the deep basement faults that were active during the collisional phase (Cuban Orogeny) are no longer in play. The Cuban Orogeny started at the end of the Cretaceous, culminated in the late Eocene and waned during the early part of the Miocene.

**SSHAC Process and TI Team Activities**

The work was performed under SSHAC Level 2 guidelines (FSAR Reference 2.5.2-318). The TI Team was comprised of Dean Ostenaa, Phil Hogan, Roland LaForge, Ross Hartleb, and Scott Lindvall. Dean Ostenaa, followed by Phil Hogan, served as the TI Team Lead.

As noted previously, the TI Team attempted to contact and interact with numerous experts to develop a response to the new information posed with this RAI. The key contact was Prof. Eberli, as discussed above. The TI Team found no proponents for Kula's long, through-going active faults along the eastern margin of Cay Sal Bank, or other significant new seismic sources in the vicinity.

The TI Team evaluated publicly available information, including available seismic data from the region. Figure 12 shows University of Hamburg Cruise M95 line locations, Kula's (Reference 1) interpreted fault locations, Masaferro et al.'s (1999) (FSAR Reference 2.5.1-426) Santaren fold locations, and six GSI line locations for those profiles presented in this response. The GSI lines were shot in 1981 and 1982, and are available on the web at: https://walrus.wr.usgs.gov/NAMSS/ (Reference 5).

The six interpreted lines include, from north to south, BH82-49A_mig, BH81-11_mig, BH81-34_mig, BH81-12B__mig, BH82-62_mig, and BH81-15_mig (Figures 13 through 18). Both migrated and unmigrated versions of the GSI seismic reflection lines are available at the NAMSS (Reference 5) website. All of the GSI lines that were downloaded to support this response are migrated sections, hence the "_mig" (i.e., "migrated") suffix. For traceability, this response retains the line names exactly as they appear in the NAMSS database (Reference 5), including the "_mig" suffix. Kula (Reference 1) and Bergman (2005) (FSAR Reference 2.5.1-906) also include interpretations of some of these GSI lines, but they do not use the "_mig" suffix. Approximately half of the GSI seismic lines used by Bergman (2005) (FSAR Reference 2.5.1-906) were unmigrated paper copies, while the other half were digitized migrated sections. It is not clear which seismic lines in Bergman (2005) (FSAR Reference 2.5.1-906) are migrated and which are unmigrated.

All six lines are presented with a vertical exaggeration of 5:1, with a full 5 second two-way travel time (TWTT) record. The seismic stratigraphy on the 1981/1982 GSI lines was derived from Miocene to Late Quaternary chronostratigraphic data from Ocean Drilling Project (ODP) Well 1006 (Eberli et al., 1997 [FSAR Reference 2.5.1-385]; Shipboard Scientific Party, 1997 [Reference 6]) and Cretaceous to Pleistocene age-correlated reflectors presented in Bergman (2005) (FSAR Reference 2.5.1-906). The interpretations shown on the six GSI lines are generally consistent with and follow the same methodology followed by Bergman (2005) (FSAR Reference 2.5.1-906). Uninterpreted versions of the six GSI lines are presented as an enclosure to this

response (see Enclosure 1). The approximated locations of Kula's faults are shown on each line.

The vertical resolution of the deep-penetration seismic data evaluated by the TI Team is lower than the resolution of the limited-penetration Cruise M95 data interpreted by Kula (Reference 1). Sheriff (1985) (Reference 7) established that the vertical resolution of a seismic dataset is approximately equal to one-quarter of the p-wave velocity of the geologic zone of interest divided by the dominant frequency. Based on a dominant signal frequency of approximately 16 Hz for the GSI data examined for this RAI response, the 2D seismic reflection datasets are estimated to have a vertical resolution of 100 feet (about 30 m). However, Widess (1973) (Reference 8) established that the minimum vertical detection length where a geologic feature will elicit a seismic response but not be fully resolved to be approximately one-eighth of the p-wave velocity of the geologic zone of interest multiplied by the dominant frequency. In the case of the 2D marine seismic data within the Santaren Channel presented herein, constructive interference from reflections from beds as thin as 50 feet (15 m) or faults with offset as little as 50 feet (15 m) should result in enough constructive interference of reflections to build up the sampled amplitude to large enough values to register on the recorded seismic trace. Hence, very small faults and fractures with cumulative vertical separation of less than about 50 to 100 feet (15 to 30 m) may not be clearly imaged, and minor Quaternary displacements or features confined to a stratigraphic interval of less than 100 feet (30 m) may not be detected on these data. However, for seismic source characterization, the marine seismic data provide a robust data set that allows resolution of significant structural features, with vertical separations much less than the vertical separation values of 90 to 150 m (Table 1) reported by Kula (Reference 1).

Figure 13 presents Line BH82-49A_mig, which is located in the Straits of Florida about 40 miles (about 70 km) southeast of the Turkey Point Units 6 & 7 site (Figure 12). Continuous, parallel to slightly sub-parallel, unbroken seismic reflections are apparent across the entire length of the profile. These data provide evidence for no faulting or folding of the area since pre-Cretaceous time, and clearly demonstrate the tectonic stability of the region between the Santaren Channel and Florida.

Figure 14 presents Line BH81-11_mig, which is located in the Straits of Florida at the northern end of the faults mapped by Kula (Reference 1) (Figure 12). On this line, a small fault is mapped in the Miocene section above a small anticline near the margin of a buried carbonate bank. The buried carbonate bank is primarily Cretaceous in age, although final drowning of the carbonate bank did not occur in the northern Santaren Channel until the early Miocene (Bergman, 2005) (FSAR Reference 2.5.1-906). The fault mapped above the anticline is confined to the stratigraphic interval between 3.6 Ma and 23.7 Ma. It does not cut the 23.7 Ma horizon, and may have formed as a result of differential subsidence along the carbonate bank margin. The small anticline near the carbonate bank margin may have formed as the result of Cretaceous salt migration and diapirism, as documented elsewhere in the region (Ball et al., 1985; Echevarria-Rodriguez et al., 1991) (FSAR References 2.5.1-501 and 2.5.1-497). Bergman presents an interpretation of this profile showing maps of several short, non-tectonic, old faults with minor normal offset bounding the edge of the buried carbonate platform along the

basin margin (Bergman, 2005, Figure 6.8) (FSAR Reference 2.5.1-906). None of the faults identified by Bergman (2005) (FSAR Reference 2.5.1-906) are younger than 23.7 Ma. The deepest mapped horizon is interpreted to be pre-Cretaceous in age, and appears unfaulted and unfolded.

Figure 15 presents Line BH81-34_mig, which is located at the northern end of the Santaren Channel and crosses Kula's (Reference 1) Faults B and C near Cruise M95 Line 20 (Figures 3, 10, and 12). Several small faults are mapped on this northeast-trending line. One of the faults is above a small anticline near the approximate location of Kula's Fault C. The other two mapped faults are near the margin of the buried Cretaceous carbonate bank. These two faults may have formed as a result of differential subsidence along the carbonate bank margin, as previously suggested by other workers (Eberli, 2004 [Reference 2]; Bergman, 2005 [FSAR Reference 2.5.1-906]). Bergman presents an interpretation of this profile and maps several short faults with minor normal offset near the edge of the buried carbonate platform along the basin margin (Bergman's (2005) Figure 6.6 [FSAR Reference 2.5.1-906]). The deepest mapped horizon on Figure 15 is interpreted to be pre-Cretaceous in age, and does not exhibit any apparent vertical separation (faulting) within the resolution of the data.

Figure 16 illustrates Line BH81-12B_mig, which crosses the northern margin of Cay Sal Bank and Santaren Channel. This line (Figure 12) crosses Faults B, C, and D of Kula (Reference 1), and coincides with Cruise M95 Line 15. The broad antiformal structure of Cay Sal Bank is clearly imaged on this profile. Cretaceous and older units exhibit a broad anticlinal fold, the axis of which underlies eastern Cay Sal Bank.

Acoustically transparent and in some cases chaotic reflections are visible beneath the seafloor on the steep eastern margin of Cay Sal Bank; these are interpreted by the TI Team to result from mass wasting events along this progradational shelf margin, similar to interpretations by Bergman (2005) (FSAR Reference 2.5.1-906), Kula (Reference 1), and are consistent with Prof. Eberli's interpretations. A seismic reflection of mid-Miocene (12.2 Ma) age appears unfaulted. The deepest mapped horizon is interpreted to be pre-Cretaceous in age, and also appears to be unfaulted. These two seismic horizons show no apparent vertical offset along the eastern margin of Cay Sal Bank where Kula (Reference 1) mapped 3 "deep-rooted" tectonic faults, suggesting that Faults B, C, and D do not exist in this area and may have instead been interpretation artifacts of vertically exaggerated shallow seismic profiles.

Kula's (Reference 1) cross section X-X' (Figures 4 and 12), which depicts >1 km of vertical offset of Cretaceous carbonate bank along several faults splaying off a subhorizontal decollement (detachment) crosses the western portion Line BH81-12B_mig (Figure 16). The mid-Miocene and pre-Cretaceous horizons do not exhibit any vertical separation and are unfaulted at this location. There is no evidence supporting the existence of either a deep detachment or tectonic Faults B, C, and D along this seismic line.

The vertical separation of these faults suggested by Kula (Reference 1) as shown on Table 1 are within the 50 to 100 feet (15 to 30 m) vertical resolution of these seismic data. Minor faulting associated with polygonal faults, acoustic pipes, and

dewatering/fluid escape features likely exist on Line BH81-12B_mig, but have not been mapped.

Figure 17 illustrates interpreted Line BH82-62_mig, which extends from the eastern margin of Cay Sal Bank across the Santaren Channel. This line crosses Faults B, C, and D of Kula (Figure 12). A small listric normal fault of mid-Cretaceous age exhibits minor offset and a rollover geometry along the carbonate bank margin. Many continuous, unbroken seismic reflections extending from the seafloor back to pre-Miocene age document no faults are apparent on this seismic line.

Figure 18 presents interpreted Line BH81-15_mig, which is located between Cay Sal Bank and the Santaren anticline. This line crosses Faults C and D of Kula (Figure 12). Many continuous, unfaulted seismic reflections extending from the mid-Miocene to pre-Cretaceous time onlap the buried Cretaceous age carbonate bank. Mid- to late-Miocene age strata onlap and overlap the buried carbonate bank margin. The buried carbonate margin has remained tectonically inactive since the early- to mid-Miocene; minor bedding dips prior to that time result mainly from depositional slopes and differential compaction (Figure 9 of Masaferro et al., 2002) (FSAR Reference 2.5.1-479). The observed relationships clearly document no tectonic faults on this seismic line, and no connection between the Santaren anticline tectonic structures mapped by Masaferro to the south with any minor structures to the north.

The publicly available seismic lines do not support Quaternary active, long tectonic faults along the eastern margin of Cay Sal Bank or in the Straits of Florida to the north. Continuous, unfaulted seismic reflections across the Santaren Channel and along the eastern flank of Cay Sal Bank are clearly apparent on seismic profiles that cross the fault locations mapped by Kula (Reference 1). The most dominant feature apparent in the seismic profiles is the buttress unconformity and onlap of the sedimentary section in the Santaren Channel onto the buried Cretaceous carbonate reef beneath Cay Sal Bank. The seismic profiles show evidence for the absence of through-going fault structures as interpreted by Kula (Reference 1).

As previously discussed, Prof. Eberli concurs with the interpretation that there are no long, tectonic faults in this area, and suggests only a single, small, low slip rate fault northeast of Cay Sal Bank that coincides with the north-northeast-trending Cay Sal anticline. The TI Team concurs with the observation that there is a fault with seafloor expression in this area, but notes that there are several non-seismogenic mechanisms that may plausibly result in this structural expression. The observed features may be the result of salt migration and diapirism above an unfaulted pre-Cretaceous seismic reflection apparent on GSI Lines BH81-11_mig, BH81-34_mig, and BH81-12B_mig (Figures 14, 15, and 16), with fluid and gas migration along the fault, and potential fluid expulsion at the seafloor.

Based on evaluations of the data, the TI Team concludes the following:

- Most of Kula's (Reference 1) neotectonic interpretations are not technically defensible, as they are unsupported and contradicted by data. Kula's fault interpretations are generally not technically defensible, and the geomorphic interpretations of the MTC landslide headscarps visible on MBES bathymetry

data as faults are flawed and not defensible. Although not highlighted in the published abstract (Eberli et al., 2015) (Reference 4), the same feature was presented and discussed by Prof. Eberli in his oral presentation at AAPG as an example of an old, modified MTC headscarp along the Cay Sal Bank.

- There is some evidence for possible Quaternary growth of Cay Sal anticline, with minor faulting and fluid migration along the axis of the fold. The orientation of the fold (N20°E strike) is not consistent with the roughly N15°E convergence direction between the North American and Caribbean Plates (Demets et al., 2000, 2007; Mann, 2006) (FSAR References 2.5.1-502, 2.5.1-635, and 2.5.1-636) as it is almost parallel to the direction of plate convergence. However, Kula (Reference 1) and Prof. Eberli's hypothesis that the Cay Sal anticline may represent an oblique wrench structure is feasible and falls within the range of technically defensible interpretations. Prof. Eberli does not consider these local faults and fold as seismogenic, and the observed features alternatively may be the result of salt diapirism, non-tectonic faulting, and fluid expulsion at the seafloor.
- Polygonal faulting, gas migration and expulsion, and fluid migration piping are common structures throughout the area, as suggested by Bergman (2005) (FSAR Reference 2.5.1-906), Kula (Reference 1), and TI Team discussions with Prof. Eberli. . Basin-bounding normal faults are also common along carbonate bank-basin margins, and are driven by gravitational forces, as well as differential subsidence and compaction.
- The elements of Kula's interpretations that remain technically defensible or possible (those supported by Prof. Eberli, permissible by other data, and consistent with broadly based principles of geologic interpretation) include short, localized folds; a short, shallow fault zone (parts of Faults A and B) along the axis of the Cay Sal anticline; and polygonal faulting, fluid migration, and seafloor expulsion features. There are no data supporting through-going structures along the eastern margin of Cay Sal Bank capable of producing large crustal earthquakes. In fact, GSI seismic reflection lines provide direct evidence for the absence of deep-seated, through-going faults, within the limit of resolution of the seismic data (Figures 13 through 18).
- Kula's (Reference 1) suggestion that the Cay Sal Bank features are part of a presently active Cuba fold and thrust belt, and they exhibit significant young deformation of the seafloor, is not technically defensible. This interpretation requires observable deformation in the underlying strata reflecting the cumulative fault displacement that originated during Cuba subduction. The regional tectonic setting, as related to the identification of potential seismic source zones has previously been described in the COLA, and remains largely unchanged. This will be further addressed in Part (b) of this response.

***Response to Part (b): Several investigations, published by authors such as Eberli, Massafero, Bergman and Kula, make a strong case for extending the Cuba Fold and Thrust belt beneath Cay Sal Bank and as far as the northwestern end of the Santaren Channel. Even though there is no seismicity in the area beneath Cay Sal Bank and the Santaren Channel, distinct seafloor scarps argue for very recent and significant displacement. Provide an analysis of how this northward extension of the Cuban Fold and Thrust belt terrane with associated Quaternary fault displacement and seafloor scarps on at least 2 faults impacts the site seismic hazard assessment and seismotectonic boundaries.***

This part of the response is subdivided into the following four sections:

- Summary of the Cuba fold and thrust belt interpretations and why some authors have proposed its northward extension to include the Cay Sal Bank and how this interpretation is more strongly supported in the southern Santaren Channel in the vicinity of the Santaren anticline as opposed to the northern Santaren Channel.
- Discussion of possible implications of an expanded Cuba fold and thrust belt on how the Cuba areal source zone is represented in the seismic source model.
- Evaluation of the structures identified by Kula (Reference 1), Bergman (2005) (FSAR Reference 2.5.1-906), and Masaferro et al. (1999; 2002) (FSAR References 2.5.1-426 and 2.5.1-479) and whether they could represent viable seismic sources.
- Presentation of a sensitivity analysis that demonstrates minimal impact on site hazard for an assumed reverse fault coring the Santaren anticline.

The possibility of an expanded Cuba fold and thrust belt is assessed with respect to the Cuba areal source zone and expected impacts on seismic hazard at the site. This assessment indicates that alternative characterizations of the Cuba fold and thrust belt are not significant to the seismic hazard at the Turkey Point Units 6 & 7 site (see discussion in FSAR Subsection 2.5.2.4.4.3.4.2). The existing boundaries of regional seismic source zones such as the Cuban areal source zone which includes much of the Cuba fold and thrust belt along the northern coast of Cuba are based on multiple lines of evidence including geologic structure, evidence of Quaternary deformation, and historical seismicity. While some investigators extend the Cuba fold and thrust belt northeast to include Cay Sal Bank and the Santaren Channel, the analyses provided in this response indicate that there is insufficient evidence from Quaternary faulting and historical seismicity to support a revision to the Cuban areal source zone for the purposes of seismic hazard calculation.

**Summary of Cuba Fold and Thrust Belt Interpretations**

Kula (Reference 1) indicates that there are two general views on the extent of the Cuba fold and thrust belt. One view is that the arcuate belt is largely restricted to the island of Cuba (Iturralde-Vinent, 1994 [FSAR Reference 2.5.1-440]; Saura et al., 2008 [FSAR Reference 2.5.1-485]) and the other is a broader interpretation that would extend the margin eastward to the southern Santaren Channel to include the Santaren anticline (Ball et al., 1985; Masaferro, 1997) (FSAR References 2.5.1-501 and 2.5.1-477]. In the regional literature, there does not appear to be a strict definition of the Cuba fold and thrust belt, in terms of style, intensity, and magnitude of deformation. Very few researchers (Schenk, 2008, 2010 [References 9 and 10]; Pindell, 2013 [Reference 11]) have delineated a margin or limit of Cuba deformation on maps. While the literature contains several descriptions of the Cuba fold and thrust belt and Cuba foreland basin, most descriptions concentrate on field relationships exposed on the island of Cuba (e.g., Iturralde-Vinent et al., 2008) (FSAR Reference 2.5.1-786).

Large regional maps such as Figure 19 illustrate the evolution of the Caribbean crust and call out a "Cuban foredeep", but no discussion is provided by Pindell (2013) (Reference 11) on this region. As shown in Figure 19, the "Cuban foredeep" includes only the southern part of Cay Sal Bank and Santaren Channel.

Perhaps one of the more consistent characterizations that provides mapped boundaries is from the U.S. Geological Survey's assessment of oil reserves in the Cuba region (Schenk, 2008; 2010) (References 9 and 10). In this assessment, a Total Petroleum System (TPS) is defined to represent the integration of the tectonic, sedimentary, and thermal histories of an area. These studies define a Jurassic-Cretaceous "North Cuba Basin" TPS of Jurassic-Cretaceous age, shown as a yellow polygon in Figure 20 (Schenk, 2008; 2010) (References 9 and 10). This North Cuba Basin TPS is further subdivided into the North Cuba Fold and Thrust Belt, North Cuba Foreland Basin, and North Cuba Platform Margin assessment units (AU) in Figures 20 and 21, based on differences in geologic structure and reservoir types. Schenk (2008) (Reference 9) describes the North Cuba Fold and Thrust Belt AU, which encompasses all reservoirs within potential structural traps of the fold and thrust belt, as mainly onshore, but includes some offshore areas (Figure 20). The North Cuba Fold and Thrust Belt AU is dominated by structural traps such as folds, fault-related folds, faulted anticlines, and duplex structures and seismic data generally illustrate a stack of thrust sheets forming the thrust belt. (Schenk, 2008; 2010) (References 9 and 10). Schenk (2008) (Reference 9) notes that the North Cuba Fold and Thrust Belt AU typically is characterized by a greater degree of tectonic deformation than the more distal North Cuba Foreland Basin AU and the North Cuba Platform Margin AU (Figure 21).

Kula (Reference 1) proposes a modification to Schenk's (2008; 2010) (References 9 and 10) boundary of the Cuba Fold and Thrust Belt by incorporating the Cay Sal Bank in the Cuba fold and thrust belt (Figure 22). In the Kula modification of this boundary, the Cuba Fold and Thrust Belt and North Cuba Platform Margin of Schenk (2010) (Reference 10) remain undifferentiated in the Cay Sal Bank area (Figure 22). Kula's modification, included here as Figure 22, leaves unclear the question of whether Cay Sal Bank should be considered part of the fold and thrust belt or platform margin in

Schenk's nomenclature or the Cuban foredeep of Pindell (2013) (Reference 11) (Figure 19).

Deformation in the southern Santaren Channel was first described in a study by Ball et al. (1985, p. 1281) (FSAR Reference 2.5.1-501) that proposed the northern edge of the Bahamian Cuban collision zone was defined by "a 10-km broad, low relief anticline." This anticline is the same Santaren anticline that was the focus of later studies by Masaferro (1997) and Masaferro et al. (1999; 2002) (FSAR References 2.5.1-477, 2.5.1-426, and 2.5.1-479) in which they better quantified the fold geometry, growth strata, uplift history, and timing of deformation. These later studies suggest that fold growth may persist to the present.

Masaferro et al. (1999) (FSAR Reference 2.5.1-426) notes that Ball et al. (1985) (FSAR Reference 2.5.1-501) characterized the Santaren anticline as a fault-related anticline that formed during the Late Cretaceous-Early Cenozoic compression associated with the Cuban orogeny. The Santaren anticline is interpreted by Masaferro (1997) and Masaferro et al. (1999; 2002) (FSAR References 2.5.1-477, 2.5.1-426, and 2.5.1-479) as a detachment fold involving limb rotation and similarly related to the northeastern extent of contractional deformation within the Bahamian foreland of the Cuba fold and thrust belt. The fold location and 70 km extent depicted in Figure 1c of Masaferro et al. (1999) (FSAR Reference 2.5.1-426) is based, in part, on earlier data of Ball et al. (1985) (FSAR Reference 2.5.1-501) and a similar type of anticline shown by Echevarria-Rodriquez et al. (1991) (FSAR Reference 2.5.1-497) that is interpreted to be an extension of the Santaren anticline.

According to Masaferro and Eberli (1999) (FSAR Reference 2.5.1-294), the study of the seismic stratigraphy in the southern Great Bahama Bank has distinguished different episodes of tectonic deformation that have impacted the development of the carbonate bank, including the Cuba collision. Internal architecture of the carbonate bank is interpreted as resulting primarily from the interaction between tectonic destructive processes and platform recovery through sedimentation. Seismic data suggest the southern Great Bahama Bank experienced three segmentation events. The first two events were related to Jurassic rifting and probable mid-Cretaceous re-activation of west-northwest-striking faults. The third and final segmentation event during the Late Cretaceous to middle Tertiary Cuba collision is interpreted to be transtensional and synsedimentary and characterized by oblique faults with reverse and sinistral strike-slip components that disrupted the carbonate bank and formed symmetric intraplatform depressions (Masaferro and Eberli, 1999) (FSAR Reference 2.5.1-294). While reverse faulting or folding have not been observed northeast of the Santaren anticline, Masaferro and Eberli (1999) (FSAR Reference 2.5.1-294) interpret far-field effects of the Cuba subduction in the formation of the southern Great Bahama Bank.

The model originally proposed by Masaferro (1997) (FSAR Reference 2.5.1-477) to explain the southern Bahamas structural and sedimentary evolution as it relates to the Cuba-Bahama collision was expanded upon by Bergman (2005) (FSAR Reference 2.5.1-906). In a PhD dissertation, Bergman evaluated the progressive northward drowning of carbonate banks in Cretaceous through Miocene time attributed to

forebulge migration and interpreted folds and reverse faults from seismic profiles to the north of the Santaren anticline (Figures 23 and 24).

Bergman (2005, p. 172) (FSAR Reference 2.5.1-906) describes the Santaren anticline as a detachment growth fold that "is underlain by a detachment horizon over which reflections are folded." On GSI Line BH82-59_mig (Figure 23), Bergman interprets two imbricated thrust blocks located directly northwest of the Santaren anticline as mapped by Masaferro et al. (1999) (FSAR Reference 2.5.1-426).

At the northern margin of Cay Sal Bank, Bergman (2005) (FSAR Reference 2.5.1-906) interprets steep normal faults bounding the drowned carbonate bank margins (Figures 25 and 26). These two figures illustrate that the reverse faults interpreted in Figure 23 do not persist up the entire eastern margin of Cal Say Bank. Bergman did note a large, broad fold underlying the Cay Sal Bank region (Figure 25) and this structure is shown with a northeast-trending axis on the map in Figure 24.

Bergman (2005) (FSAR Reference 2.5.1-906) concludes that loading of the North American plate migrated northward away from the collision zone and caused differential subsidence along the margins of the paleo-reentrant of the Santaren Channel. Bergman also concludes that thrust faulting and other compressional features associated with the late stage Cuba collision propagated as far north as the central Santaren Channel, which is farther north than previously estimated. These compressional features of the Cuba-Bahama thrust belt were long-lived and one structure (thrust fault block B on Figure 23) appears to be active into the late Miocene and possibly Pliocene (Bergman, 2005) (FSAR Reference 2.5.1-906).

More recently, Kula (Reference 1) interprets a series of active and inactive faults bounding the eastern margin of Cay Sal Bank and two anticlines (Cay Sal and SantaMiocene) as evidence that the Cuba fold and thrust belt extends north of Cay Sal Bank (Figure 8). Kula argues that these structures are parallel to the Cuba fold and thrust belt. However, they clearly are not subparallel to the arcuate northern coast of Cuba. The Santaren anticline is subparallel to the Cuba fold and thrust belt and is consistent with northeast directed shortening. However, the Kula structures at the northern Cay Sal Bank (faults and Cay Sal anticline) are oriented north-northeast and are nearly orthogonal to the Cuba fold and thrust belt. As described in Part (a) of this response, many of the Kula (Reference 1) interpretations are not supported by the data.

**Implications of an expanded Cuba fold and thrust belt on Seismic Source Model**

The Cuba fold and thrust belt refers to the belt of fold and thrust deformation associated with the Cuba collision. The nature of deformation within a fold and thrust belt in terms of style, intensity, fault density, and earthquake potential vary considerably with distance from the subduction zone. Contractional features in the southern Santaren Channel (e.g., Santaren anticline) (Figures 12, 24, and 27) suggest the Cuba fold and thrust belt may have extended north of the island of Cuba and beyond what was defined as the Cuba areal source zone (Figure 28). While tectonic terranes and areas of similar geologic histories can assist in subdividing the crust into regional seismic source zones, the criteria for defining areal source zones are primarily the size, rate, and

characteristics of future earthquake production. Areal source zones need not be defined solely based on tectonic or geologic boundaries and nomenclature such as "Cuban foredeep" (Figure 19) or a new interpretation of the Cuba fold and thrust belt to the northeast of Cuba. Areal seismic sources, first and foremost, should be defined based on their earthquake potential.

The Cuba areal source zone (FSAR Figure 2.5.2-217) was defined by incorporating the majority of seismicity, faults, and the highly deformed region surrounding Cuba. The Cuba areal source zone was modeled assuming a uniform seismicity rate. Apparent spatial variations in seismicity rates within the Cuba areal source zone were evaluated in a sensitivity study that subdivided Cuba into smaller subzones. The decision to model Cuba as a single areal source zone or as multiple subzones has negligible impact on seismic hazard at the Turkey Point Units 6 & 7 site (see discussion in FSAR Subsection 2.5.2.4.4.3.4.2). However, there is a significant difference in seismicity rates between Cuba and the region to the north. When defining areal source zones with uniform seismicity rate and a common completeness period, areas with relatively similar seismicity rates are segregated from areas displaying very different rates of seismicity. The Cuba areal source zone was defined to capture the higher rate of seismicity in Cuba from the surrounding offshore regions of the Site Region covering the Bahamas and Straits of Florida, which were included in separate supplemental background zones, characterized by very low rates of seismicity. It would be inappropriate to expand the Cuba areal source zone into the Santaren Channel or beyond to capture the northwest limit of minor contractional deformation. This is especially true since the regions north of the Cuba areal source zone, as currently defined, exhibit a markedly different rate of seismicity. An expansion of the Cuba areal source zone to match a poorly defined margin of the Cuba fold and thrust belt would not be appropriate because it would reduce the Cuba background seismicity rate (increasing area without increasing number of earthquakes) and artificially push the Cuban seismicity rate into the Cay Sal Bank and Santaren Channel region where that rate is not observed.

Delineation of the Cuba areal source zone and the computation of recurrence parameters therein were based on conditions of a moderate, relatively spatially uniform level of seismicity throughout the island, and the availability of completeness period estimates for the island from Garcia et al. (2008) (FSAR Reference 2.5.2-255). The region north of the Cuba areal source zone, in contrast, is marked by extremely low seismicity. Figures 27 and 28 show that there are only two earthquakes within the area proposed to be added if Kula (Reference 1) meant to include the North Cuba Platform Margin and North Cuba Foreland Basin of Schenk (2008; 2010) (References 9 and 10), and only one earthquake if just the Cay Sal Bank were to be included. For either case the density of seismicity in the added regions is clearly less than in the existing Cuba areal source zone.

Completeness periods for the proposed extended regions north of the Cuba areal source zone, being an unpopulated oceanic environment and far from Cuban seismograph stations, are likely to be very different than on the island of Cuba. Extending the zone northward would therefore violate the assumption of uniform levels

of seismicity that supported delineating the original Cuba areal source zone and the completeness periods required for computing its recurrence parameters.

Kula (Reference 1) cites the January 9, 2014 $M_W$ 5.0 earthquake and aftershocks that occurred near Coralillo, Cuba as supporting evidence that a northward extension of the Cuba fold and thrust belt is warranted. A National Earthquake Information Center (NEIC) search (NEIC, 2015) (Reference 14) within the green box shown in Figure 27 from January 1, 2013 through June 25, 2015 resulted in the identification of six earthquakes as shown in the figure. The location of the $M_W$ 5.0 mainshock in its relation to the Cuba areal source zone is shown in Figure 28. The 2014 earthquakes lie within the Cuba areal source zone and thus do not provide a rationale for extending it northward.

An important consideration is that the hazard from the Cuba areal source zone is based primarily on seismicity. While the geologic data may suggest that Cay Sal Bank contains tectonic structures, the seismicity data indicate that the Cay Sal Bank presents an area of much lower seismicity rate and hazard than the Cuba areal source zone. This implies that if seismogenic structures north of the Cuba areal source zone are to be added to the seismic source model, they should be in the form of faults with discrete geometry that permits a credible estimate of Mmax and slip rates.

**Evaluation of Potential Seismic Sources**

Several faults and folds have been mapped and interpreted from the southern Santaren Channel northward along the eastern margin of Cay Sal Bank (Ball et al., 1985 [FSAR Reference 2.5.1-501]; Masaferro, 1997 [FSAR Reference 2.5.1-477]; Bergman, 2005 [FSAR Reference 2.5.1-906]; and Kula, 2014 [Reference 1]). The Santaren anticline represents the most-well-studied of these structures (Masaferro et al., 1999; 2002) (FSAR References 2.5.1-426 and 2.5.1-479). While a fault has yet to be imaged in the core of the relatively symmetrical Santaren anticline (Figures 29 and 30), this structure represents a candidate for a potential seismic source for two reasons: (1) the fold deformation appears to be Quaternary in age (e.g., Jo, 2013 [Reference 12]; Jo et al., 2015 [Reference 13]); and (2) a fold uplift rate has been determined for this structure (Masaferro et al., 2002) (FSAR Reference 2.5.1-479).

The Santaren anticline has been active at least since Mid-Eocene time to possibly Pliocene/present day (Masaferro et al., 1999) (FSAR Reference 2.5.1-426). The rate of deformation has been extremely low and the analysis of growth strata, sedimentation and fold uplift rates have documented the episodic nature of the growth of the Santaren anticline (Masaferro et al., 2002) (FSAR Reference 2.5.1-479). Masaferro et al. (1999) (FSAR Reference 2.5.1-479) indicate that the Santaren anticline is not an isolated structure and that a second anticline located south of the Santaren anticline has also folded much of the same sedimentary section (Figure 29). New high-resolution seismic data and subbottom profiles (Figure 30) illustrate Quaternary growth strata and steeply dipping secondary faults associated with the Santaren anticline, further suggesting ongoing deformation of the anticline (Jo et al., 2015) (Reference 13). The faults and folds interpreted by Bergman (2005) (FSAR Reference 2.5.1-906) to the north do not

represent seismic sources since none of these features were interpreted to be younger than Pliocene in age.

Kula (Reference 1) interprets Quaternary features along the northeastern margin on Cay Sal Bank, but as discussed in Part (a) of this response, many of these interpretations are not considered technically defensible. Seafloor breaks (Figures 6 through 8) interpreted as fault scarps by Kula (Reference 1) in Profile 24 are reinterpreted by Prof. Eberli and the TI Team as the headscarp of an MTC. Subsurface reflections are continuous and unbroken beneath the seafloor break, indicating the absence of a fault at that location (Figure 11).

There is one feature mapped by Kula (Reference 1) that appears to be a fault that extends upward to the seafloor along the Cay Sal anticline axis near the eastern edge of the buried carbonate bank margin. This feature is shown in Figures 3 and 10 (Line 20) as a high-angle zone of small displacement faults that extends to the seafloor and is coincident with a seafloor break. Prof. Eberli interprets this as a young fault; however, he acknowledges that compaction and subsidence along the buried platform margin accompanied by fluid migration could be causing the apparent disruption of subsurface seismic reflections and the seafloor. There is little apparent vertical separation of the Plio-Pleistocene horizon mapped by Kula on this seismic profile. If this fault is tectonic and capable of generating earthquakes, its dimensions, and therefore earthquake magnitudes, would be limited. Seismic reflection profiles both north and south of Line 20 (from Kula) demonstrate continuous, unfaulted pre-Cretaceous seismic reflections and the absence of faulting at depth. Minor offsets and faulting are apparent high in the section (above the 23.7 Ma horizon) in GSI Lines BH81-11_mig (Figure 14) and BH81-34_mig (Figure 15), but this faulting does not appear to offset deeper seismic reflections.

As described in NUREG/CR-5503 (1999) (Reference 15), faults that penetrate less than 5 km depth may reasonably be considered non-seismogenic features. Within the 15 to 30 m vertical resolution of the deep GSI seismic data evaluated in this response and by Bergman (2005) (FSAR Reference 2.5.1-906), minor faults along the axis of the Cay Sal anticline do not penetrate below the top of the Miocene, which is less than 1 km below the seafloor (Figures 14, 15, and 25). As noted in Part (a) of this response, Prof. Eberli does not consider any faults mapped by Kula (Reference 1) as seismogenic because they are very short and discontinuous. Consequently, the TI Team favors a non-tectonic, non-seismogenic nature of the feature imaged in Kula's Line 20 given the numerous non-tectonic, shallow faults in the area and the absence of apparent vertical separation of the top of the Miocene and pre-Cretaceous reflections at depth.

**Santaren Anticline Fault Source Sensitivity Analysis**

A sensitivity analysis was conducted to assess the sensitivity of the Probabilistic Seismic Hazards Alalysis (PSHA) results in the FSAR to a Santaren anticline fault source. Masaferro et al. (1999) (Reference 2.5.1-426) interpret the Santaren anticline in the southern Santaren Channel as a detachment fold with possible Quaternary activity. For the purpose of this sensitivity analysis, it is conservatively assumed that the

anticline is cored by a seismogenic fault. The results of the sensitivity analysis consist of quantification of the increase in hazard and ground motion amplitude at annual frequencies of exceedance (AFEs) of $10^{-4}$ and $10^{-5}$, for frequencies of 1 Hz and 10 Hz. The selected AFEs were chosen because they control the ground motion response spectrum (GMRS) (see discussion in FSAR Subsection 2.5.2.6). The selected frequencies were chosen because they represent the low and high frequency portions of the GMRS.

Figure 31 shows the location of the modeled Santaren anticline fault source. The Santaren anticline fault source is assumed to follow the northernmost surface trace of the Santaren anticline, as depicted in Masaferro et al. (1999; their Figure 1c) (FSAR Reference 2.5.1-426).

*Hicacos Fault Source as Proxy for Santaren Anticline Fault Source*

As described in FSAR Subsection 2.5.2.4.4.3.4.2.2, 15 faults in Cuba were characterized for a PSHA sensitivity analysis. Hazard curves were computed for the faults shown in Figure 31. The strategy for this analysis was to identify one of the Cuba faults at a similar distance as the Santaren Anticline fault source to the site, and scale its hazard curves by the ratio of the two slip rates.

Although the Hicacos fault source is 26.9 km (43.3 miles) closer to the site than the Santaren anticline fault source, ruptures on each fault as modeled in the PSHA are distributed uniformly on the fault plane. Given an average magnitude of $M_w$ 7.15 and the Wells and Coppersmith (1994) (FSAR Reference 2.5.1-662) magnitude to fault length relation ("all" fault types), the average rupture distance to the site for each fault can be calculated. Comparing these distances shows that the average rupture distance to the site for the Hicacos fault source is 11.4 km (7.1 miles) shorter than the average distance to the Santaren anticline fault source. This shows that using the Hicacos fault source as a proxy for the Santaren anticline fault source provides a comparable and slightly conservative assessment.

FSAR Table 2.5.2-236 indicates a mean slip rate of 0.037 mm/yr for the Hicacos fault source. For the Santaren anticline fault source, the uplift rate of 0.05 mm/yr from Masaferro et al. (2002) (FSAR Reference 2.5.1-479) is used. Masaferro et al. (1999; 2002) (FSAR References 2.5.1-426 and 2.5.1-479) show the Santaren anticline to be nearly symmetric in map view. As progressively shallower dip angles for the hypothetical fault underlying the anticline are assumed, these would produce a progressively more asymmetric appearance of the anticline. Because the slip rate on the fault can be approximated by the uplift rate divided by the sine of the fault dip angle, progressively shallower dip angles produce increasingly higher slip rates on the fault. Given the nearly symmetric appearance of the anticline, an angle of 45 degrees is assumed as a conservative estimate of the dip of the hypothetical fault underlying the anticline. This results in a slip rate of 0.071 mm/yr for the Santaren anticline fault source.

Hazard Curve Development for the Santaren Anticline Fault Source

Dividing 0.037 by 0.071 provides a scale factor of 1.92. The Hicacos fault source hazard AFE, which is portrayed as the y-axis of the hazard curves, is then multiplied by this factor, and added to FSAR total hazard curves from FSAR Table 2.5.2-223.

Comparison to FSAR Total Hazard Curves

Hazard curves for the Santaren anticline fault source, FSAR total hazard, and total hazard plus the Santaren anticline fault source are shown for frequencies of 1 Hz and 10 Hz in Figures 32 and 33. The increase in the FSAR total hazard due to the addition of the Santaren anticline fault source is very small and barely discernible in these plots.

Because the GMRS relies on hazard curve results at AFEs of $10^{-4}$ and $10^{-5}$, the percent hazard increase (y-axis of the hazard curves) caused by addition of the Santaren anticline fault source is computed. The increase in the ground motions in g, and the percent increase in ground motion (x-axis of the hazard curves) at these AFE levels are also computed.

Table 2 shows the new AFE levels at the original FSAR total amplitude values, with the percent increase. These range from 1.4% to 8.8%.

Table 3 shows that ground motion amplitudes at AFEs of $10^{-4}$ and $10^{-5}$ were found to increase by 0.8% to 3.5%, which indicates increases in ground motion amplitudes from 0.0006 to 0.003 g.

Conclusions

The sensitivity of the FSAR PSHA hazard curves for 1 Hz and 10 Hz to a Santaren anticline seismic source was assessed by using the Hicacos fault source in Cuba as a proxy for magnitude and distance, and scaling the Hicacos hazard curves by the Santaren:Hicacos slip rate ratio. Ground motion amplitudes at AFEs of $10^{-4}$ and $10^{-5}$ were found to increase by 0.8% to 3.5%, with increases in ground motion amplitudes ranging from approximately 0.0006 to 0.003 g for AFEs of $10^{-4}$ and $10^{-5}$.

**Response to Part (c):** ***Provide appropriate illustrations and maps to support your analyses and discussions. Update any RAI responses and associated COLA revisions that pertain to the Santaren Anticline; the Cuban Fold and thrust belt; boundaries of the Cuba Areal source term, and sensitivity analysis for the Cuban source term. Include interpretation of Santaren Anticline based on Bergman, 2005.***

Illustrations and maps are presented in Parts (a) and (b) of this response. The Part (b) response also includes a description of the Santaren anticline by Bergman (2005) (FSAR Reference 2.5.1-906).

This RAI response provides additional information and does not require any revisions to previous RAI responses. The COLA will be revised to include updated descriptions of: (1) hypothesized tectonic structures in the Santaren Channel; (2) northern extent of the

Cuba fold and thrust belt; and (3) a hazard sensitivity analysis for a hypothetical fault source associated with the Santaren anticline.

**Table 1.** Fault descriptions from Kula (p. 88-89) (Reference 1).

| Fault | Style | Length | Vertical Separation | Seafloor Break | Quaternary Active |
|---|---|---|---|---|---|
| A | Wrench | 41 km | 150 m | Yes | Yes |
| B | Wrench | 115 km | 120 m | Yes | Yes |
| C | Thrust | 180 km | 120 m | No | No |
| D | Thrust | 160 km | 90 m | No | No |

**Table 2.** Summary of Rock Hazard Sensitivity to Santaren Anticline Fault Source: Comparison of MAFEs at FSAR Amplitudes

| | **FSAR** | | **FSAR + Santaren anticline fault source** | |
|---|---|---|---|---|
| | **$10^{-4}$ mean annual frequency of exceedance** | | | |
| **Freq** | *MAFE* | *Amp. (g)* | *MAFE* | *MAFE % Diff* |
| **1 Hz** | 1.00E-04 | 0.0343 | 1.0605E-04 | 6.05% |
| **10 Hz** | 1.00E-04 | 0.0822 | 1.0726E-04 | 7.26% |
| | **$10^{-5}$ mean annual frequency of exceedance** | | | |
| **Freq** | *MAFE* | *Amp. (g)* | *MAFE* | *MAFE % Diff* |
| **1 Hz** | 1.00E-05 | 0.0663 | 1.0880E-05 | 8.80% |
| **10 Hz** | 1.00E-05 | 0.278 | 1.0142E-05 | 1.42% |

**Table 3.** Summary of Rock Motion Sensitivity to Santaren Anticline Fault Source: Ground Motion Amplitudes in Comparison to FSAR Ground Motion Amplitudes

| | **FSAR** | **FSAR + Santaren anticline fault source** | | |
|---|---|---|---|---|
| | **Rock motions (g) at $10^{-4}$ mean annual frequency of exceedance** | | | |
| **Freq** | *Amp. (g)* | *Amp. (g)* | *Amp. Diff* | *Amp. % Diff* |
| **1 Hz** | 0.0343 | 0.034899 | 0.000599 | 1.75% |
| **10 Hz** | 0.0822 | 0.085058 | 0.002858 | 3.48% |
| | **Rock motions (g) at $10^{-5}$ mean annual frequency of exceedance** | | | |
| **Freq** | *Amp. (g)* | *Amp. (g)* | *Amp. Diff* | *Amp. % Diff* |
| **1 Hz** | 0.0663 | 0.067900 | 0.001600 | 2.41% |
| **10 Hz** | 0.278 | 0.280139 | 0.002139 | 0.77% |

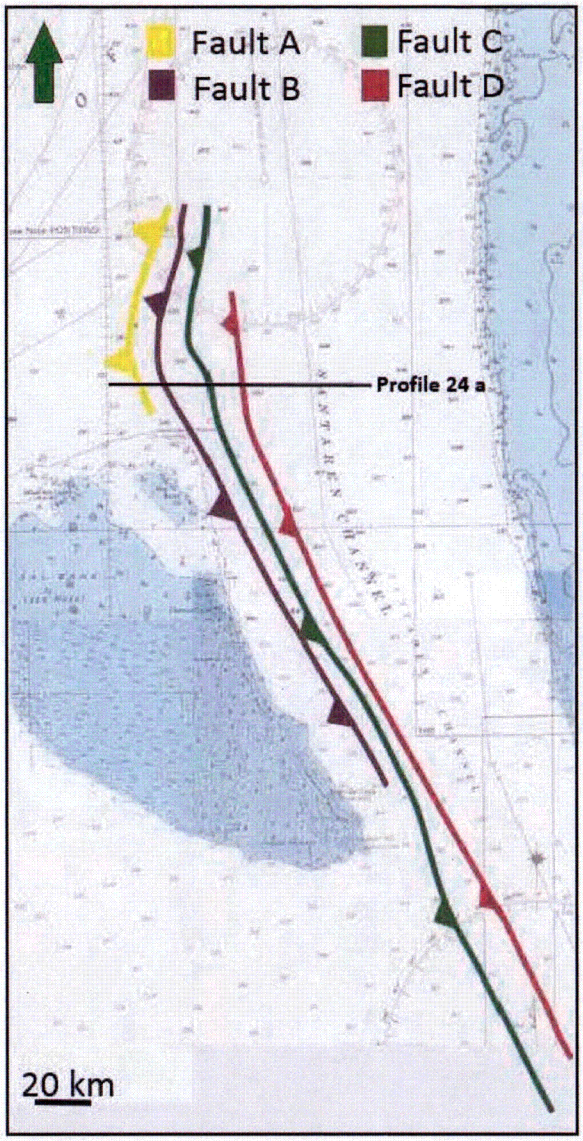


**Figure 1.** Kula's (Reference 1) Figure 4-6 location map of deep-rooted faults mapped showing, from west to east, Faults A (yellow), B (blue), C (Green), and D (Purple). Kula only considered Faults A and B to be active

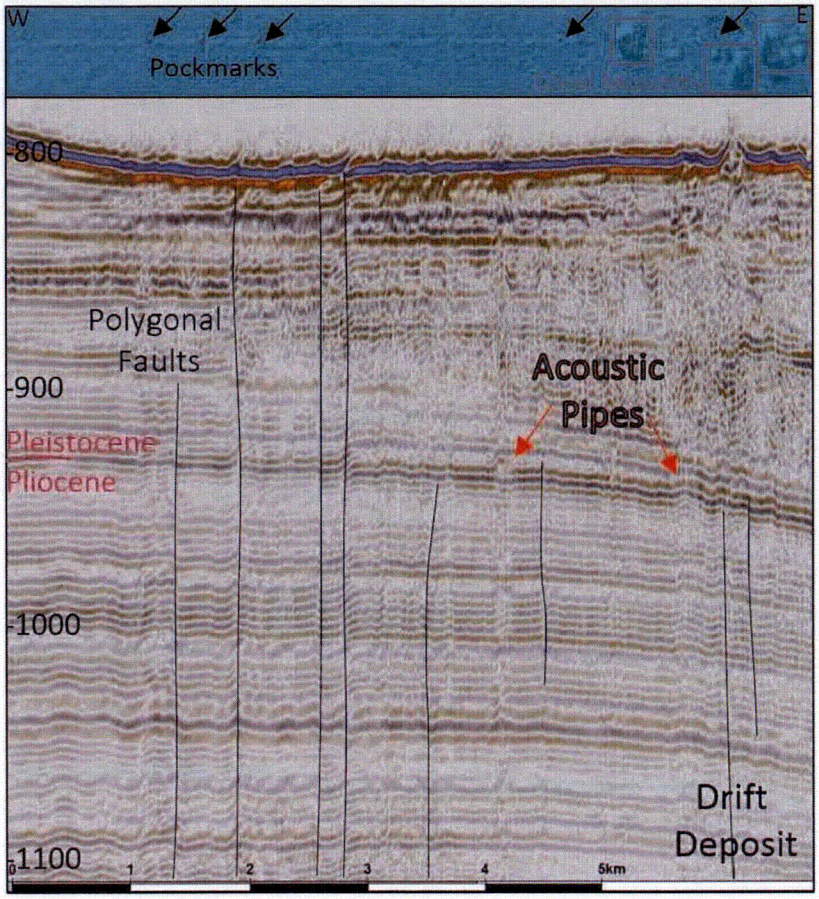


**Figure 2.** Kula's (Reference 1) Figure 4-17 showing Profile 27 illustrating fluid escape features such as polygonal faults and acoustic pipes at and below the seafloor. Profile location shown on Figure 12.

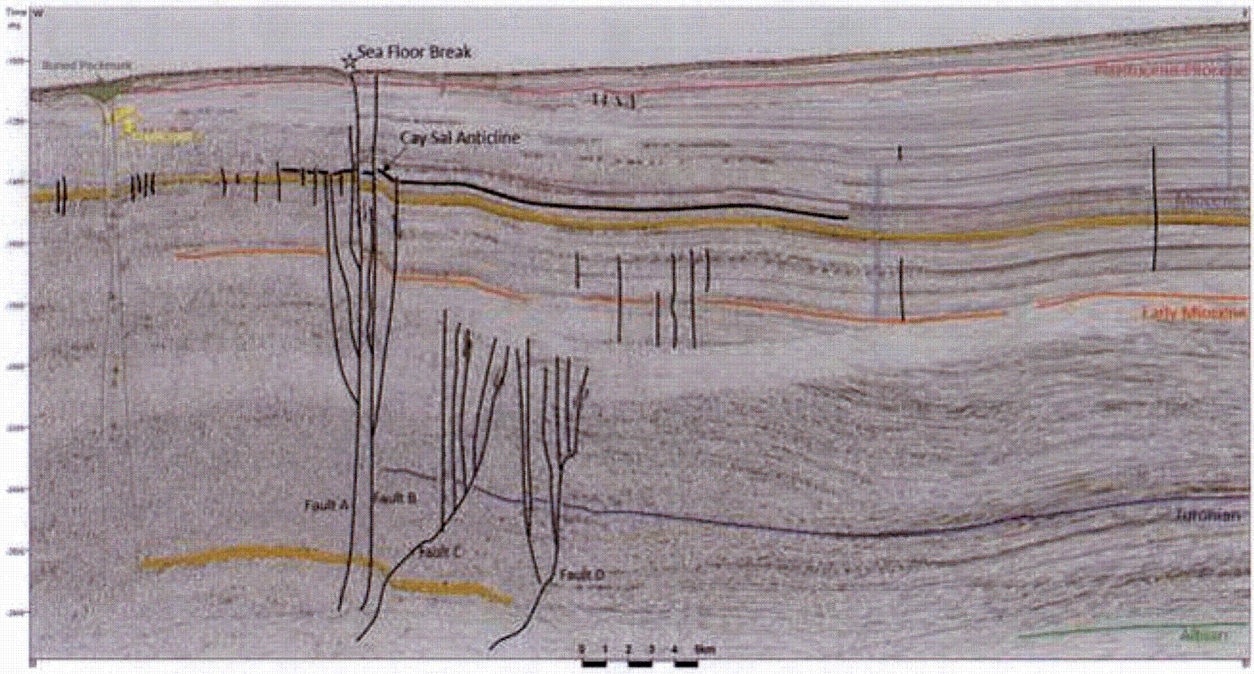


**Figure 3.** Kula's (Reference 1) Figure 5-3 showing interpreted Profile 20, mapped horizons, and Faults A through D. Note seafloor break above Fault A and fluid escape acoustic pipe near western end of profile, and the Cay Sal anticline between Faults A and B. Profile location shown on Figure 12.

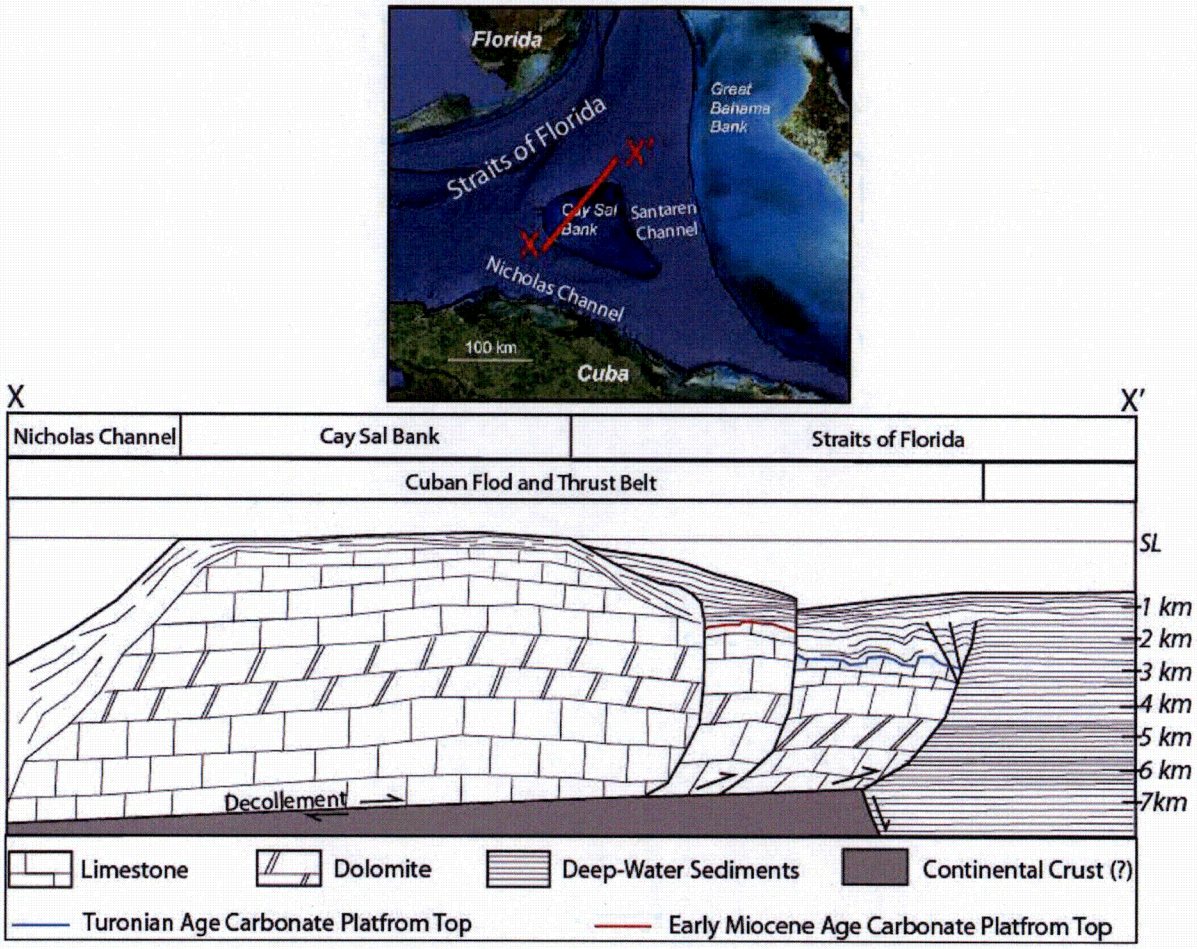


**Figure 4.** Idealized cross Section X-X' Across Cay Sal Bank (Kula, 2014, Figure 5-18 [Reference 1]).

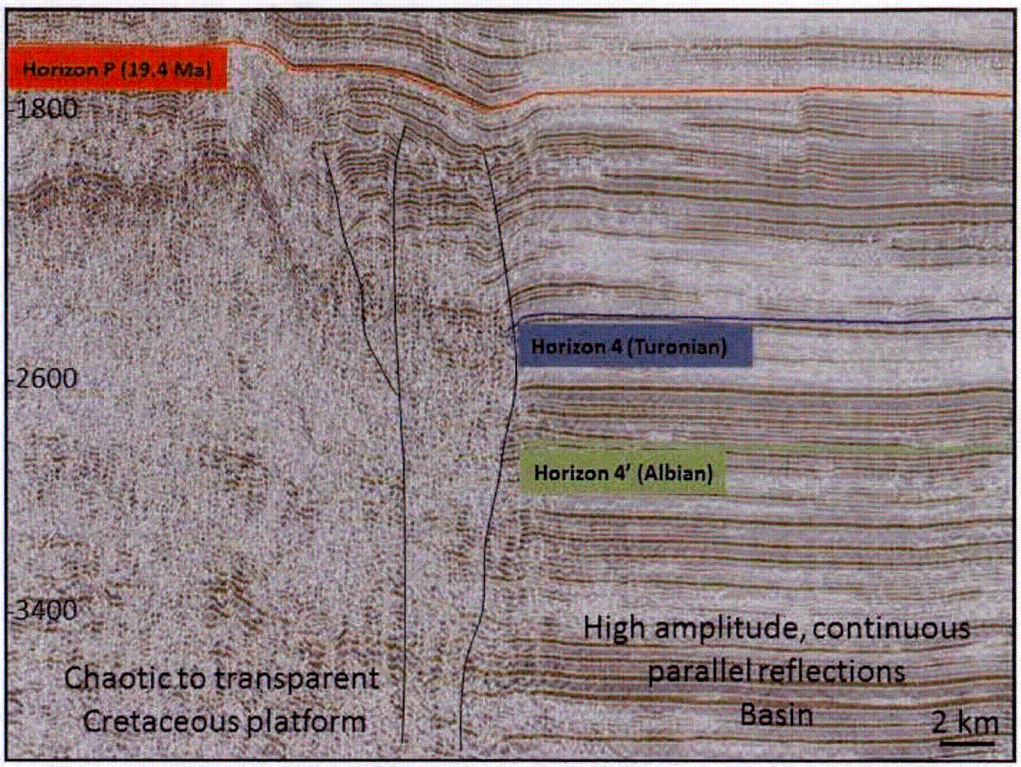


**Figure 5.** Kula's (Reference 1) Figure 4-6 showing portion of GSI Line BH81-34 from northern Cay Sal Bank showing buried Cretaceous shallow-water carbonate platform margin and pre-early Miocene faults. These are presumably Kula's faults C and D, but are not labeled on the figure. Line location shown on Figure 12.

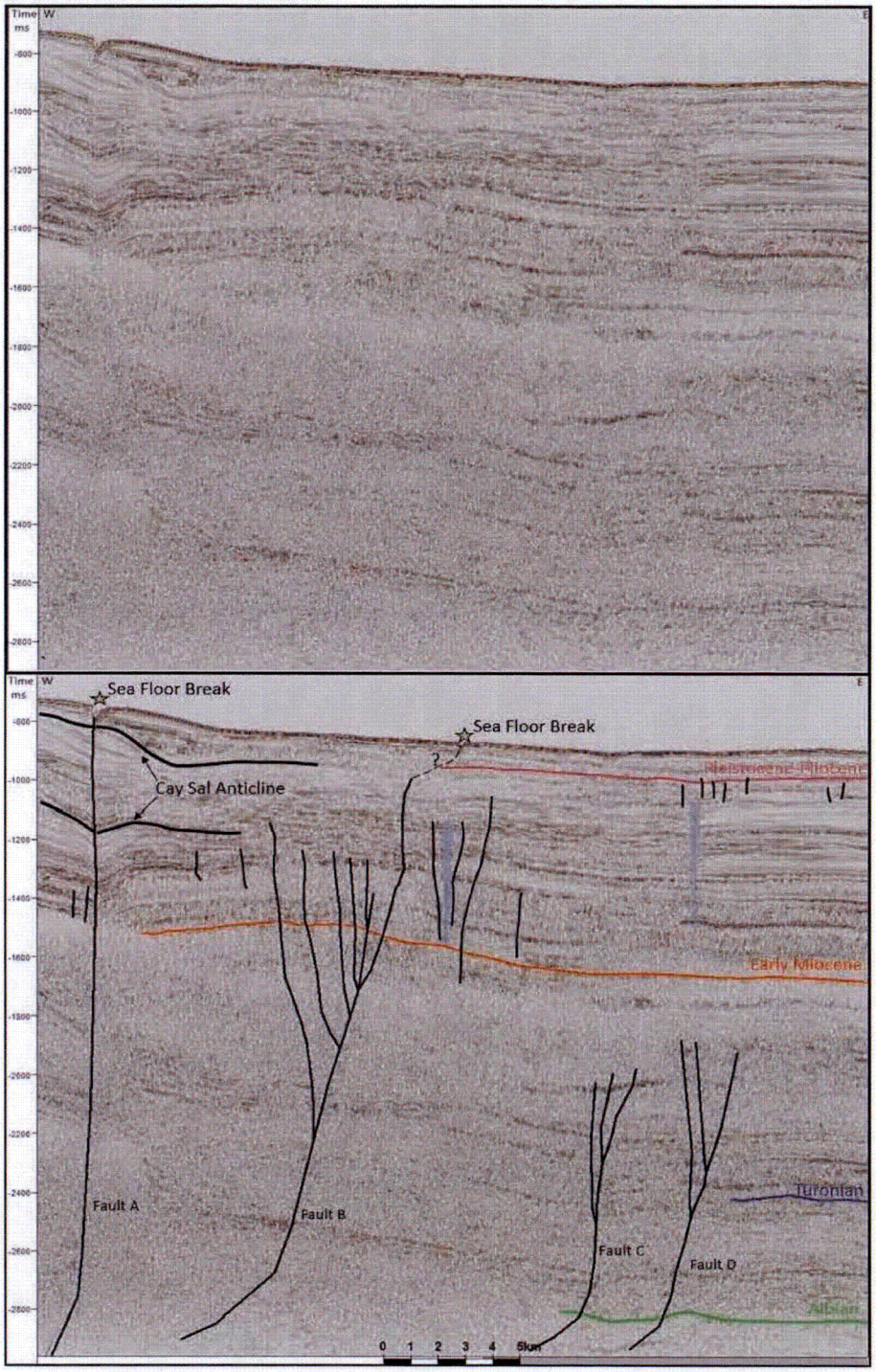


1.

**Figure 6**. Kula's (Reference 1) Figure 5-7 showing interpreted Profile 24A along eastern margin of Cay Sal Bank showing Faults A, B, C, and D. Also note seafloor breaks mapped above faults A and B. Profile location shown on Figure 12.

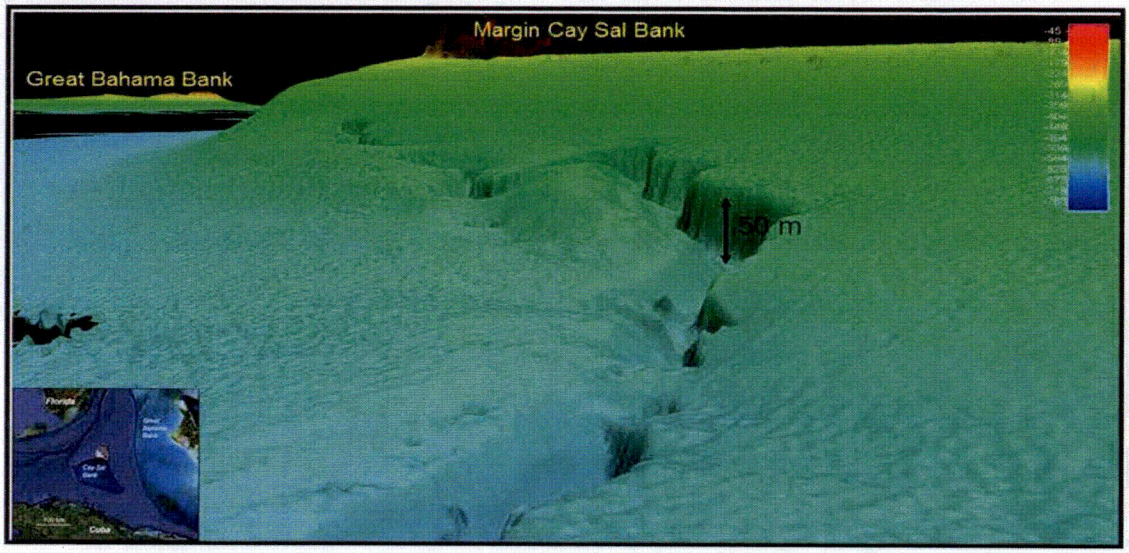


**Figure 7a.** Kula's (Reference 1) Figure 5-12 showing seafloor break and 50-m-high scarp on northeastern margin of Cay Sal Bank. View to the southeast.

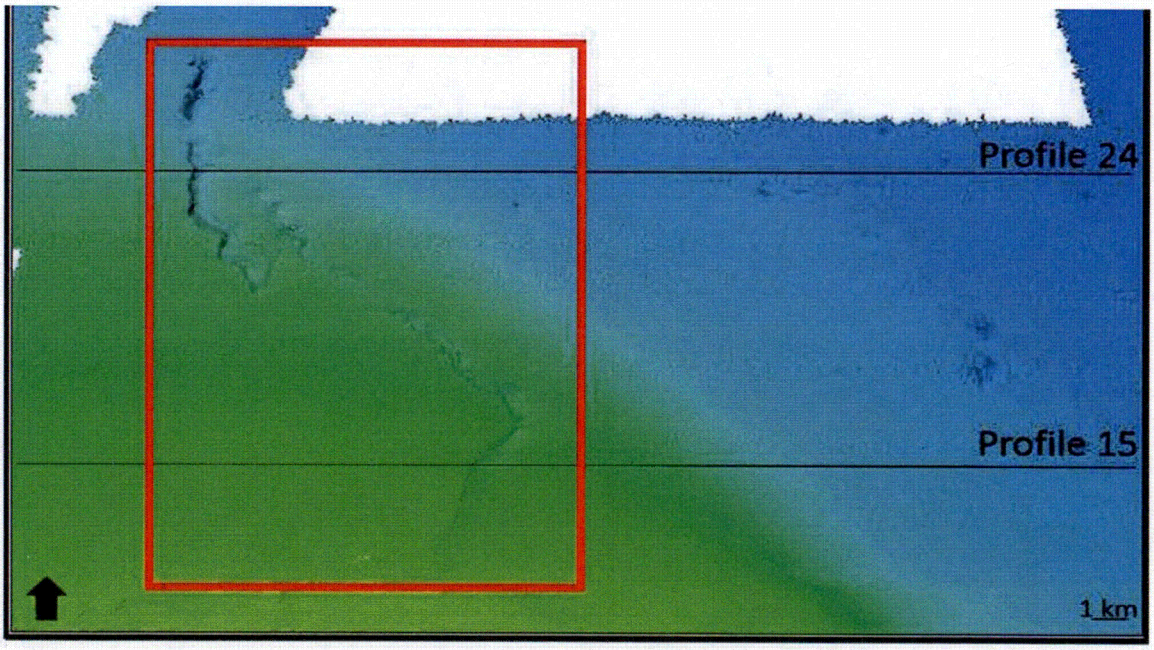


**Figure 7b.** Kula's (Reference 1) Figure 5-13 showing bathymetric expression of seafloor break on northeastern margin of Cay Sal Bank.

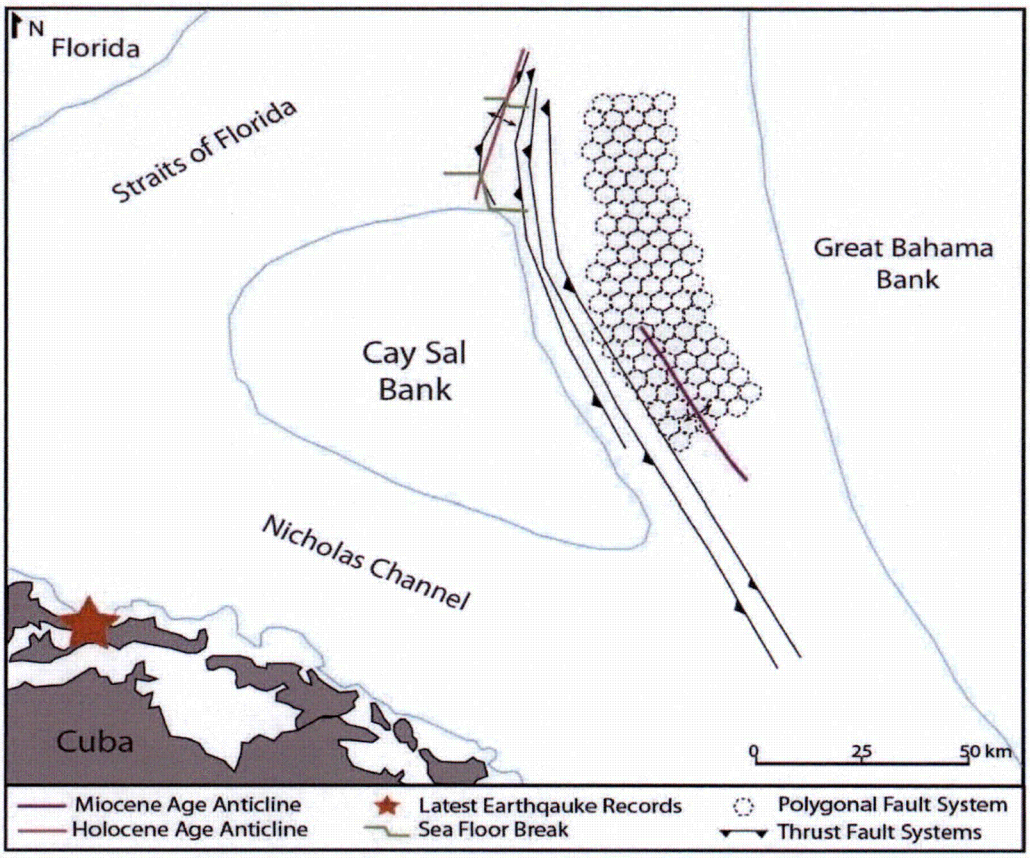


**Figure 8.** Kula's (Reference 1) Figure 5-16 location map of structural features along the eastern margin of Cay Sal Bank.

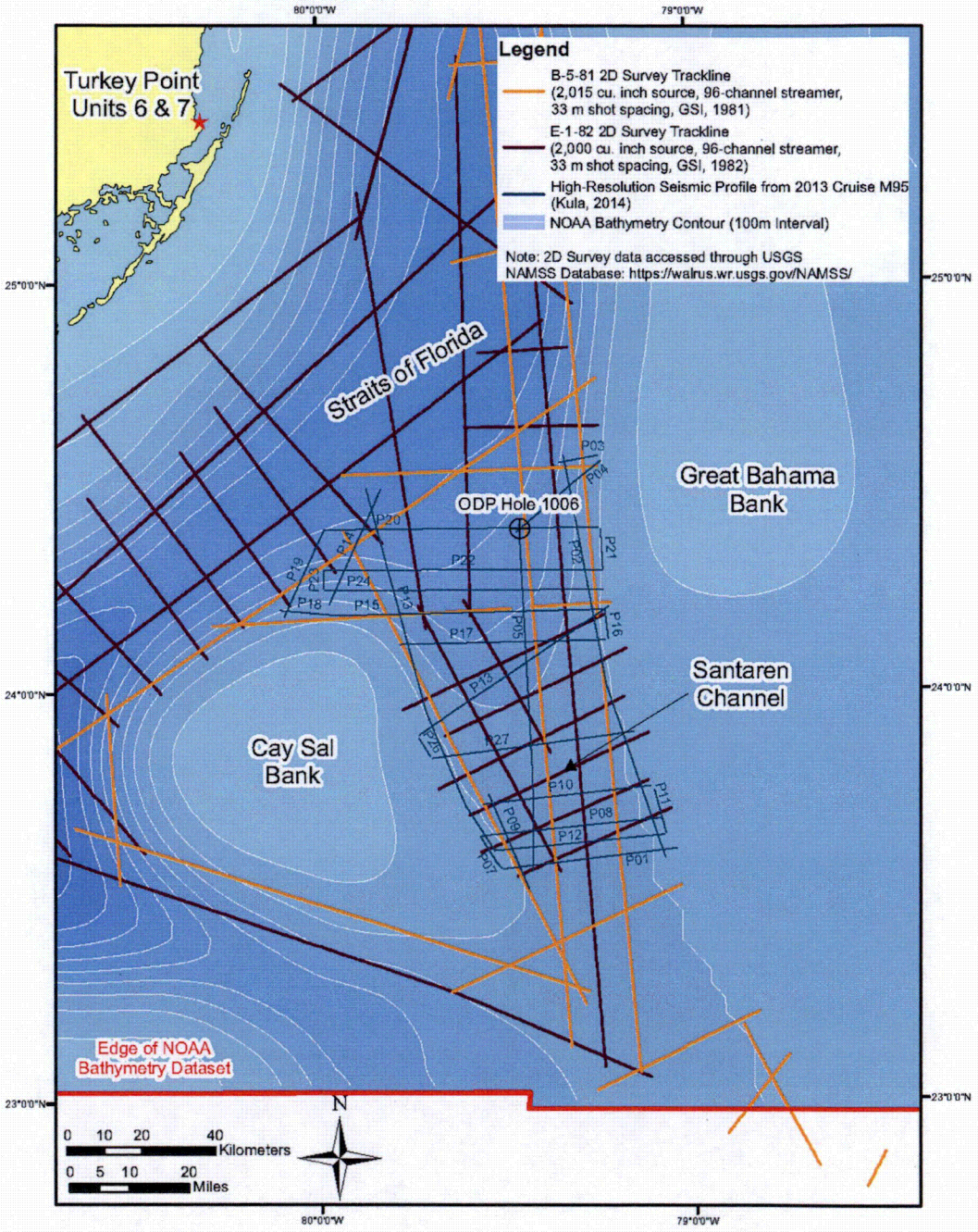


**Figure 9.** Cruise M95 seismic profiles and publicly available seismic data.

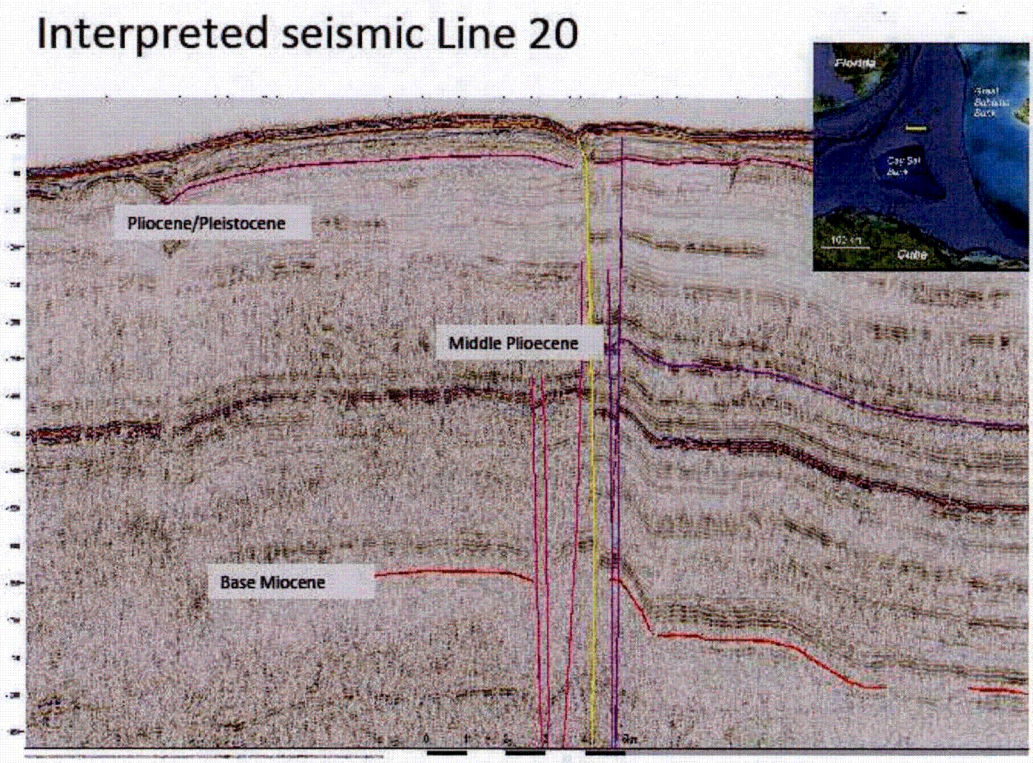


**Figure 10.** Enlarged version of Kula's (Reference 1) Figure 5-3 showing interpreted seismic Line 20. Line location shown on Figure 12

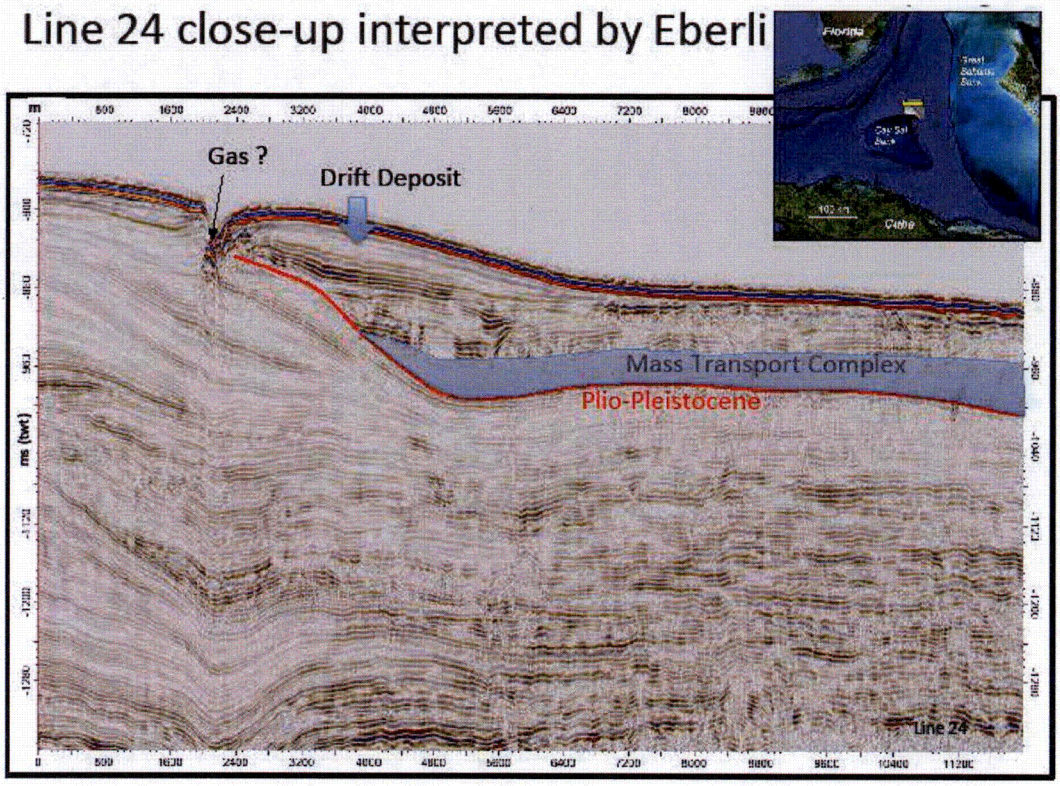


**Figure 11.** Enlarged version of Kula's (Reference 1) Figure 5-7 Profile 24 with Prof. Eberli's interpretation. See Figure 6 for un-interpreted seismic line 24 and for Kula's interpretation. Profile location shown on Figure 12.

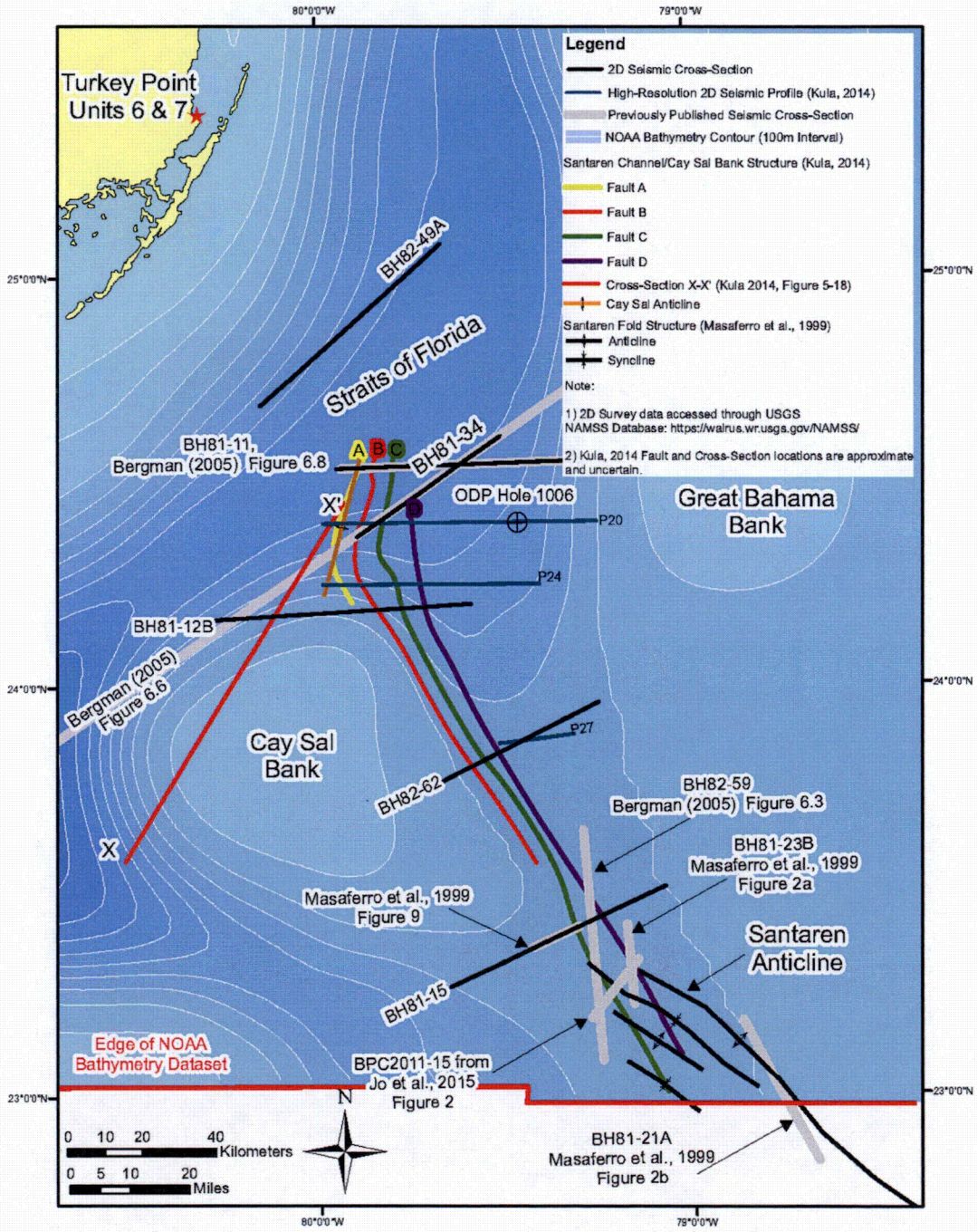


**Figure 12.** Tectonic features and locations of seismic lines and geologic cross-sections in the Santaren Channel region.

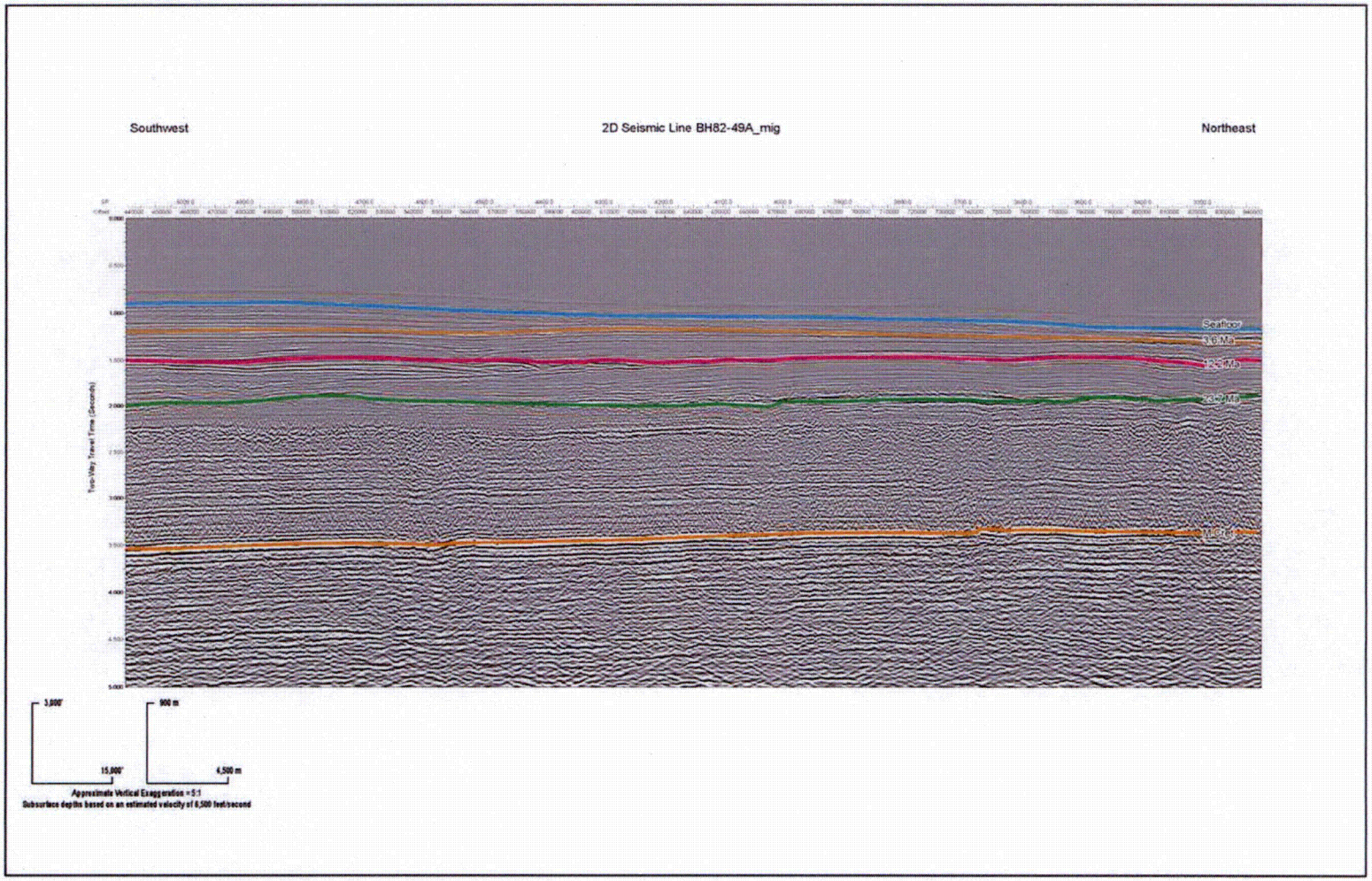


**Figure 13.** Interpreted GSI seismic reflection line BH82-49A_mig. (Modified after data from Reference 5).

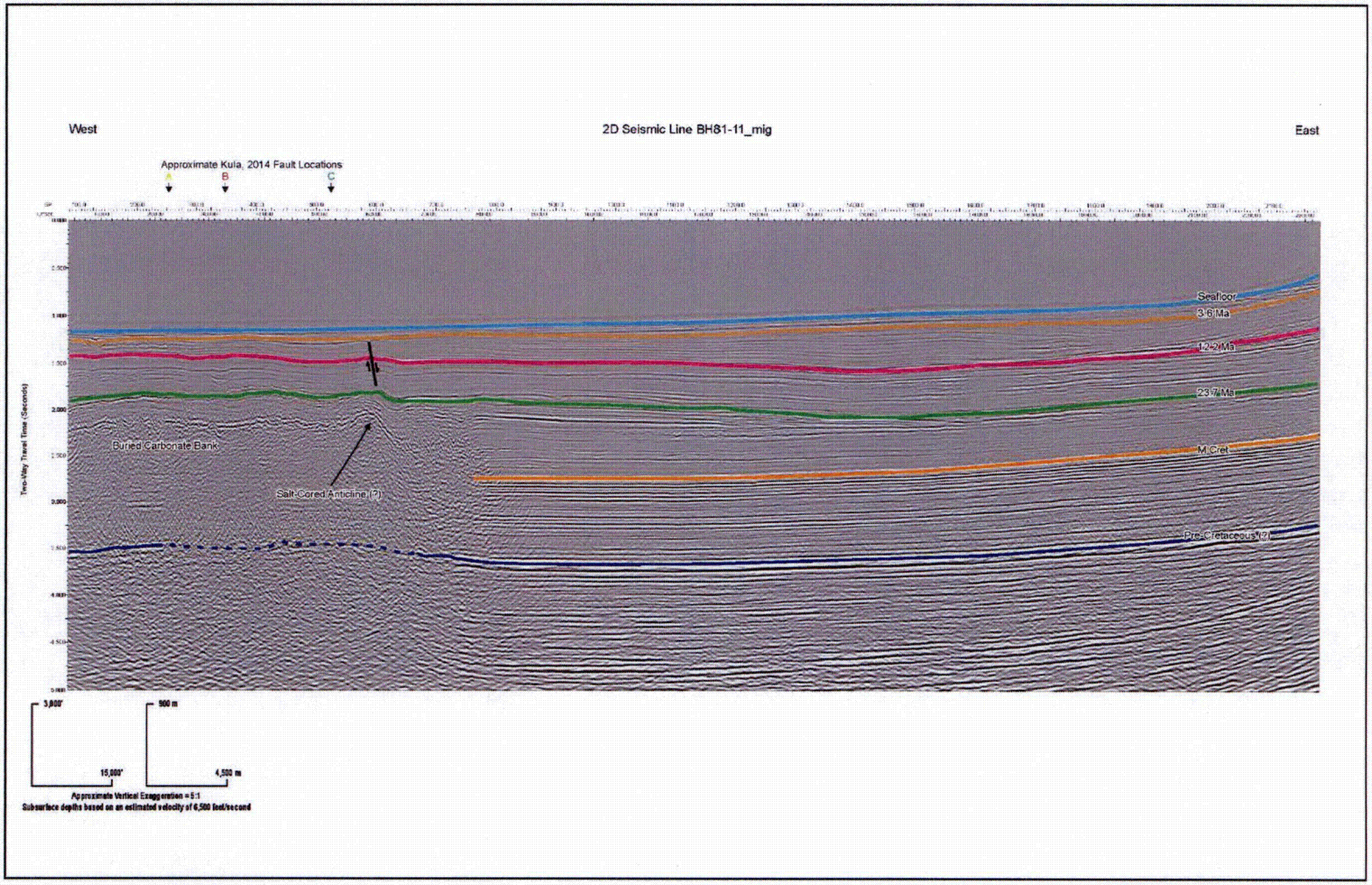


**Figure 14**. Interpreted GSI seismic reflection line BH81-11_mig. Stratigraphic horizons and fault location modified from Bergman (2005). (Modified after data from Reference 5).

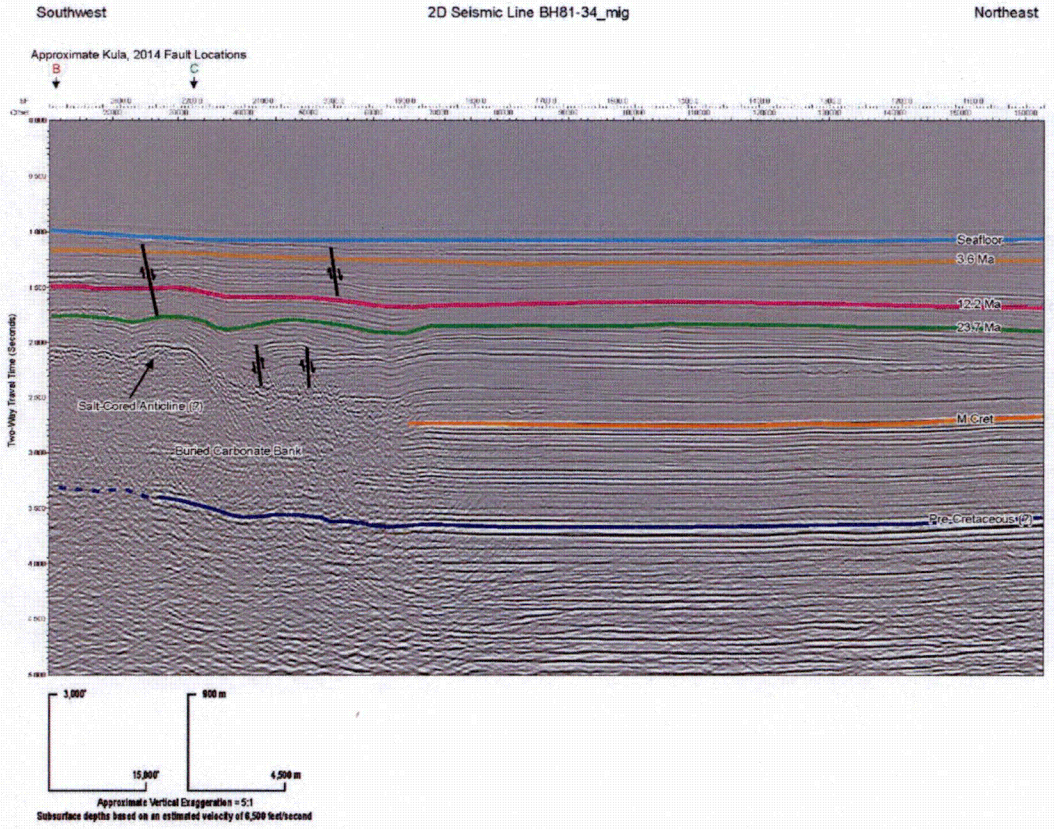


**Figure 15.** Interpreted GSI seismic reflection line BH81-34_mig. (Modified after data from Reference 5).

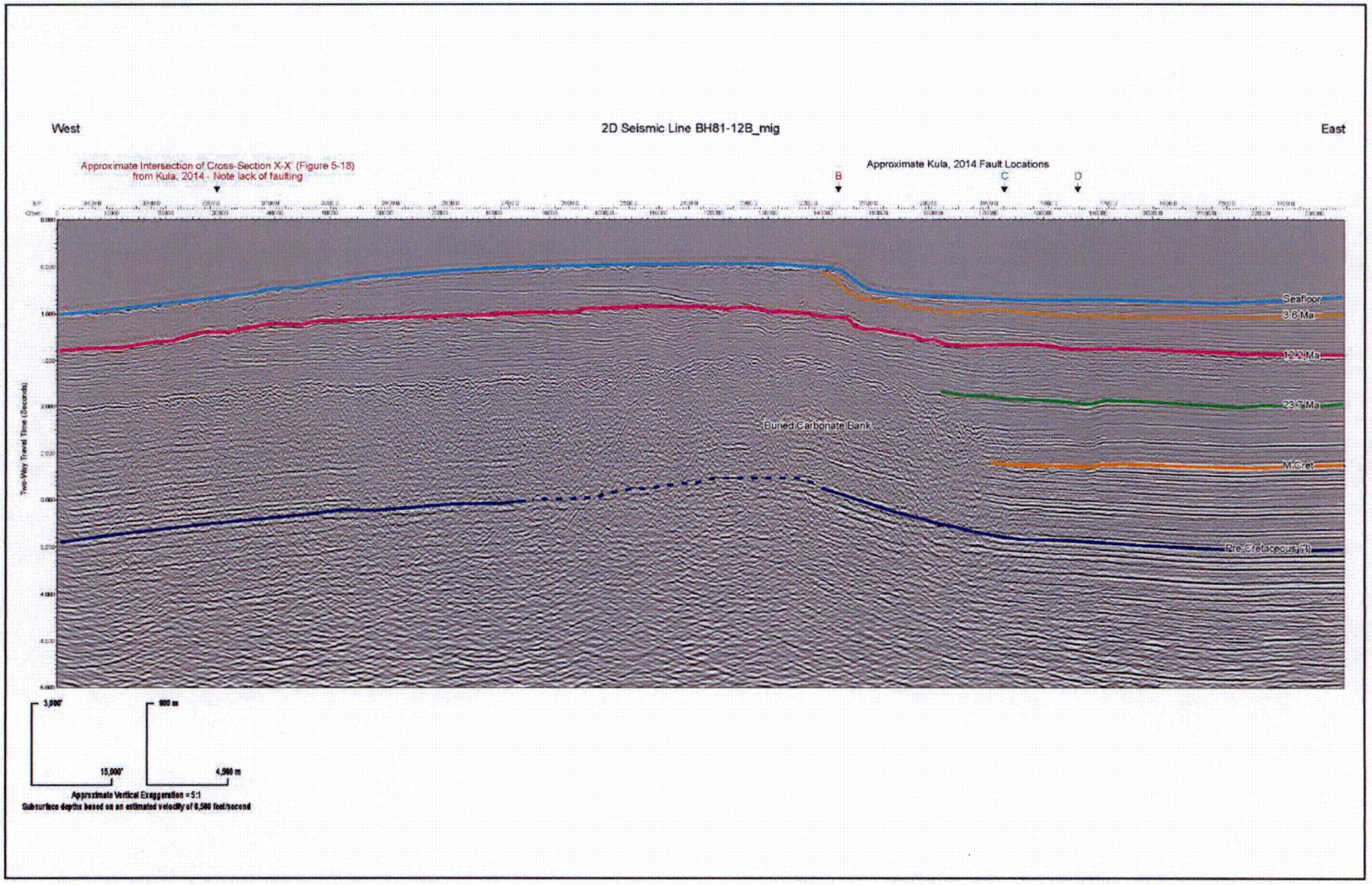


**Figure 16.** Interpreted GSI seismic reflection line BH81-12B_mig. (Modified after data from Reference 5).

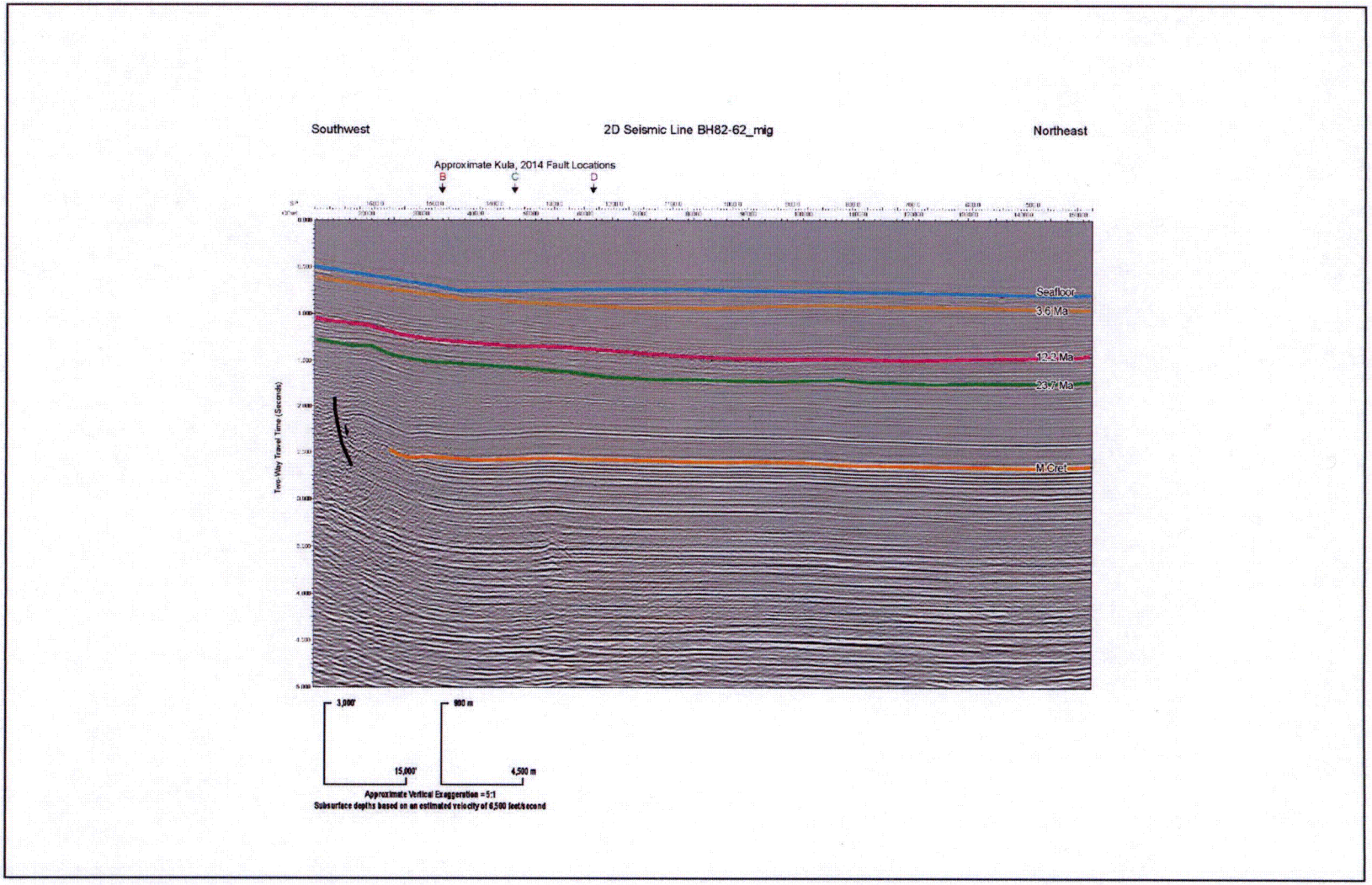


**Figure 17.** Interpreted GSI seismic reflection line BH82-62_mig. (Modified after data from Reference 5)

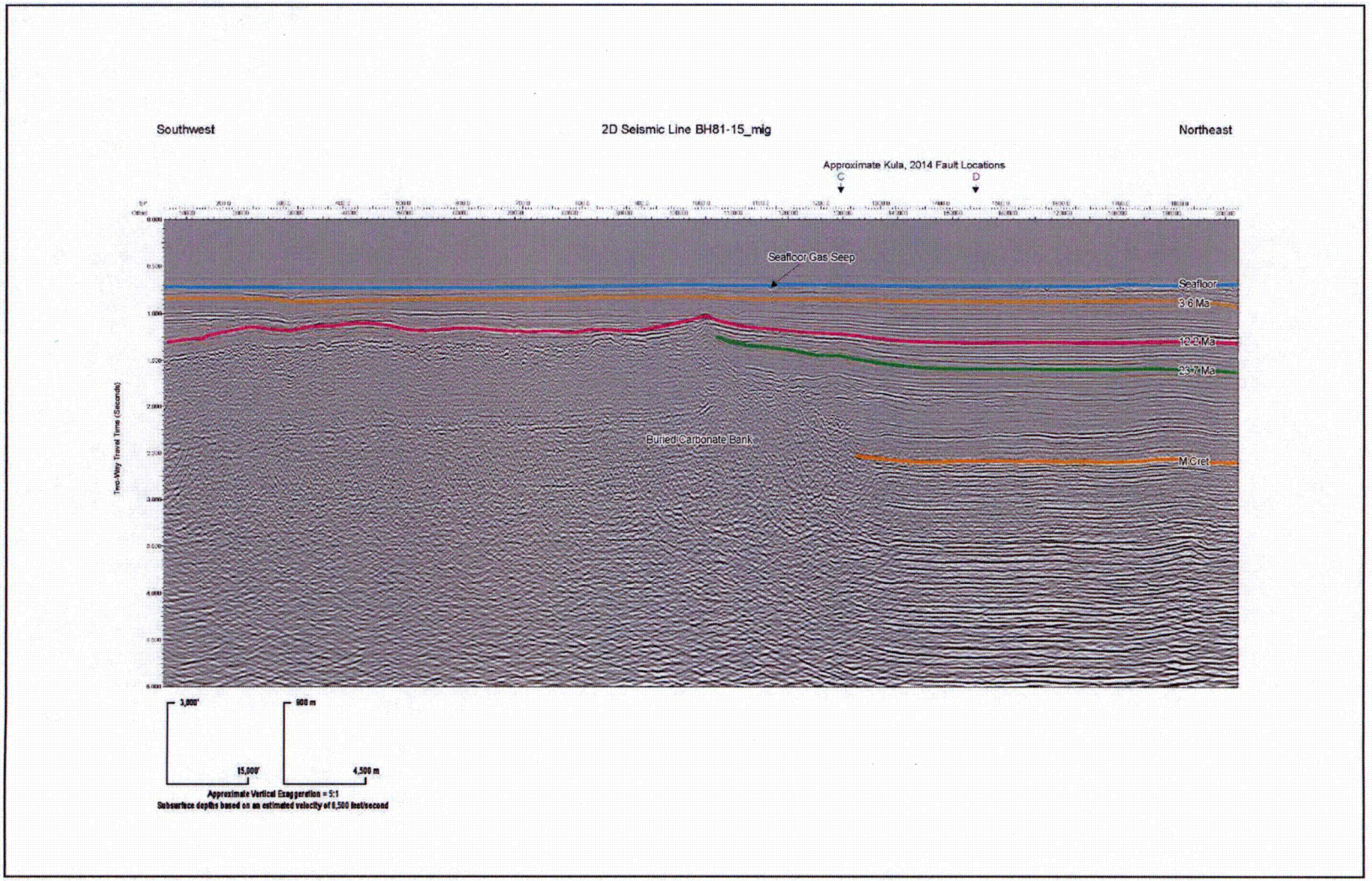


**Figure 18.** Interpreted GSI seismic reflection line BH81-15_mig. (Modified after data from Reference 5).

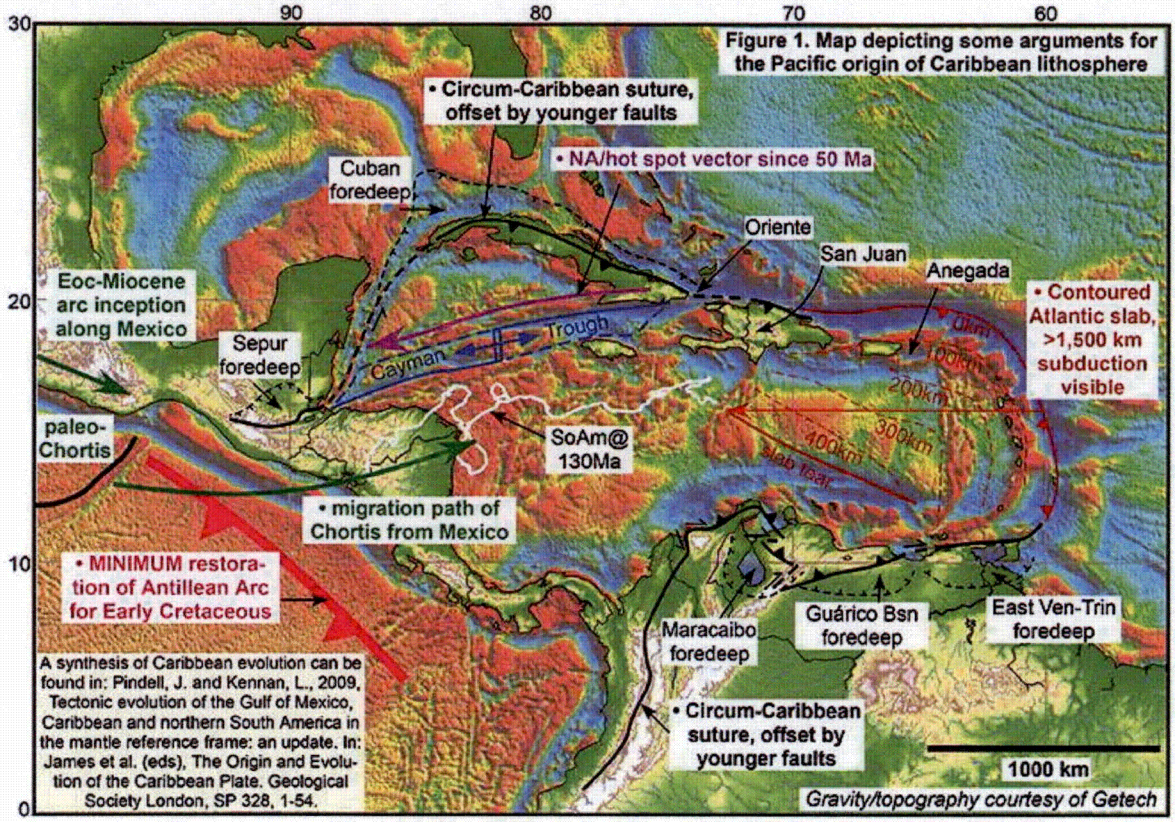


**Figure 19**. Regional map depicting arguments for a Pacific origin of Caribbean lithosphere from Pindell (2013) (Reference 11). Note the designation of the "Cuban foredeep" with short dashed line that includes only the southern part of Cay Sal Bank and Santaren Channel.

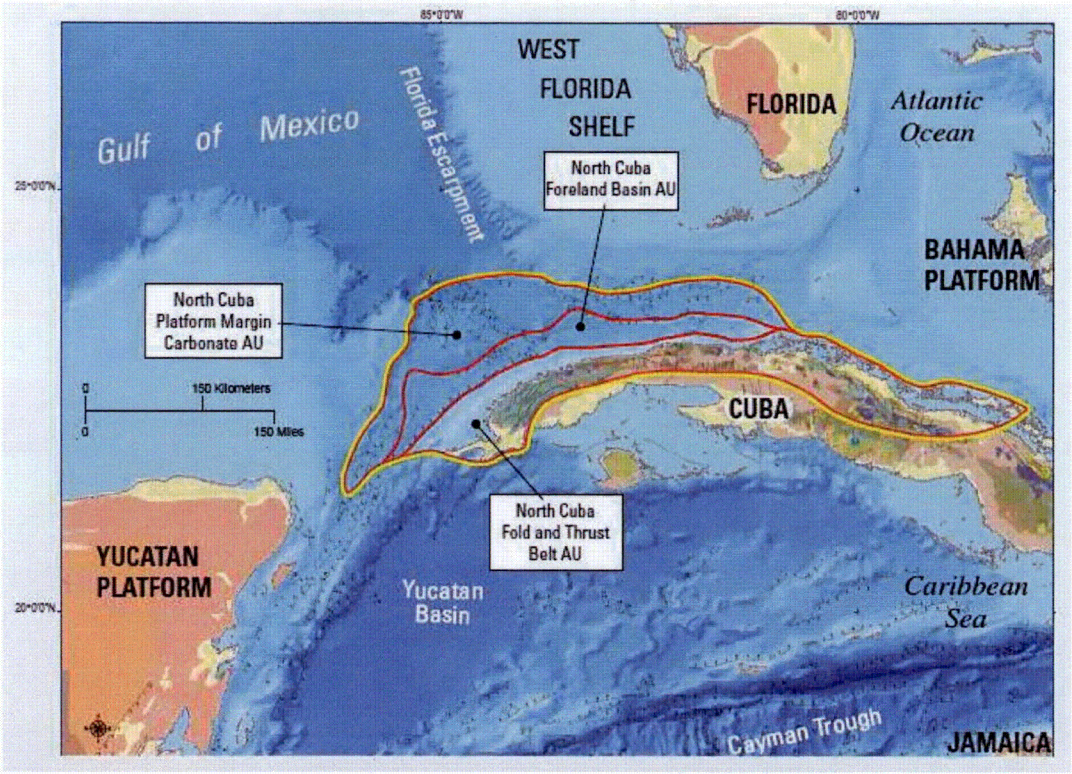


**Figure 20**. Extents of the North Cuba Fold and Thrust Belt, North Cuba Foreland Basin, and North Cuba Platform Margin assessment units (AUs) within the Jurassic-Cretaceous Total Petroleum System (TPS) (yellow line) from Schenk (2010) (Reference 10). The AUs were subdivided based on geologic structure and reservoir type.

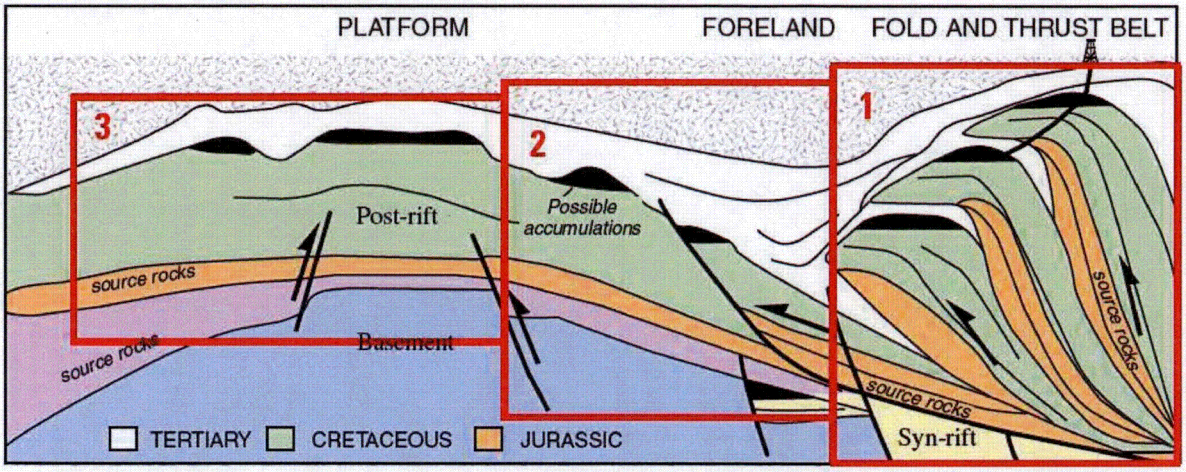


**Figure 21**. Schematic illustration from Schenk (2008) (Reference 9) showing the general boundaries and characteristics of the three assessment units (AU) outlined in red rectangles: North Cuba Fold and Thrust Belt (1), North Cuba Foreland Basin (2), and North Cuba Platform Margin Carbonate (3).

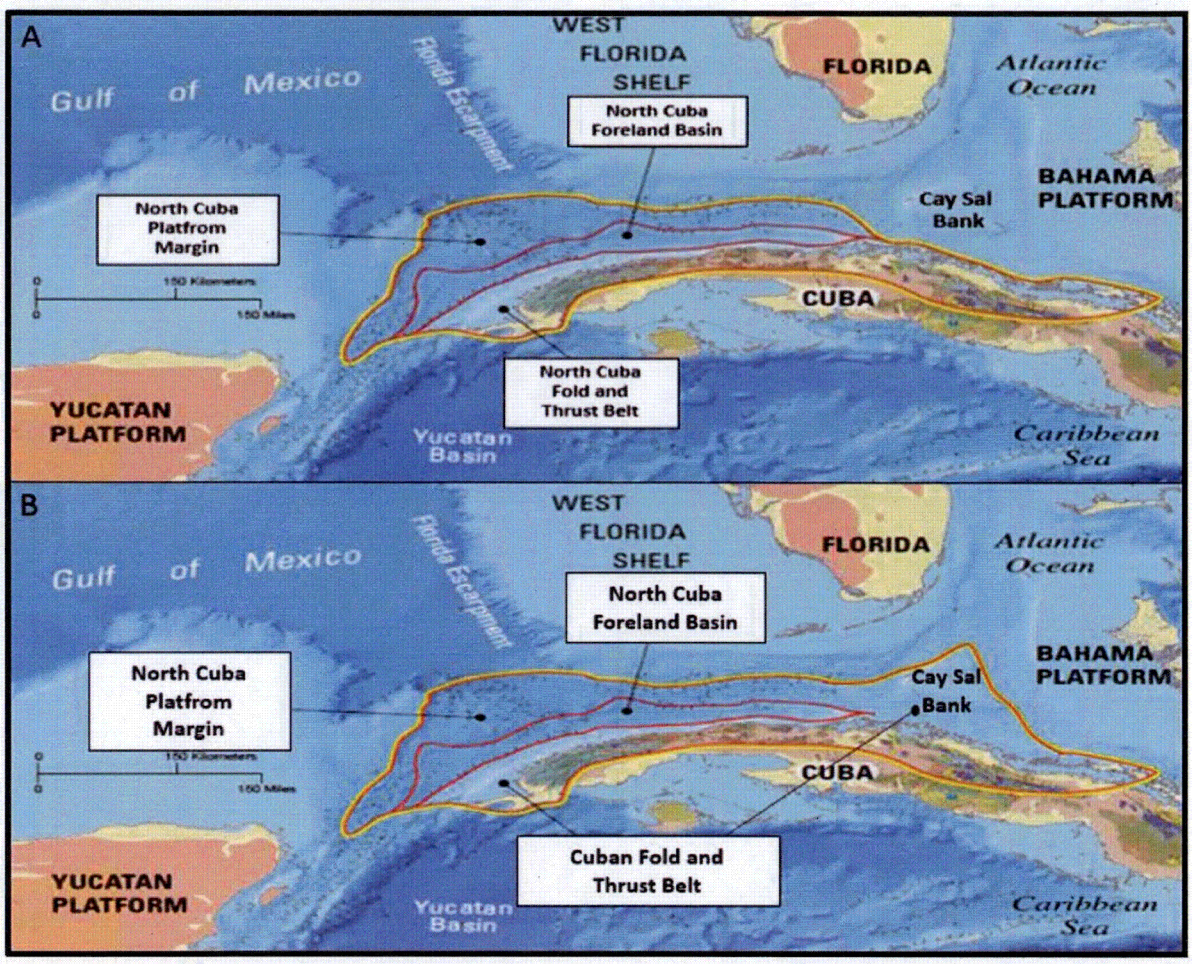


**Figure 22**. Schenk (2008; 2010) (References 9 and 10) assessment units shown in A and proposed modification of boundaries by Kula (Reference 1) shown in B. Note that the platform margin and fold and thrust belt remain undifferentiated in the eastern portion of the region modified by Kula (Reference 1). Figure 6-1 from Kula (Reference 1).

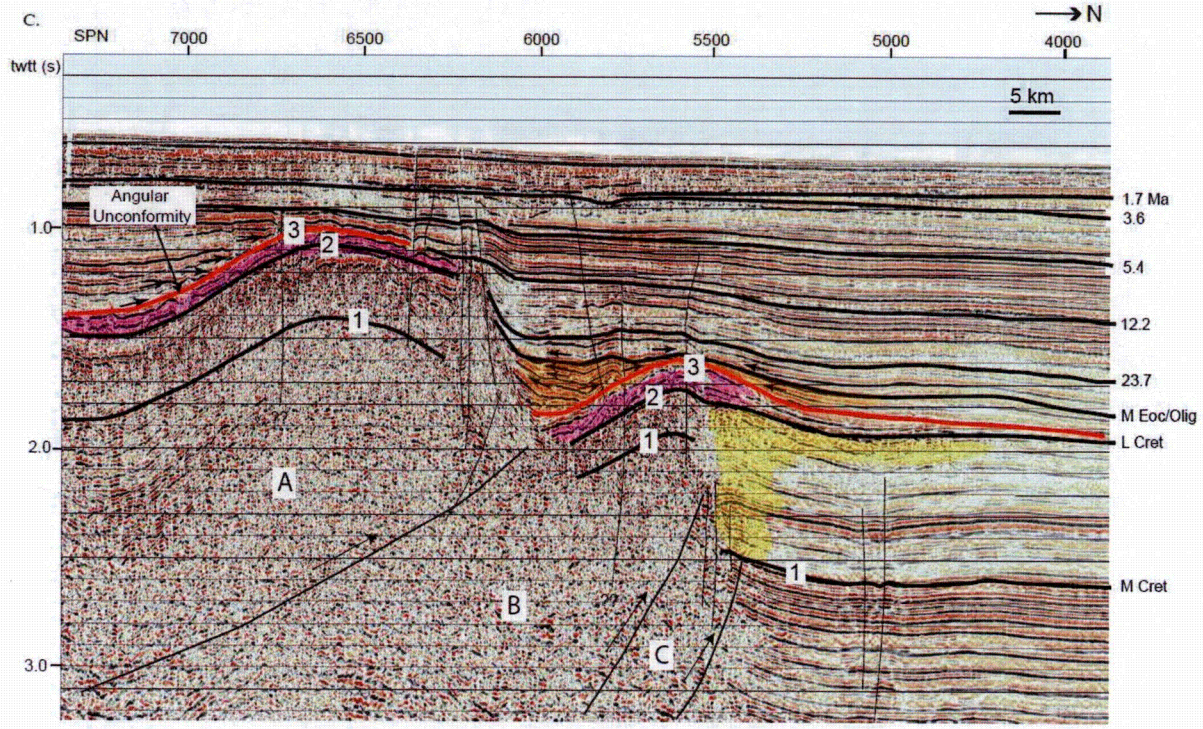


**Figure 23**. Thrust-bound folds along the buried shallow-water carbonate margin. Reflection 2 represents a disconformity between underlying marginal facies of late Cretaceous age and an overlying hemipelagic facies of Paleogene age. Reflection 3 is an angular unconformity that marks the onset of folding and thrusting of the buried margin. From Figure 6.3 of Bergman (2005) (FSAR Reference 2.5.1-906). Location of profile is shown in Figure 12.

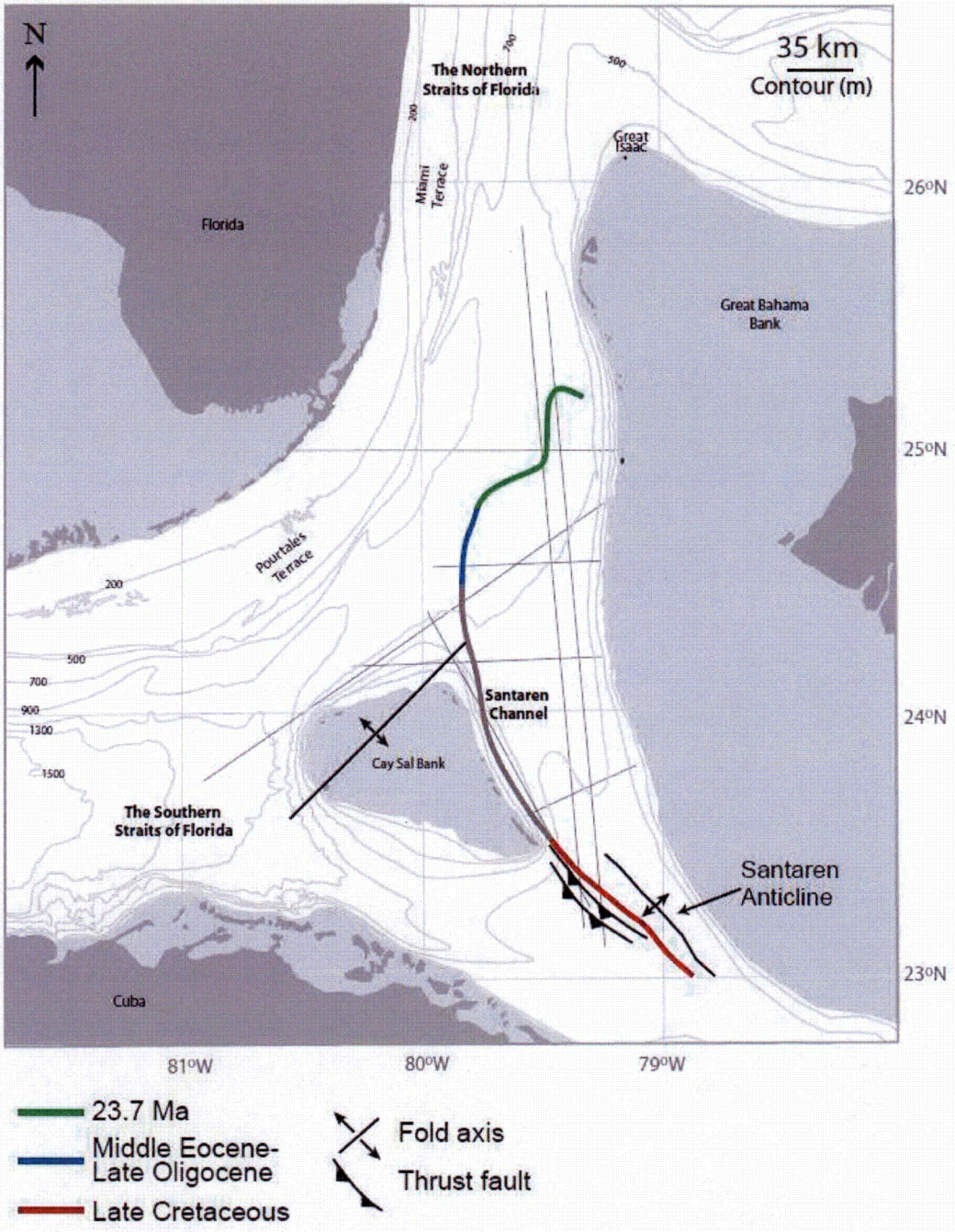


**Figure 24**. Map of compressional features (faults and folds) and ages of buried platforms along the Santaren Channel. From Figure 6.9 of Bergman (2005) (FSAR Reference 2.5.1-906).

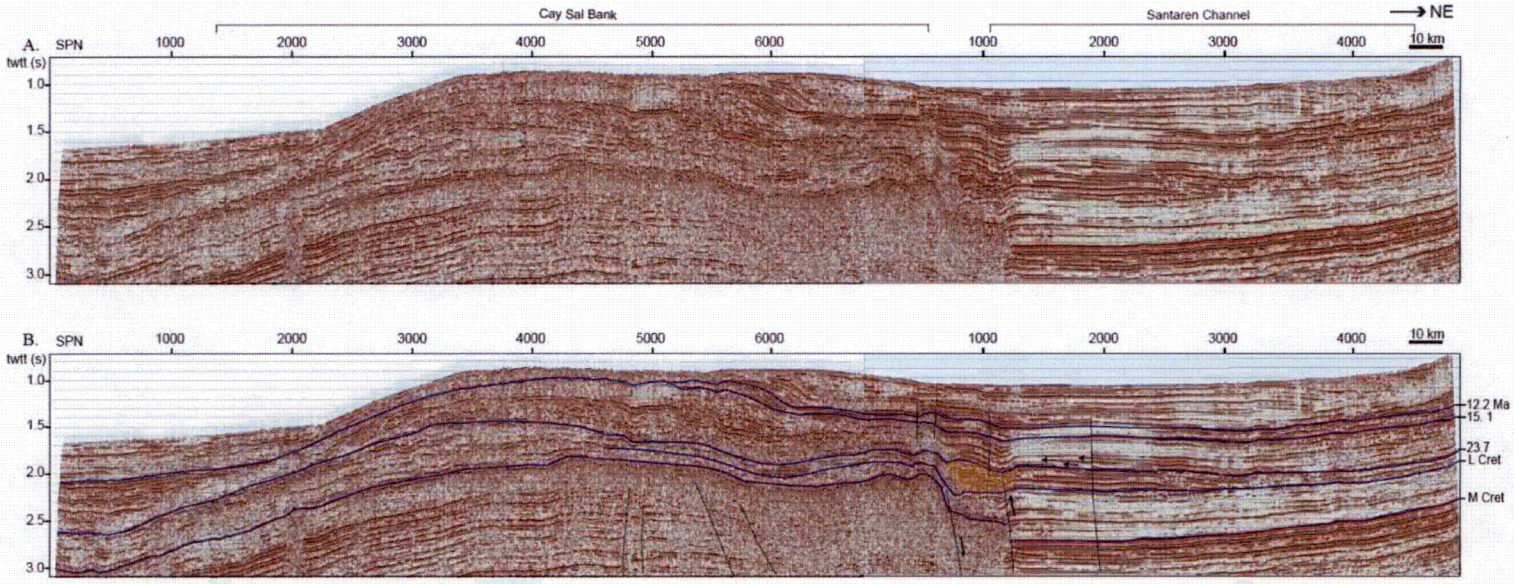


**Figure 25**. Seismic Line BH81-34 oriented northeast-southwest along the northwest margin of Cay Sal Bank. From Figure 6.6 of Bergman (2006) (FSAR Reference 2.5.1-906).

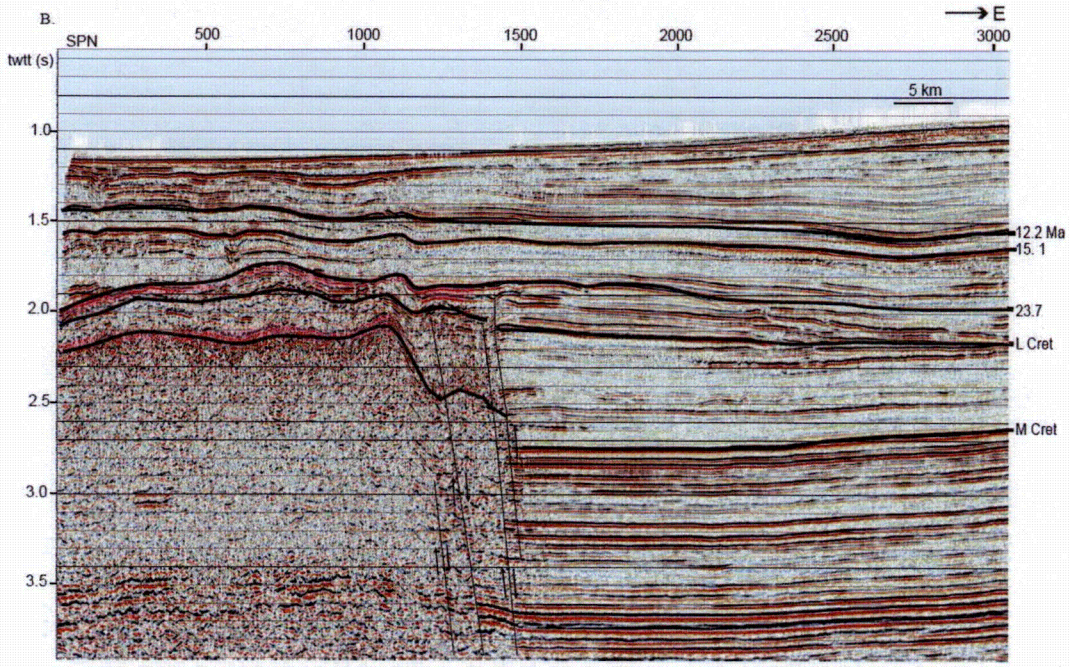


**Figure 26**. Easterly oriented line (GSI Line BH81-11) that crosses the eastern margin of Cay Sal Bank. The upper portion of the margin is interrupted by packages of the high-amplitude cap facies (shaded pink). An unconformity adjacent to the margin indicates the shallow-carbonate platform foundered between the middle Eocene and late Oligocene. From Figure 6.8 of Bergman (2005) (FSAR Reference 2.5.1-906).

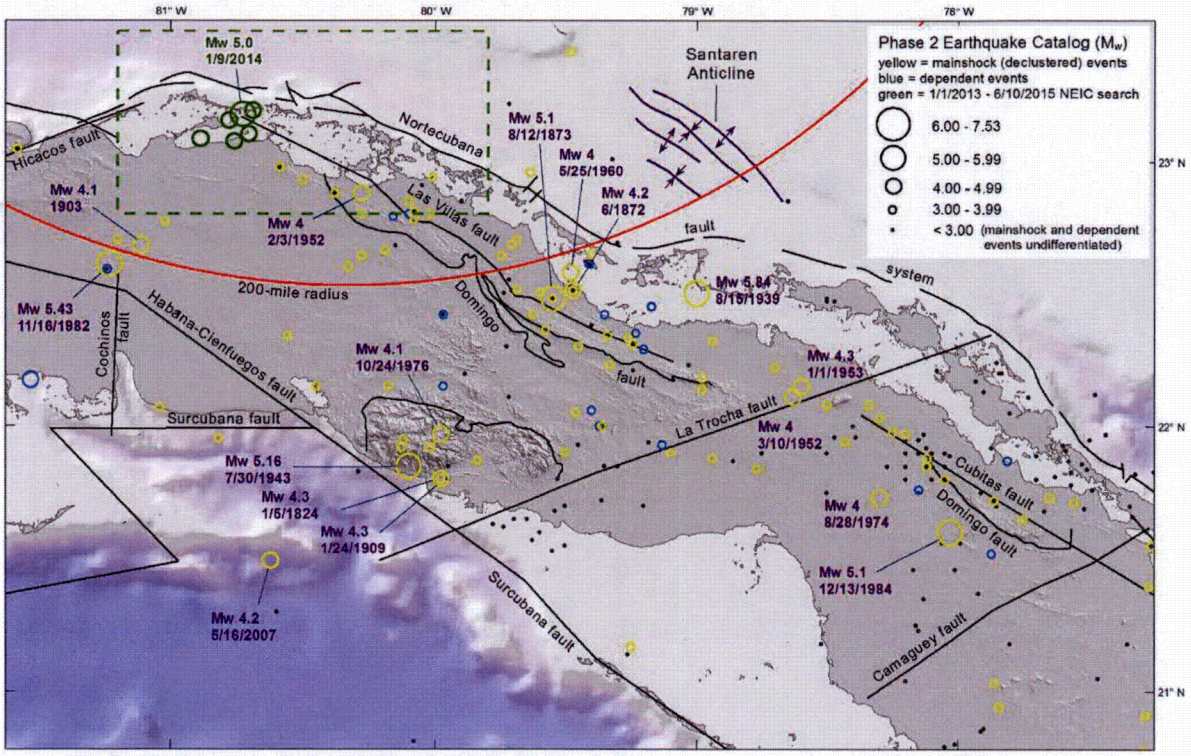


**Figure 27**. Fault map of Cuba showing earthquakes from the Phase 2 earthquake catalog. Additional earthquakes (shown in green) are from online search of the National Earthquake Information Center (NEIC) earthquake catalog for events that occurred between January 1, 2013 and June 10, 2015, performed at http://earthquake.usgs.gov/earthquakes/search/ (accessed 6/25/2015) (Reference 14). Dashed green line shows extent of NEIC search area. Red line shows portion of the 200-mile radius Site Region.

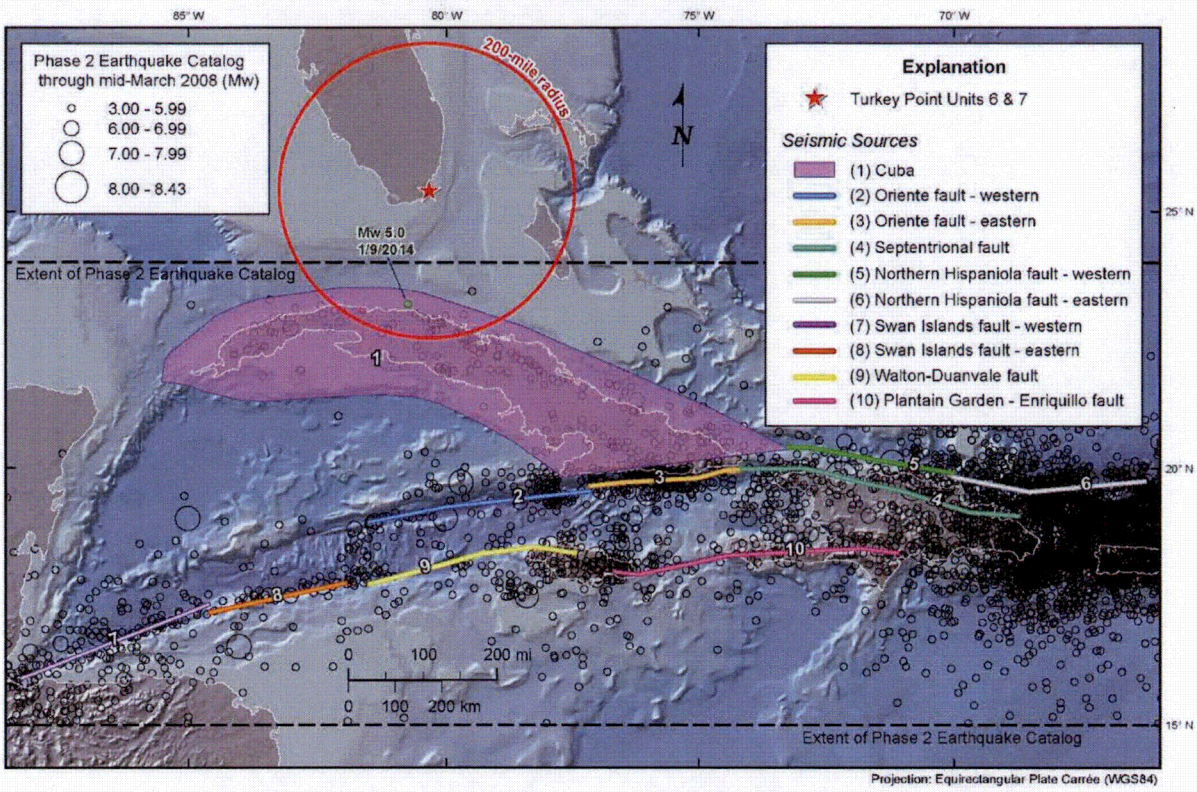


**Figure 28**. Cuba and northern Caribbean seismic source model sources and the January 9, 2014 $M_w$ 5.0 earthquake offshore north of Cuba. See FSAR Section 2.5.2.1 for discussion on the Phase 2 mainshock earthquake catalog as shown. Magnitude and location of the 2014 earthquake (shown in green) are from http://earthquake.usgs.gov/earthquakes/search/ (accessed 6/25/2015) (Reference 14).

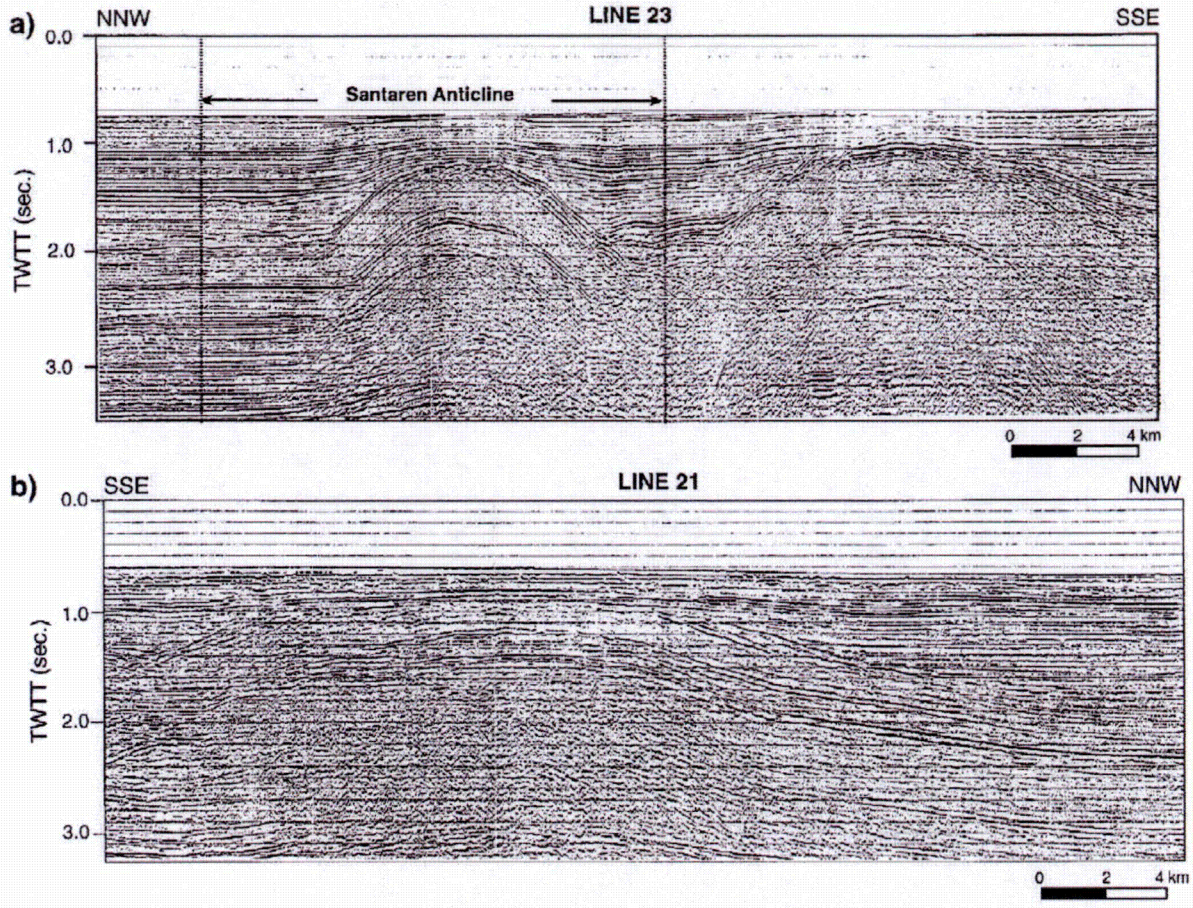


**Figure 29.** GSI seismic reflection Profiles BH81-23B (upper panel a) and BH81-21A_mig (lower panel b) across the Santaren anticline (from Masaferro et al., 1999 [FSAR Reference 2.5.1-426]). Line location shown on Figure 12.

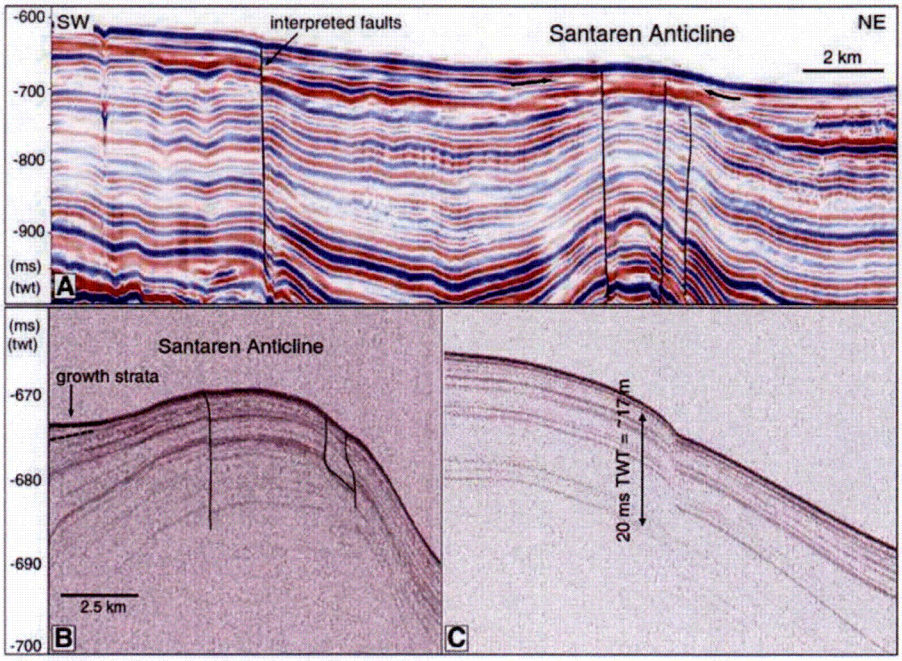


**Figure 30.** High resolution seismic reflection Line BPC2011-15 (A) and subbottom profiles (B and C) that illustrate shallow Quaternary secondary faulting associated with the Santaren anticline (Jo et al. 2015 [Reference 13]). Line location shown on Figure 12.

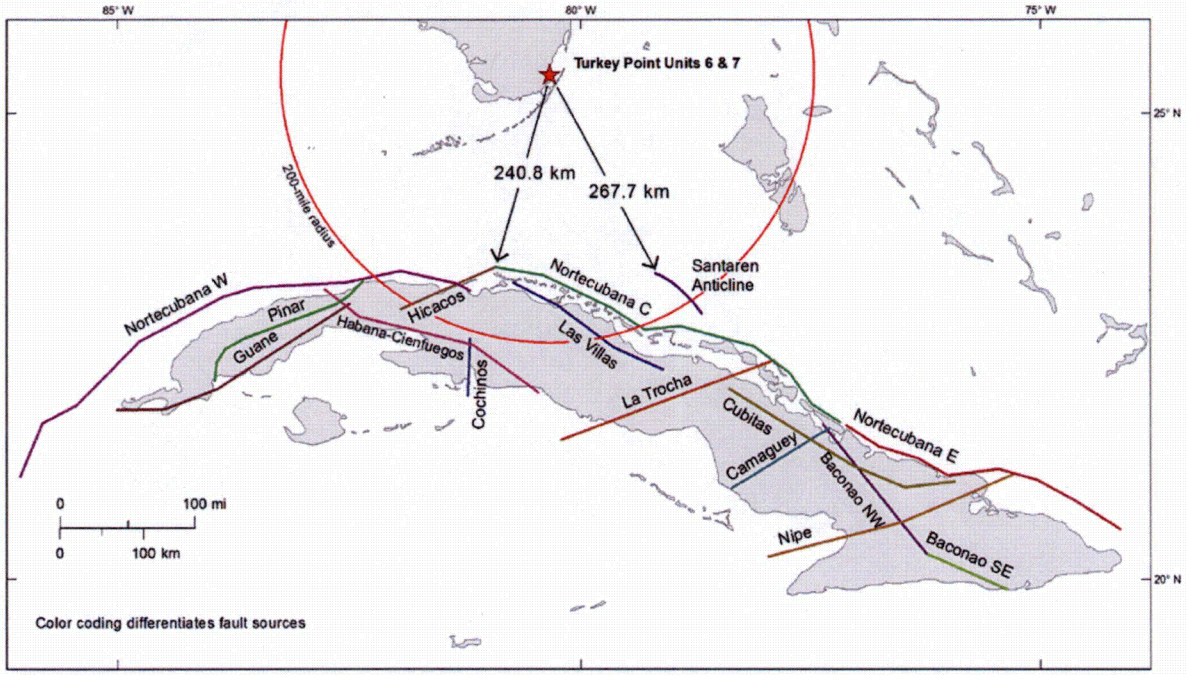


**Figure 31.** Location of Cuba fault sources and Santaren anticline fault source, and nearest distances.

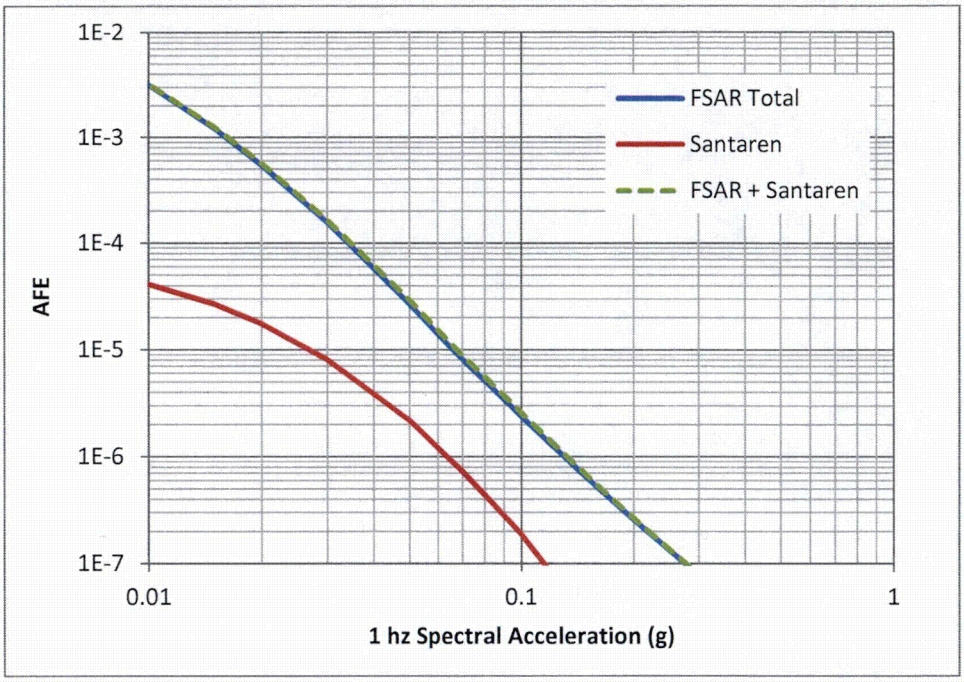


**Figure 32.** Hazard curves for 1 Hz: Santaren anticline fault source, FSAR Total, and FSAR total + Santaren anticline fault source.

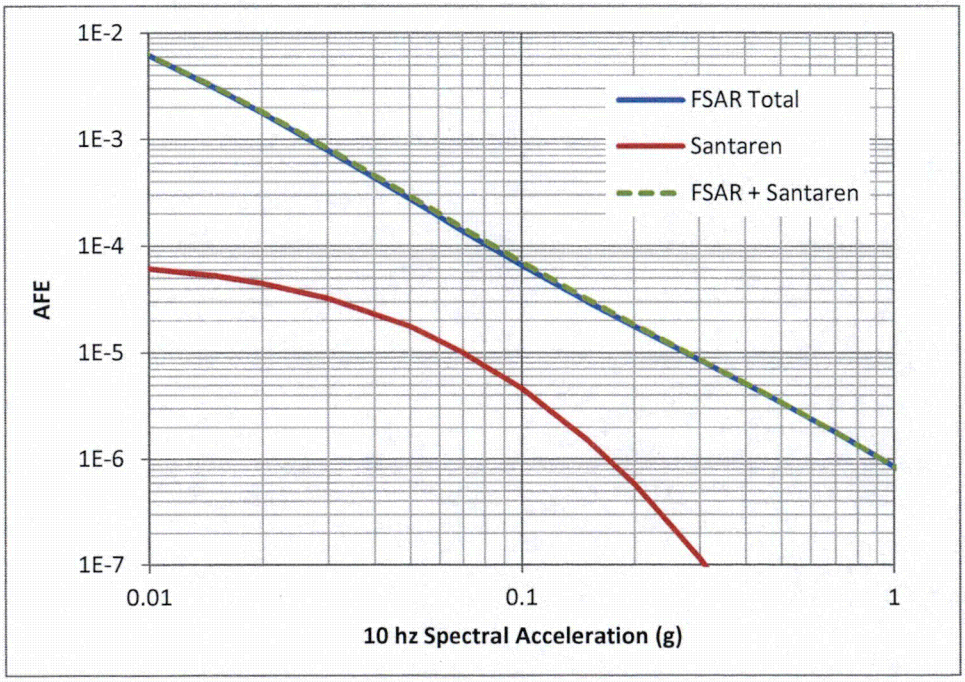


**Figure 33.** Hazard curves for 10 Hz: Santaren anticline fault source, FSAR Total, and FSAR total + Santaren anticline fault source.

This response is PLANT SPECIFIC.

**References:**

1. Kula, D., *Neotectonics on the Edge of the Cuban Fold and Thrust Belt*, unpublished Master's thesis, University of Miami, 133 p., 2014.
2. Eberli, G.P., Anselmetti, F.S., Betzler, C. Van Konijnenburg, J.-. H., and Bernoulli, D., *Carbonate Platform to Basin Transition on Seismic Data and in Outcrop – Great Bahama Bank and the Maiella Platform,* Italy, in Eberli, G.P., Massaferro, J.L., Sarg, J.F. (eds.) Seismic Imaging of Carbonate Reservoirs and Systems, AAPG Memoir 81, pp. 207-250. 2004.
3. Tournadour, E., Mulder, T., Borgomano, J., Hanquiez, V., Ducassou, E., and Gillet, H., *Origin and architecture of a Mass Transport Complex on the northwest slope of Little Bahama Bank (Bahamas): Relations between off-bank transport, bottom current sedimentation and submarine landslides*, Sedimentary Geology, Vol. 317, pp. 9-26, 2015.
4. Eberli, G.P., Kula, D., Jo, A., Masaferro, J.L., Ludemann, T., and Betzler, C., *Influence of Neo-Tectonic Activity in the Cuban Fold and Thrust Belt on the Slope and Margin Failures of Cay Sal and Great Bahama Bank* (abstract), AAPG Annual Convention and Exhibition, Denver, CO, June 2015.
5. U.S. Geological Survey, *National Archive of Marine Seismic Surveys (NAMSS)*, Available at https://walrus.wr.usgs.gov/namss/, accessed June 22, 2015.
6. Ocean Drilling Program Shipboard Scientific Party, *Chapter 9* Site 1006, Eberli, G.P., Swart, P.K., Malone, M.J., et al., *Proceedings of the Ocean Drilling Program, Initial Reports.,* Vol., 1997.
7. Sheriff, R.E., *Aspects of Seismic Resolution*, O.R. Berg and D. Woolverton (eds.), Seismic Stratigraphy II: An Integrated Approach to Hydrocarbon Exploration: AAPG Memoir 39, pp. 1–10, 1985.
8. Widess, M.B., *How thin is a thin bed?,* Geophysics, Vol. 38, pp. 1176-1180, 1973.
9. Schenk, C.J., *Jurassic-Cretaceous Composite Total Petroleum System and geologic models for oil and gas assessment of the North Cuba Basin, Cuba*, in U.S. Geological Survey North Cuba Basin Assessment Team, (eds.), Jurassic-Cretaceous Total Petroleum System and geologic assessment of oil and gas resources of the North Cuba Basin, Cuba: U.S. Geological Survey Digital Data Series DDS–69–M, Chapter 2, 94 p., 2008.
10. Schenk, C.J., *Geologic Assessment Of Undiscovered Oil And Gas Resources of the North Cuba Basin, Cuba*, U.S. Geological Survey Open-File Report 2010–1029, Version 1.0., 2010.

11. Pindell, J., *Origin of the Caribbean? Look to the Pacific*, American Association of Petroleum Geologists (AAPG) Explorer, available at: https://www2.aapg.org/explorer/2013/07jul/historical0713.cfm, accessed June 26, 2015.

12. Jo, A., *Carbonate Slope Morphology and Sedimentary Processes along Southwestern Great Bahama Bank*, unpublished Master's thesis, University of Miami, 122 p., 2013.

13. Jo, A., Eberli, G.P., and Grasmueck. M., *Margin collapse and Slope Failure along Southwestern Great Bahama Bank,* Sedimentary Geology, Vol. 317, pp. 43-52, 2015.

14. NEIC (2015) Earthquake Search, National Earthquake Information Center of the U.S. Geological Survey. Available at http://earthquake.usgs.gov/earthquakes/search/, accessed June 25, 2015.

15. Hanson, K.L., Kelson, K.I., Angell, M.A., and Lettis, W.R., *Techniques for Identifying Faults and Determining Their Origins, prepared for Division of Engineering Technology*, U.S NRC, NUREG/CR-5503, 1999.

## ASSOCIATED COLA REVISIONS

FSAR Subsection 2.5.1 will be revised in a future COLA revision as follows:

The following text will be inserted in FSAR Subsection 2.5.1.1.1.3.2.2, following the text with subheading titled, Jacksonville Fracture Zone, in a future COLA revision as follows:

**Possible Faults and Folds Near Cay Sal Bank**

**Based on new limited-penetration seismic reflection and bathymetry data, Kula (2014) (Reference 1022) and Eberli et al. (2015) (Reference 1023) proposed that four faults and related folding east and northeast of Cay Sal Bank may be tectonically related to a northeast extension of the Cuban fold-and-thrust belt, similar to previous suggestions by Bergman (Reference 906). As shown by Bergman (Reference 906), movement on the faults was primarily older than Paleocene and Eocene in age, but some waning movement may have continued into the late Miocene and possibly Pliocene. Kula's (Reference 1022) interpretation of the two eastern-most and longer faults suggests ages similar to Bergman (Reference 906), but also suggests that two shorter faults (Faults A and B) east and north of Cay Sal Bank have evidence of neotectonic activity including seafloor breaks up to 50 m high (Figure 2.5.1-229.)**

**Evaluation of additional seismic data, discussions with Kula's principal thesis advisor Prof. G. Eberli, and comparisons to features identified by other researchers working with similar high-resolution data in the region (e.g., Tournadour et al. (Reference 1024); Jo et al. (Reference 1025)) indicate that most of the features interpreted by Kula (Reference 1022) and Eberli et al. (Reference 1023) as evidence of neotectonic activity are more credibly interpreted as**

**evidence of mass movements and gravity-driven slope failures, and that other non-seismogenic processes including polygonal faults, fluid expulsion, and sediment compaction are likely the primary origin of features mapped by Kula (Reference 1022). The youngest fault interpreted by Kula (Reference 1022), which extends to the seafloor, is not continuous either in depth or length, indicating a non-tectonic origin. Therefore, the possible faults and folds near Cay Sal Bank do not represent capable tectonic sources.**

In FSAR Subsection 2.5.1.1.1.3.2.2, a new paragraph will be added following the text under subheading Cuban Fold-and-Thrust Belt, in a future COLA revision as follows:

**While most investigators confine the extent of the Cuban fold and thrust belt near the north shore of Cuba as described above, others have suggested that the relatively more subdued folding and faulting found to the northeast onto the Bahama Platform represents an extension of the Cuban fold-and-thrust belt (Masaferro et al. [Reference 426]; Masaferro et al. [Reference 479]; Bergman [Reference 906]). Structural features such as the Santaren anticline (Masaferro et al. [References 426 and 479]) and reverse faults interpreted by Bergman (Reference 906) in the southern and central Santaren Channel are taken as an indication of a greater northeastern extent for the Cuban fold-and-thrust belt style of deformation.**

FSAR Subsection 2.5.1.3 will be revised in a future COLA revision to incorporate an editorial change to FSAR Reference 906 and add new references as follows:

2.5.1.3 References

906. Bergman, K., Seismic Analysis of Paleocurrent Features in the Florida Straits: Insights into the Paleo-Florida Current, Upstream Tectonics, and the Atlantic-Caribbean Connection, University of Miami, Coral Gables, Florida, p. ~~238~~ **222**, 2005.

**1022. Kula, D., *Neotectonics on the Edge of the Cuban Fold and Thrust Belt*, unpublished Master's thesis, University of Miami, 2014.**

**1023. Eberli, G.P., Kula, D., Jo, A., Masaferro, J.L., Ludemann, T., and Betzler, C., *Influence of Neo-Tectonic Activity in the Cuban Fold and Thrust Belt on the Slope and Margin Failures of Cay Sal and Great Bahama Bank* (abstract), AAPG Annual Convention and Exhibition, Denver, CO, June 2015.**

**1024. Tournadour, E., Mulder, T., Borgomano, J., Hanquiez, V., Ducassou, E., and Gillet, H., *Origin and architecture of a Mass Transport Complex on the northwest slope of Little Bahama Bank (Bahamas): Relations between off-bank transport, bottom current sedimentation and submarine landslides,* Sedimentary Geology, Vol. 317, pp. 9-26, 2015.**

**1025. Jo, A., Eberli, G.P., and Grasmueck. M., *Margin collapse and Slope Failure along Southwestern Great Bahama Bank,* Sedimentary Geology, Vol. 317, p. 43-52, 2015.**

FSAR Figure 2.5.1-229 will be revised in a future COLA revision as follows. Note this version of FSAR Figure 2.5.1-229 supersedes that provided in the response to RAI 02.05.01-36 under FPL Letter L-2015-156.

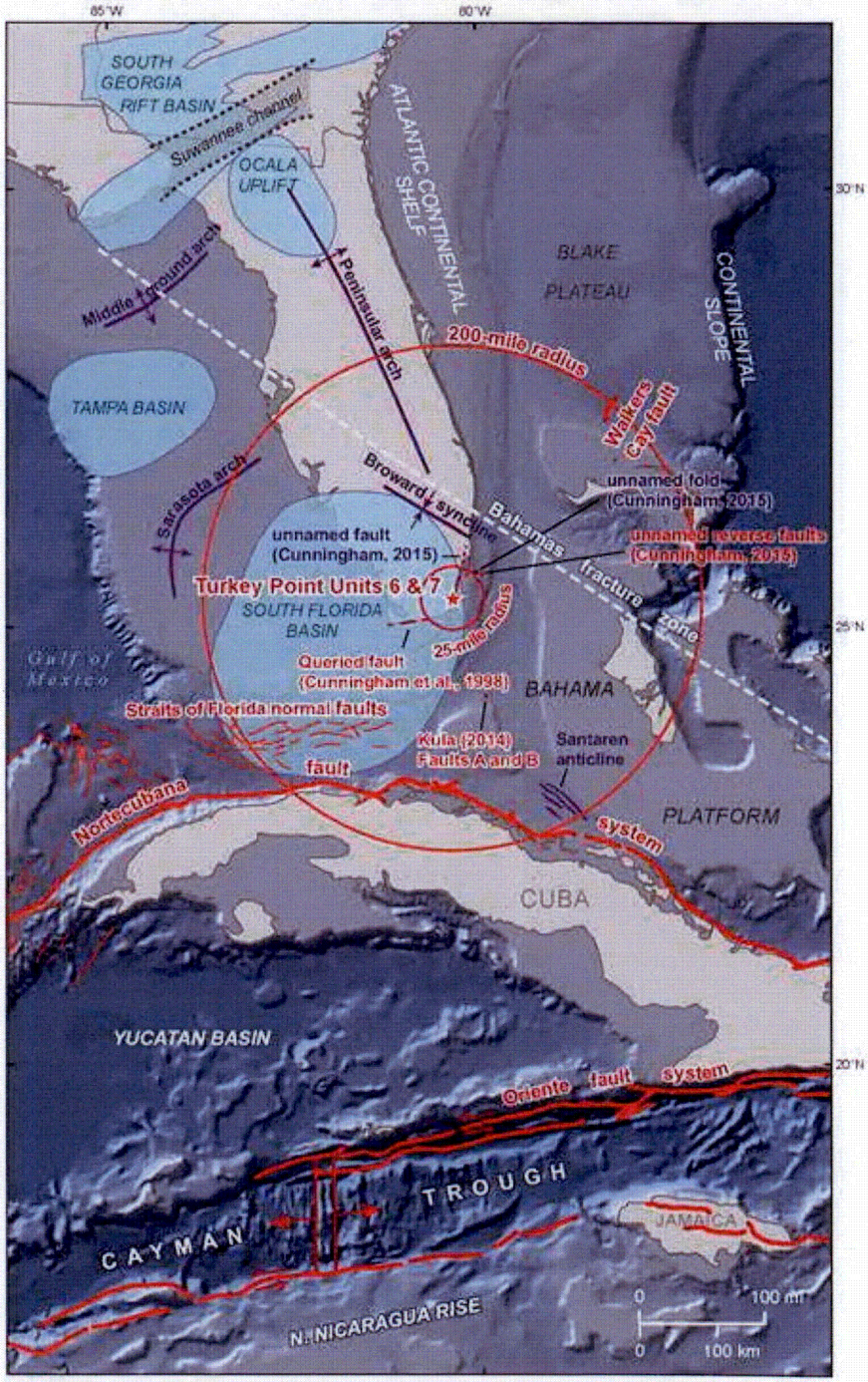


**Sources: References 822, 482, 823, 457, 212, ~~and~~ 421, 373, 999, and 1022.**

FSAR Figure 2.5.1-350 and figure title will be revised in a future COLA revision as follows:

**Figure 2.5.1-350 Seismicity in the Vicinity of the Santaren Anticline. ~~Regional Seismicity Plotted on a Map of the Nortecubana Fault and Santaren Anticline~~**

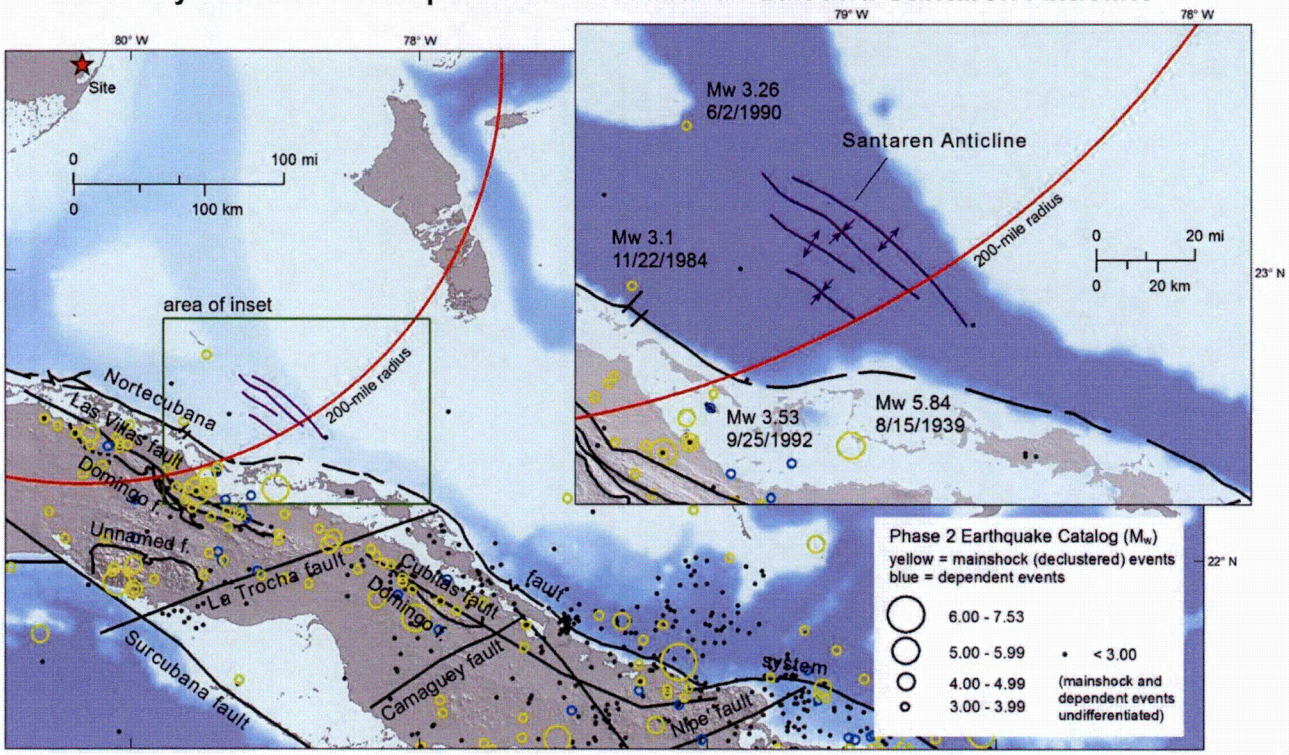


Source: 439, 443, 448, 477, 492, 494, and 770

A new Subsection 2.5.2.4.4.3.4.3, titled Santaren Anticline Fault Source Hazard Sensitivity Calculation, will be added in a future COLA revision as follows:

**2.5.2.4.4.3.4.3 Santaren Anticline Fault Source Hazard Sensitivity Calculation**

**A seismic source characterization for a potential fault underlying the Santaren Anticline for use in a hazard sensitivity calculation was performed to assess the impact on hazard at the Turkey Point Units 6 & 7 site.**

**Masaferro et al. (Reference 362) interpret the Santaren anticline in the southern Santaren Channel as a detachment fold with possible Quaternary activity. For the purpose of this sensitivity analysis, it is conservatively assumed that the anticline is cored by a seismogenic fault. Figure 2.5.2-272 shows the location of the Santaren anticline fault source, based on Masaferro et al. (Reference 362). A Santaren anticline fault is assumed to have the same surface trace as the anticline. Table 2.5.2-240 shows the surface rupture dimensions, assumed dip, uplift rate (from Masaferro et al. [Reference 363]), slip rate (uplift rate divided by sine of the dip), and distance of the fault endpoints to the site. The fault is assumed to reach the surface.**

**As part of the PSHA sensitivity calculations for hypothetical active faults in Cuba (Subsection 2.5.2.4.4.3.4.2), hazard curves for 1 Hz and 10 Hz spectral acceleration were developed for the 15 faults shown in Figure 2.5.2-272. One of these, the Hicacos fault source, lies about 15 miles (about 25 km) closer to the site than the Santaren anticline fault source, and was thus used as a proxy for the Santaren anticline fault source. The same magnitude distribution was assumed for the Santaren anticline fault source as for the Hicacos fault source ($M_W$ 7.3 and 7.0, equally weighted [Table 2.5.2-236]). The Hicacos hazard curve annual frequencies of exceedance were then scaled by the ratio of the Santaren anticline fault source slip rate (0.071 mm/yr) to the mean Hicacos slip rate (0.037 mm/yr, from Table 2.5.2-236), or 1.92. This strategy is conservative in that the Hicacos fault is closer to the site than the Santaren anticline fault source.**

**The Santaren anticline fault source hazard curves were added to those for the FSAR total hazard (from Table 2.5.2-223), and the increases in hazard and ground motion at annual frequencies of exceedance of $10^{-4}$ and $10^{-5}$ were computed.**

**Figure 2.5.2-286 shows the Santaren anticline fault source hazard curves, the FSAR total hazard curves, and the effect of summing the two. As depicted in Figure 2.5.2-286, adding the Santaren anticline fault source clearly has a small effect on the total hazard.**

**Table 2.5.2-241 shows the change in hazard at MAFE of $10^{-4}$ and $10^{-5}$. The hazard increases range from 1.42% to 8.80%. Table 2.5.2-242 shows the change in ground motions at these hazard levels. The ground motion increases range from 0.77% to 3.48%. The maximum ground motion increase is less than 0.003 g.**

The following new references will be added to FSAR Subsection 2.5.2.7 in a future COLA as follows:

2.5.2.7 References

**362. Masaferro, J., J. Poblet, M. Bulnes, G. Eberli, T. Dixon, and K. McClay, *Palaeogene-Neogene/Present Day(?) Growth Folding in the Bahamian Foreland of the Cuban Fold and Thrust Belt*, Journal of the Geological Society, Vol. 156, pp. 617–631, 1999.**

**363. Masaferro, J., M. Bulnes, J. Poblet, and G. Eberli, *Episodic Folding Inferred from Syntectonic Carbonate Sedimentation: the Santaren Anticline, Bahamas Foreland,* Sedimentary Geology, Vol. 146, No. 1-2, pp. 11–24, 2002.**

FSAR Tables 2.5.2-240, 2.5.2-241 and 2.5.2-242 will be added in a future COLA revision:

**Table 2.5.2-240**
**Santaren Anticline Fault Source Parameters**

| Length (km) | Nearest Distance to Site (km) | Farthest Distance to Site (km) | Uplift Rate (mm/yr) | Fault Dip (degrees) | Slip Rate (mm/yr) |
|---|---|---|---|---|---|
| 70.5 | 267.7 | 333.4 | 0.05 | 45 | 0.071 |

**Table 2.5.2-241**
**Summary of Rock Hazard Sensitivity to Santaren Anticline Fault Source: Comparison of Exceedance (MAFE) at FSAR Amplitudes**

| | FSAR | | FSAR + Santaren Anticline fault source | |
|---|---|---|---|---|
| | $10^{-4}$ mean annual frequency of exceedance | | | |
| Freq | *MAFE* | *Amp.* | *MAFE* | *MAFE % Diff* |
| 1 Hz | 1.00E-04 | 0.0343 | 1.0605E-04 | 6.05% |
| 10 Hz | 1.00E-04 | 0.0822 | 1.0726E-04 | 7.26% |
| | $10^{-5}$ mean annual frequency of exceedance | | | |
| Freq | *MAFE* | *Amp.* | *MAFE* | *MAFE % Diff* |
| 1 Hz | 1.00E-05 | 0.0663 | 1.0880E-05 | 8.80% |
| 10 Hz | 1.00E-05 | 0.278 | 1.0142E-05 | 1.42% |

**Table 2.5.2-242**

**Summary of Rock Motion Sensitivity to Santaren Anticline Fault Source: Ground Motion Amplitudes in Comparison to FSAR Ground Motion Amplitudes**

| | FSAR | FSAR + Santaren Anticline fault source | | |
|---|---|---|---|---|
| | Rock motions (g) at $10^{-4}$ mean annual frequency of exceedance | | | |
| Freq | *Amp.* | *Amp.* | *Amp. Diff* | *Amp. % Diff* |
| 1 Hz | 0.0343 | 0.034899 | 0.000599 | 1.75% |
| 10 Hz | 0.0822 | 0.085058 | 0.002858 | 3.48% |
| | Rock motions (g) at $10^{-5}$ mean annual frequency of exceedance | | | |
| Freq | *Amp.* | *Amp.* | *Amp. Diff* | *Amp. % Diff* |
| 1 Hz | 0.0663 | 0.067900 | 0.001600 | 2.41% |
| 10 Hz | 0.278 | 0.280139 | 0.002139 | 0.77% |

FSAR Figure 2.5.2-272 and figure title will be revised in a future COLA revision:

**Figure 2.5.2-272 Map of ~~Intraplate~~ Cuba Fault Sources and Santaren Anticline Fault Source for Hazard Sensitivity Calculations**

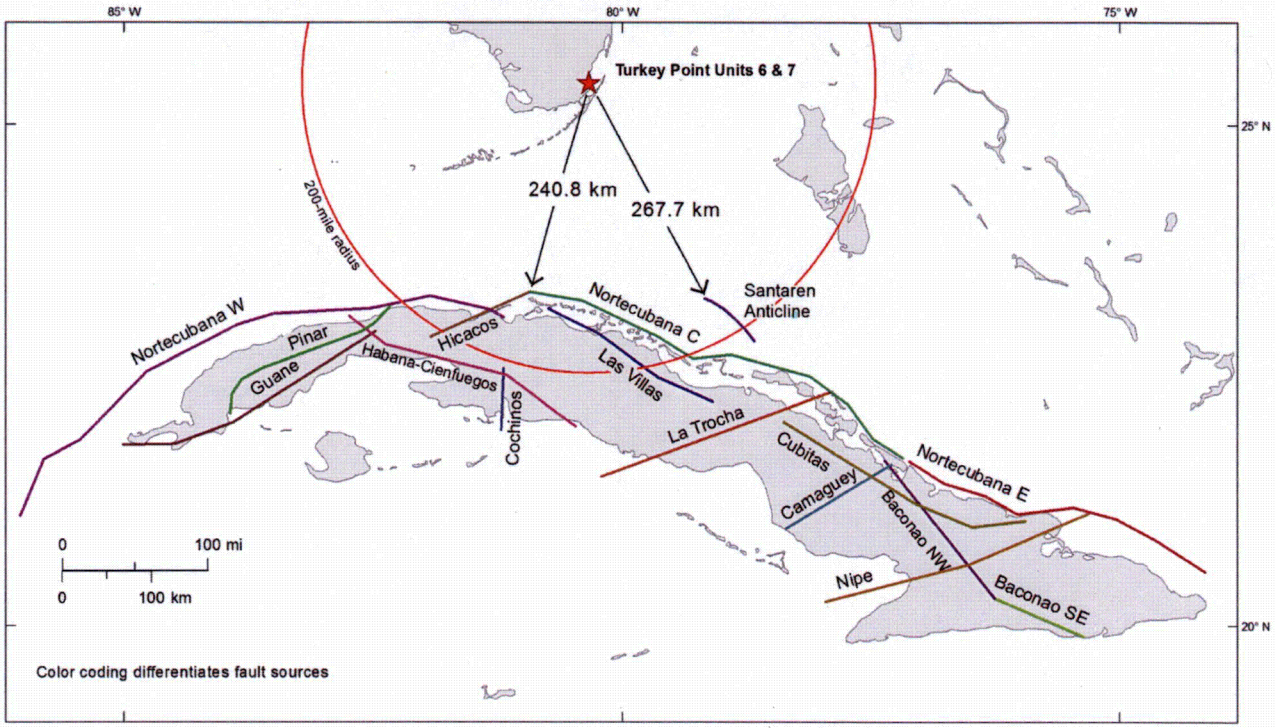

A new FSAR Figure 2.5.2-286 will be added in a future COLA revision:

**Figure 2.5.2-286 1 Hz and 10 Hz Mean Hazard Curves showing Sensitivity to Santaren Anticline Fault Source**

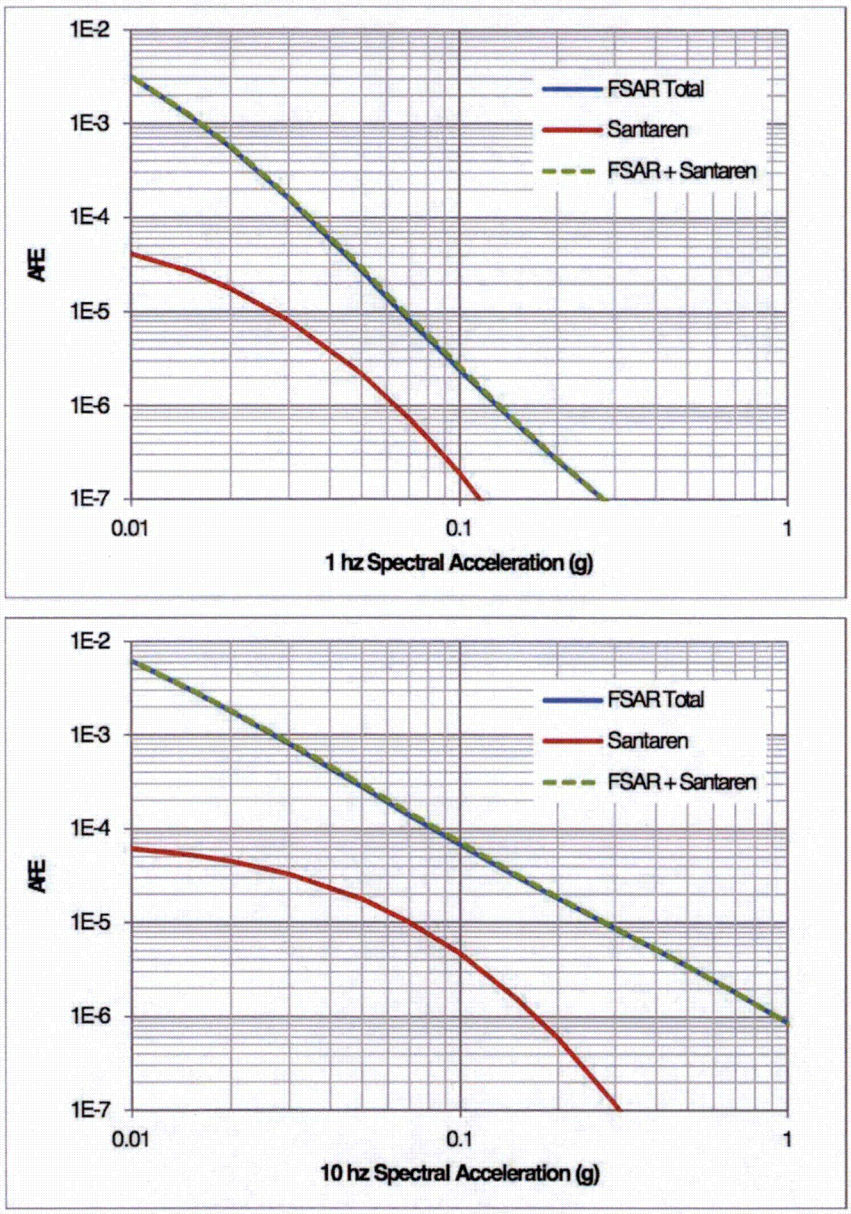


## ASSOCIATED ENCLOSURES

Enclosure 1: Supplemental Figures Showing Uninterpreted, Publicly Available GSI Seismic Lines from the Santaren Channel Region

# ENCLOSURE 1

**Supplemental Figures Showing Uninterpreted, Publicly Available GSI Seismic Lines from the Santaren Channel Region**

(7 Pages)

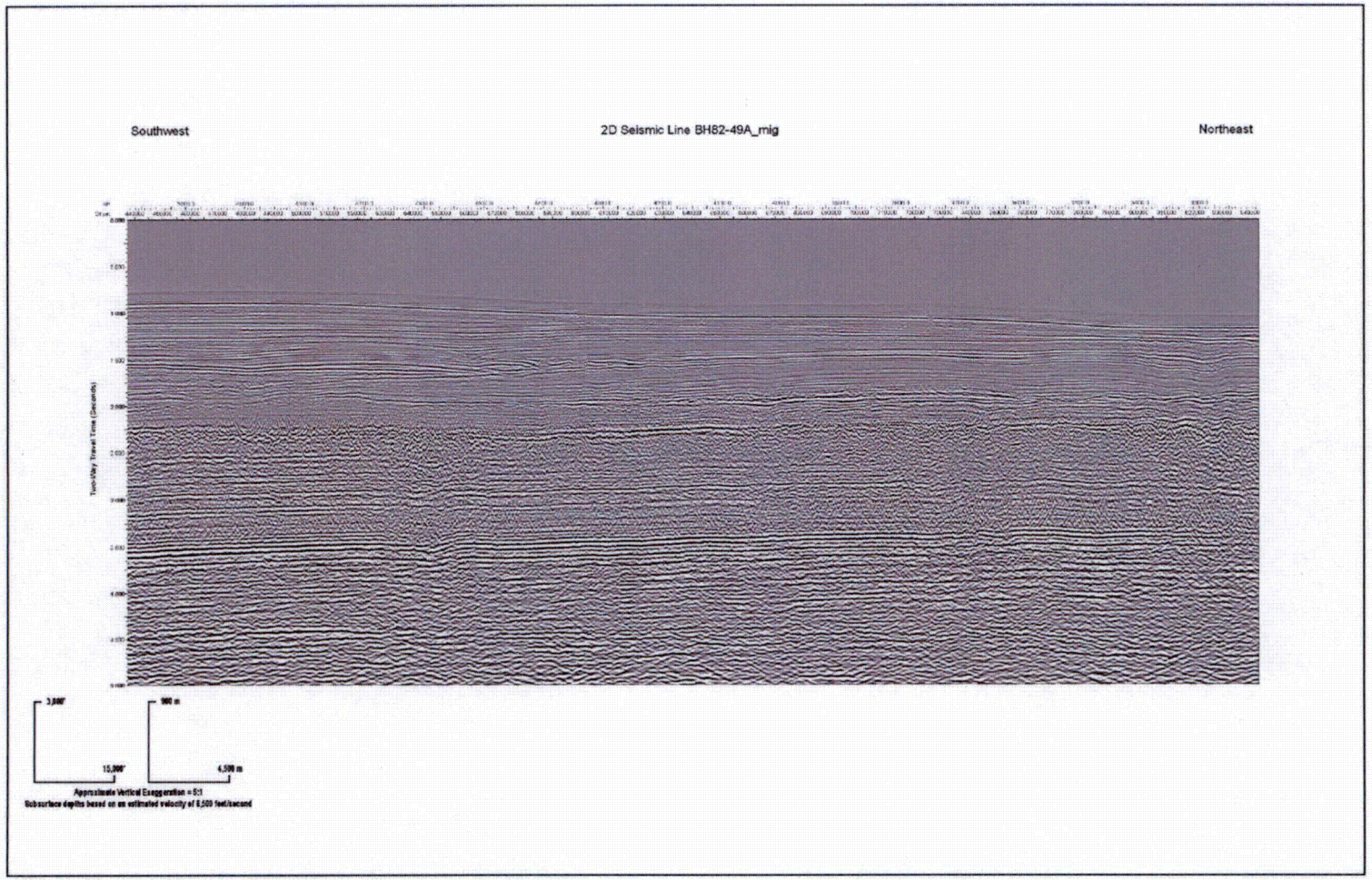


**Figure A1.** Uninterpreted GSI seismic reflection Line BH82-49A_mig (Reference 5).

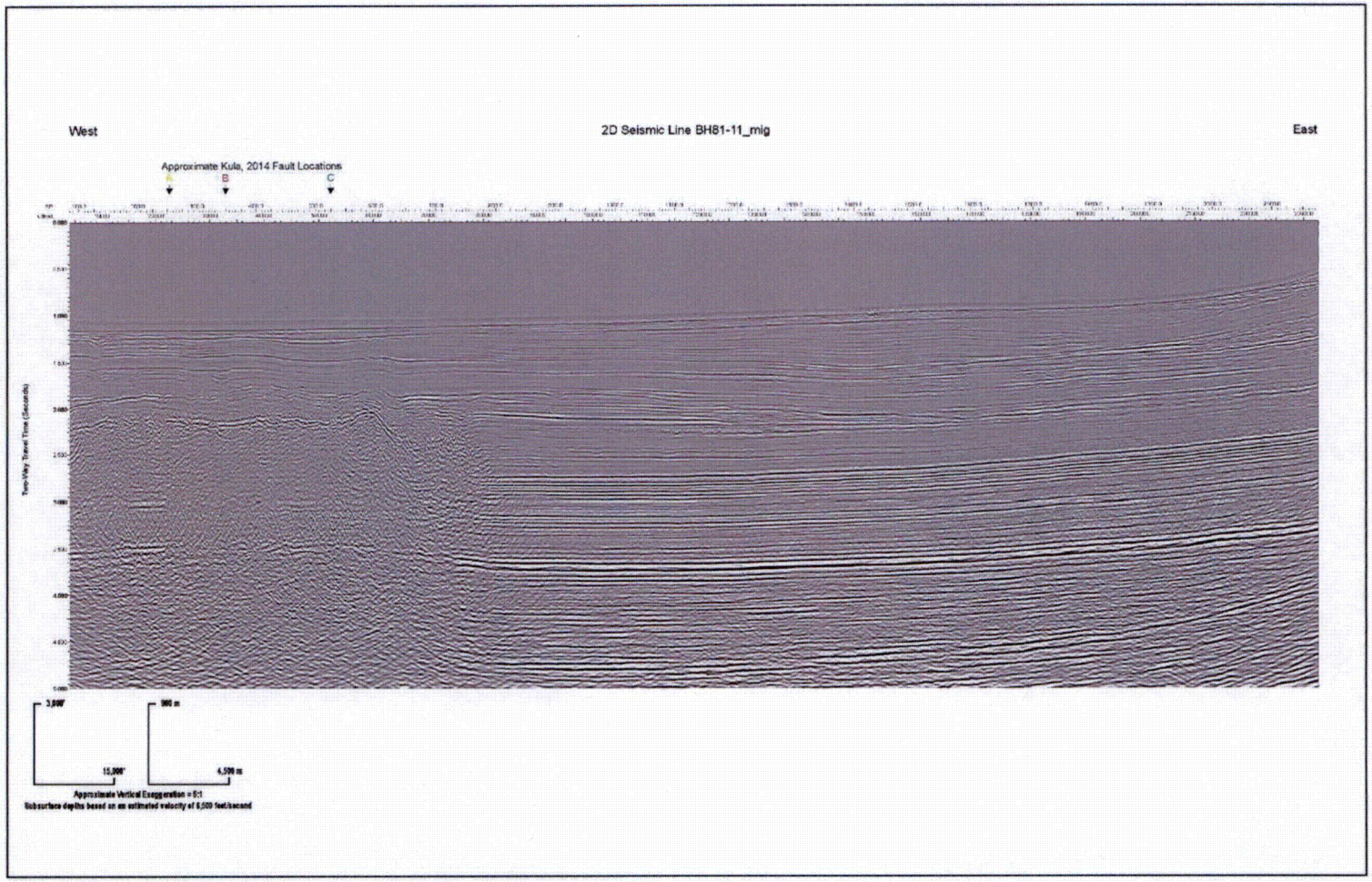


**Figure A2.** Uninterpreted GSI seismic reflection Line BH81-11_mig (Reference 5).

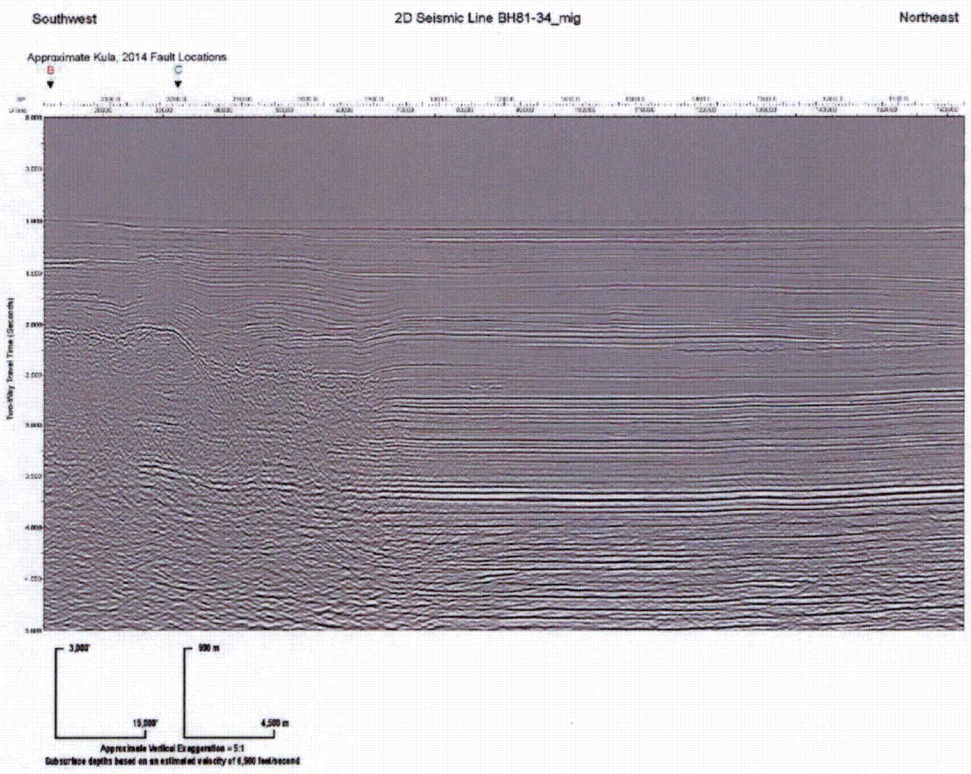


**Figure A3.** Uninterpreted GSI seismic reflection Line BH81-34_mig (Reference 5).

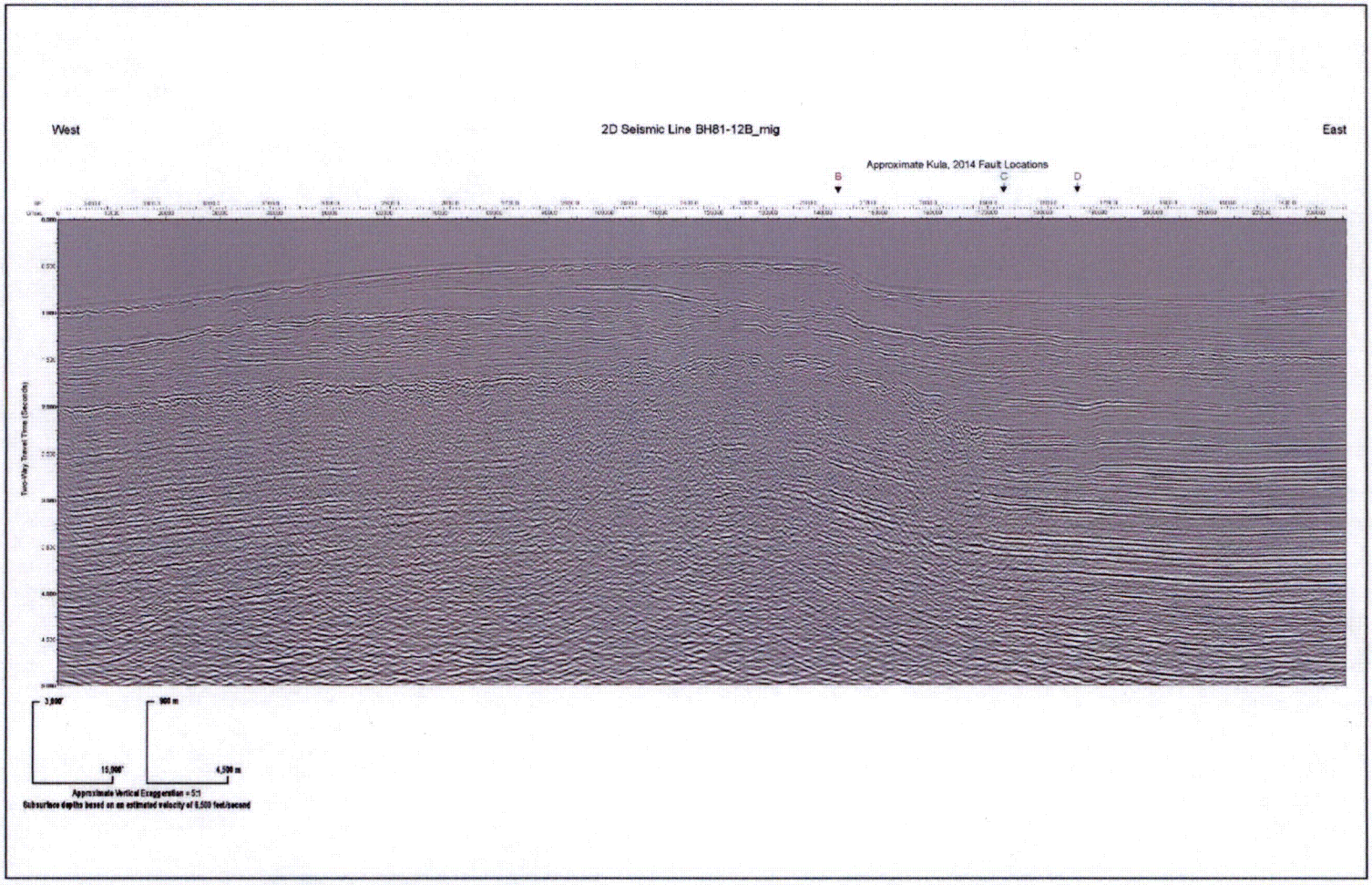


**Figure A4.** Uninterpreted GSI seismic reflection Line BH81-12B_mig (Reference 5).

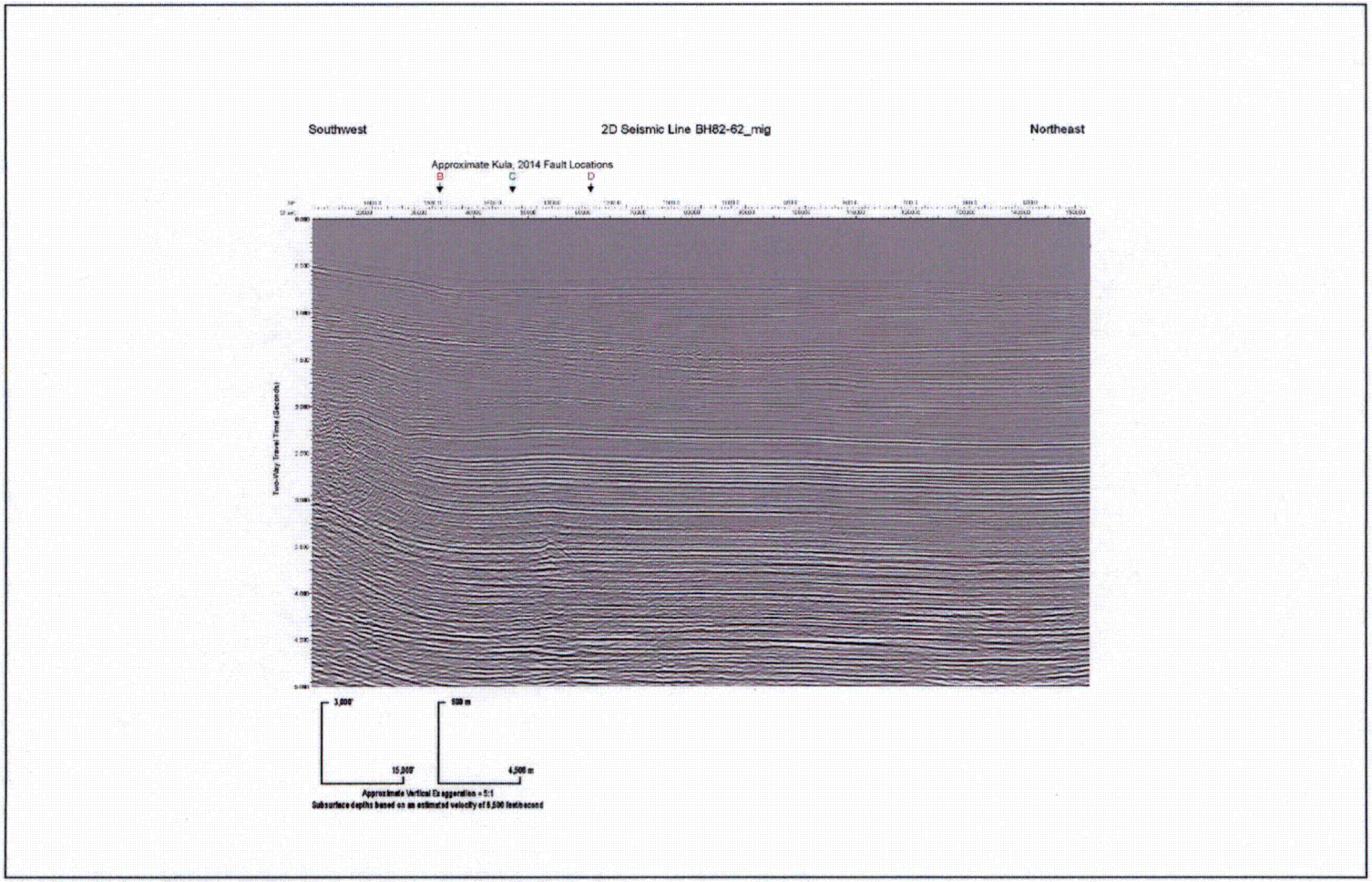


**Figure A5.** Uninterpreted GSI seismic reflection Line BH82-62_mig (Reference 5).

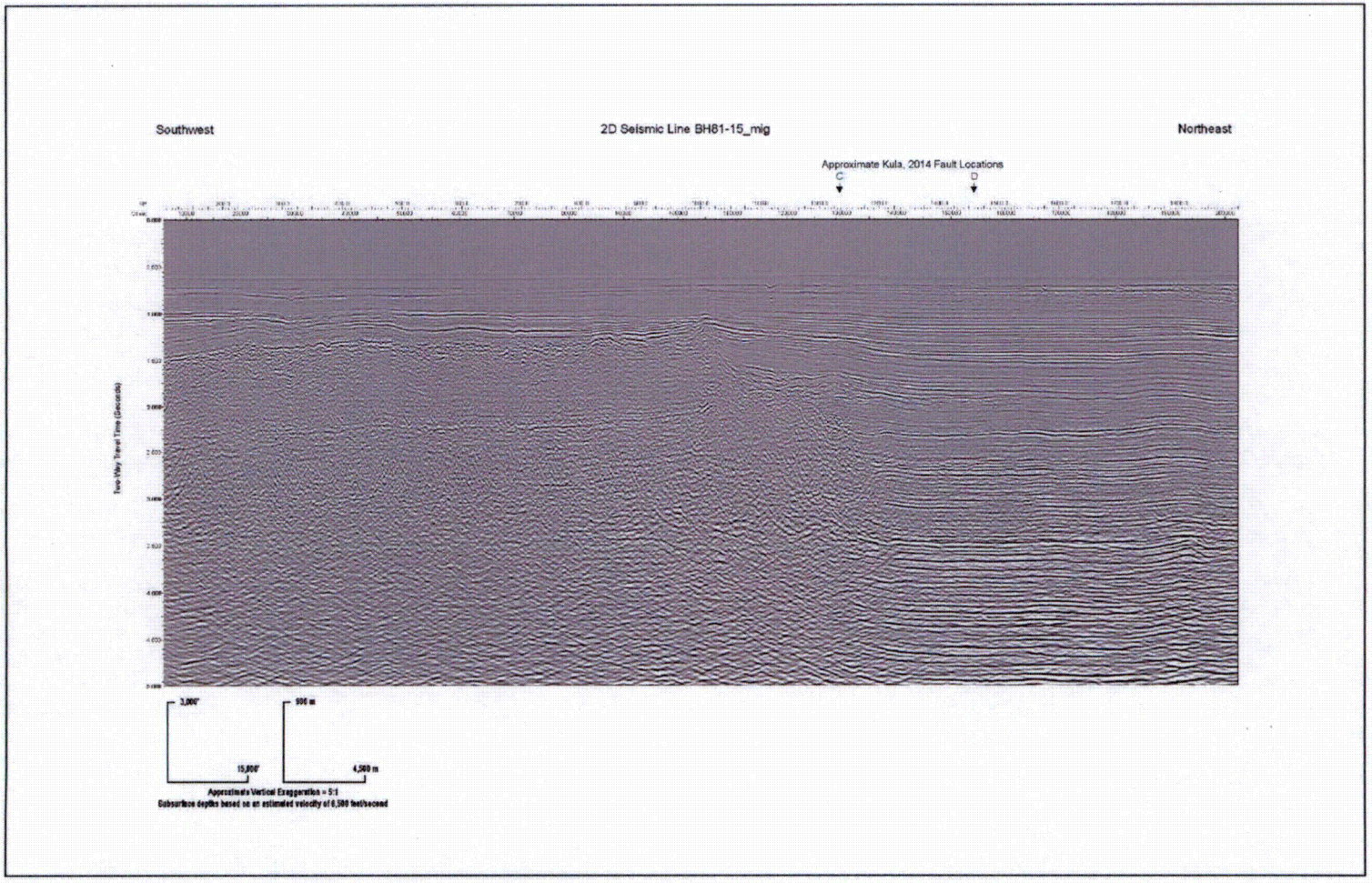


**Figure A6.** Uninterpreted GSI seismic reflection Line BH81-15_mig (Reference 5).